A High Throughput LC-MS Platform for the Discovery of Autotaxin Inhibitors

BY

YONGCHAO LI

M.D., Beijing University of Chinese Medicine, Beijing, China, 2004

DISSERTATION

Submitted in partial fulfillment of the requirements for the degree of Doctor of Philosophy in Medicinal Chemistry in the Graduate College of the University of Illinois at Chicago, 2017

Chicago, Illinois

Defense Committee:

Richard B. van Breemen, Advisor and Chair

John William Christman, Ohio State University

Douglas D. Thomas

Terry W Moore

Guofei Zhou, Pediatrics

To my beloved wife Yaxin Huang & our precious kid Austin for their love and support

ACKNOWLEDGEMENT

The thesis would not have been completed without the contributions, assistance and support from family, friends, the faculty, and my advisor, Dr. Richard B. van Breemen. To Professor van Breemen, I am very grateful for his brilliant guidance, practical advice, deep knowledge, foresight, and optimistic attitude which will deeply affect my future.

I thank my dissertation committee members, Dr. John William Christman, Dr. Douglas D. Thomas, Dr. Terry W. Moore, and Dr. Guofei Zhou for their support and guidance with my research project.

I would like to thank Dr. Dejan Nikoic for his tremendous helpful suggestions and his constant guidance during the course of my graduation education.

I would like to thank the many graduate students and postdoctoral fellows at the University of Illinois at Chicago for their help, support and fruitful discussions.

Finally, I would like to express my heartfelt gratitude to my family, especially my wife Yaxin Huang and my son, my parents Qinglian Guo and Xianbin Li, and my parents-in-law Weina Zhang and Guangye Huang. Thank you for your constant love and support as well as patience.

CONTRIBUTION OF AUTHORS

Chapter 1 is a review of research references that places my dissertation topic in the context of the larger field and addresses the potential and significance of this research project.

Chapter 2 represents a published manuscript (include incomplete citation). I generated Figures 1, 2, 3, 4, 5, 6, 7, 8, 9, 10, 11, 12, 13 and played a large role in the writing of the manuscript along with my research mentor, Dr. John W. Christman. My work was critical to the conclusions of this manuscript because my results identify the most important biomarker in this experiment. My research mentor, Dr. John W. Christman contributed to the writing of the manuscript.

Chapter 3 and represents a series of my own unpublished data directed at answering the question how to find out the inhibitor of Autotaxin and identify the inhibitor, glabridin, from *Glycyrrhiza glabra*.

TABLE OF CONTENTS

CHAPTER **PAGE**

TABLE OF CONTENTS (continued)

LIST OF TABLES

LIST OF FIGURES

LIST OF FIGURES (continued)

FIGURE PAGE

LIST OF ABBREVIATIONS

AA	Arachidonic acid
AM	Alveolar macrophages
ANOVA	One-way analysis of variance
ATX	Autotaxin
BAL	Bronchoalveolar lavage
BMDM	Bone marrow-derived macrophages
cAMP	Adenosine monophosphate
CID	collision-induced dissociation
COPD	Chronic obstructive pulmonary disease
COX	Cyclooxygenase
cPGES	Cytosolic prostaglandin E synthase
Da	Dalton
DMEM	Dulbecco's modified eagle's medium
DMSO	Dimethyl sulfoxide
DNA	Deoxyribonucleic acid
DRA	Triple antigen
EIA	Enzyme Immunoassay
ELISA	Enzyme-linked immunosorbent assay
E-NPP 2	Ectonucleotide pyrophosphatase/phosphodiesterase family member
EPO	Erythropoietin
ER	Endoplasmic reticulum
ESI	Electrospray ionization
FAK	Focal adhesion kinase
Fsp-VHL	Fibroblast-specific pVHL
GC	Gas chromatography
GPCRs	G protein-coupled receptors
GSH	Glutathione
GST	Glutathione-S-transferase

LIST OF ABBREVIATIONS (continued)

HCT	Hematocrit
HGB	Hemoglobin
HIF	Hypoxia-inducible factor
H-PGDS	Hematopoietic prostaglandin D synthase
HPLC	High performance liquid chromatography
IC 50	Concentration required to inhibit 50% of enzyme activity
IFNγ	Interferon gamma
IHC	Immunohistochemistry
IL	Interleukin
iNOS	Inducible nitric oxide synthase
IPF	Idiopathic pulmonary fibrosis
IS	Internal standard
IT-TOF	Ion trap-time-of-flight
LC	Liquid chromatography
LCAT	Lecithin-cholesterol acyltransferase
LLOQ	Lower limit of quantitation
LOD	Limit of quantitation
LPA	Lysophosphatidic acid
LPC	phosphatidylcholine
LPE	phosphatidylethanolamine
LPS	phosphatidylserine
µ	Micro
m	Milli
M	Molar
MAPK	Mitogen-activated protein kinase
mPGES-1	Microsomal prostaglandin E synthase-1
mPGES-2	Microsomal prostaglandin E synthase-2
MMP	Metoprotease
MS	Mass spectrometry

LIST OF ABBREVIATIONS (continued)

MS-MS	Tandem mass spectrometry
m/z	Mass-to-charge ratio
n	Nano
NF-kB	Nuclear factor-kappaB
NSAIDs	Nonsteroidal anti-inflammatory drugs
NOS	Nitric oxide synthase
NOX	NAD(P)H oxidase
Ofev	Nintedanib
PA	phosphatidic acid
PAS	Periodic acid–Schiff
PCNA	Proliferating cell nuclear antigen
PG	Prostaglandin
PGDS	Prostaglandin D synthase
PGES	Prostaglandin E synthase
PLA 2	Phospholipase A 2
PUF	Pulsed ultrafiltration
pVHL	Von Hippel-Lindau protein
QC	Quality control
QqTOF	Quadrupole-quadrupole-time-of-flight
RBC	Red blood cells
RIA	Radioimmunoassay
RT-PCR	Reverse transcription PCR
S1P	Sphingosine 1-phosphate
SBP-AG	Sub-Segmental Bronchoprovocation with Allergen
SD	Standard deviation
SDS-PAGE	Sodium dodecyl sulfate polyacrylamide gel electrophoresis
SET	Skin endpoint titration
SMB	Somatomedin B
S/N	Signal-to-noise

LIST OF ABBREVIATIONS(continued)

SOP	Standard operating procedure
Th	Helper T cells
TLC	Thin layer chromatography
TLR	Toll like receptor
TNF-α	Tumor necrosis factor α
TOF	Time-of-flight
UHPLC	Ultrahigh pressure liquid chromatography
UIC	University of Illinois at Chicago
ULOQ	Upper limit of quantitation
VEGF	Vascular endothelial growth factor
WB	Western blot
WT	Wild type

SUMMARY

The bioactive group of lipids, the eicosanoids, which includes lysophospholipids and their derivatives, are lipid mediators formed from arachidonic acid. Class 1 lipid mediators include sphingosine-1-phosphate (S1P), lysophosphatidic acid (LPA) and endocannabinoids. LPA binds to specific receptors which take part in various biological processes, including brain development, embryo implantation, hair growth, and inflammation. Produced by the enzymatic activity of extracellular autotoxin (ATX), LPA is involved in asthma pathogenesis. Additionally, LPA enhances the production of cytokines and chemotaxis in lymphocytes, which can lead to contractility and proliferation of airway smooth muscle cells as well as changing inflammatory signaling in the epithelial cells of the bronchus. Together, all these results indicate that LPA participates in the molecular pathogenesis of asthma.

Our hypothesis is that the ATX-LPA axis plays a critical role in the pathogenesis of asthma and makes it an ideal target for an effective anti-asthma treatment. To test our hypothesis, a human model (an IRB-approved protocol for sub-segmental broncho-provocation with allergen, SBP-AG, to induce localized allergic inflammation in human volunteers), and a mouse model (mice subjected to a triple allergen house dust mite, ragweed and aspergillus allergen; DRA) has been developed to explore the mechanism of ATX-LPA axis on the pathogenesis of asthma. To further explore the function of LPA in asthma, we used a transgenic mouse with ATX over-expression (ATX-Tg) to study the effect of triple allergen challenge compared to that of wild type mice. LPA receptor 2 knock-out mice (LPA2-/-) were also used to carry out additional experiments to provide further evidence to support our hypothesis.

The development of sensitive, efficient and high-throughput methods to study the ligand-enzyme binding affinity and their potential to inhibit ATX activity is essential to identify novel ATX inhibitors. ATX can hydrolyze phosphatidylcholine (LPC) into two products, choline and LPA, and both products can be used to measure ATX activity. Previously, several in vitro biochemical assays based on radiometry or fluorescence had been used to screen compounds for potential ATX inhibition by measuring its enzymatic products, and these tested one compound at a time for binding or inhibition. Liquid chromatography-tandem mass spectrometry (LC-MS/MS) also can be used to measure LPA, but most of the previous LC-MS based methods were used to detect naturally occurring LPA in biological fluids (i.e. plasma, bronchoalveolar lavage). Although not previously applied to ATX inhibitor screening, mass spectrometry-based bioassays are useful in the discovery of protein ligands and enzyme inhibitors. For example, pulsed ultrafiltration (PUF) LC-MS based methods, invented in our laboratory, have been used for screening of combinatorial library mixtures and natural product extracts in order to identify ligands for a wide variety of macromolecular targets including quinone reductase-2, cyclooxygenase-2, estrogen receptors, and retinoid X receptor. The main advantages of PUF-LCMS based screening over optical or radioactive detection methods are high throughput, low cost, fewer false positives, and no need to modify either the ligand or the targets by attaching a radiolabel, chromophore or fluorophore.

1. INTRODUCTION

1.1 Lysophosphatidic Acid (LPA)

Lysophosphatidic acid (LPA) is a water-soluble phospholipid derivative, and its structure is shown in figure 1.1. It is the simplest of all glycerophospholipids in vivo (1). Additionally, it is a known critical potent extracellular signaling molecule, which can act on G protein-coupled receptors (GPCRs). When LPA acts on GPCR, it leads to the altering of multiple cellular responses, including cell survival, cytoskeletal changes, proliferation, and calcium influx (2, 3). Pharmacologically active LPA was first isolated by Kirschner and Vogt from brain extracts in 1961 (4). Since then, 7696 full-text journal articles related to LPA have been published as collected in NCBI.

To date, multiple LPA receptors have been reported, which include LPA1, LPA2 and LPA3. These are also referred to as EDG2, EDG4, and EDG7, respectively. More recently discovered LPA receptors include LPA4 (P2RY9, GPR23), LPA5 (GPR92), as well as LPA6 (P2RY5, GPR87). One critical finding that has been established in research on LPA receptors is that LPA binds to the heterotrimeric G proteins, including Gi/o, G12/13, Gq, and Gs. In addition, LPA mediates effects in several types of cells as well as model systems, both in vitro and in vivo. Through gain- and loss-of-function studies, LPA has been linked to not only physiological but also pathophysiological effects on nearly every organ system. The influence of LPA extends to almost all the developmental steps and phases of an organism (5).

There are two principal pathways of LPA biosynthesis. First, LPA can be formed from lysophospholipids (phosphatidylcholine/LPC, phosphatidylethanolamine/LPE or

phosphatidylserine/LPS) by action of the enzyme, autotaxin (ATX). The production of lysophospholipids, on the other hand, involves at least two mechanisms. The secretory phospholipase A2 (PS-PLA2) and phosphatidylserine-specific phospholipase A1 (PS-PLA1), which produce lysophospholipids in active platelets. In plasma, PLA1-like enzymes, as well as lecithin-cholesterol acyltransferase (LCAT), are involved in the production of LPC (6-7). The second major pathway of LPA biosynthesis entails the conversion of diacylglycerol to phosphatidic acid (PA) by the catalytic mechanisms of diacylglycerol kinase. The pathway may also involve phospholipase D converting phospholipids D to PA. The next step involves the conversion of PA to LPA. This process is enabled by the catalytic mechanisms of either PLA1 or PLA2 (8).

LPA is present in all eukaryotic tissues that have ever been tested. The most common LPA species used in the laboratory is 18:1 oleoyl-LPA. It is also referred to as 1-acyl-2-hydroxy-sn-glycero-3-phosphate. However, there are more chemical forms of LPA in different biological systems that have been recognized (9). The observed LPA concentration in various biological systems spans from low nanomolar to micromolar levels. In addition, serum is known to contain micromolar concentrations of LPA, which is much higher than in plasma. Notably, LPA concentration in plasma, approximately 0.1 μM, is much higher than the apparent nanomolar Kd of LPA 1-6 (10, 11).

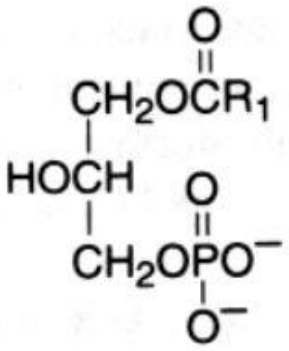

Figure 1.1 LPA structure

1.2 Autotaxin (ATX)

Autotaxin, which is also referred to as ectonucleotide pyrophosphatase/phosphodiesterase family member 2 (E-NPP 2), is a secreted catalyst involved in the conversion of lysophosphatidylcholine into LPA. It is encoded by the ENPP2 gene in human (12) and is produced as a pre-proenzyme and later discharged into the extracellular space (13). The structure of ATX is shown in figure 1.2 (14).

The ATX protein consists of four domains, which include 2 *N*-terminal somatomedins-B-like (SMB) domains followed by a catalytic domain (PDE) and a C-terminus nuclease-like domain (NUC) (15). The interaction between proteins (protein-protein interaction) is believed to be mediated by the SMB domains. The crystal structure of ATX indicates that there is an interaction between the SMB domains and the catalytic PDE domain on one side, and on the other end, it interacts with the NUC domain. Based on a sequence similarity, the structure of the PDE domain has a close resemblance to that of prototypic NPP, which is found in the bacteria *Xanthomonas axonopodis*. The structure is an evolutionary relative of alkaline phosphatases. ATX has gone through a series of evolutionary changes resulting in the development of a deep lipid-binding pocket, which is hydrophobic. The pockets are of about 15 Å in diameter and can readily accommodate monoacyl groups but will exclude diacyl phospholipids. The depth of the lipid-binding pockets is optimal for LPA (14:0) (16).

Furthermore, studies have shown that the lipid-binding pocket of ATX is permanently 'open'; meaning that the LPC substrate has continuous access to the active site. Binding of LPC to ATX might also enhance catalytic processes through 'substrate destabilization.' When this happens, LPC reduces the activation energy barrier of the phosphodiester hydrolysis reaction (16). ATX then hydrolyzes the head groups of lysophospholipids to form lysophosphatidic acid (1 or 2-acyl-sn-glycerol-3-phosphate, LPA). In addition, ATX acts on sphingosylphosphorylcholine resulting in the production of sphingosine 1-phosphate (S1P) (17). Conversely, S1P and LPA can act as potent inhibitors of ATX. They have an enzymatic affinity which is roughly 1000-fold higher than those reported for ATX substrates (18). ATX is believed to be the primary source of blood LPA but not for S1P (19, 20).

ATX is expressed in many organs in human. The brain, lungs, spinal cord, intestines, kidney, and the ovary contain the highest levels of mRNA. Medium levels of ATX mRNA have

been reported in lymph nodes, particularly at the high endothelial venules, which are involved in the control of lymphocyte entry (21, 22).

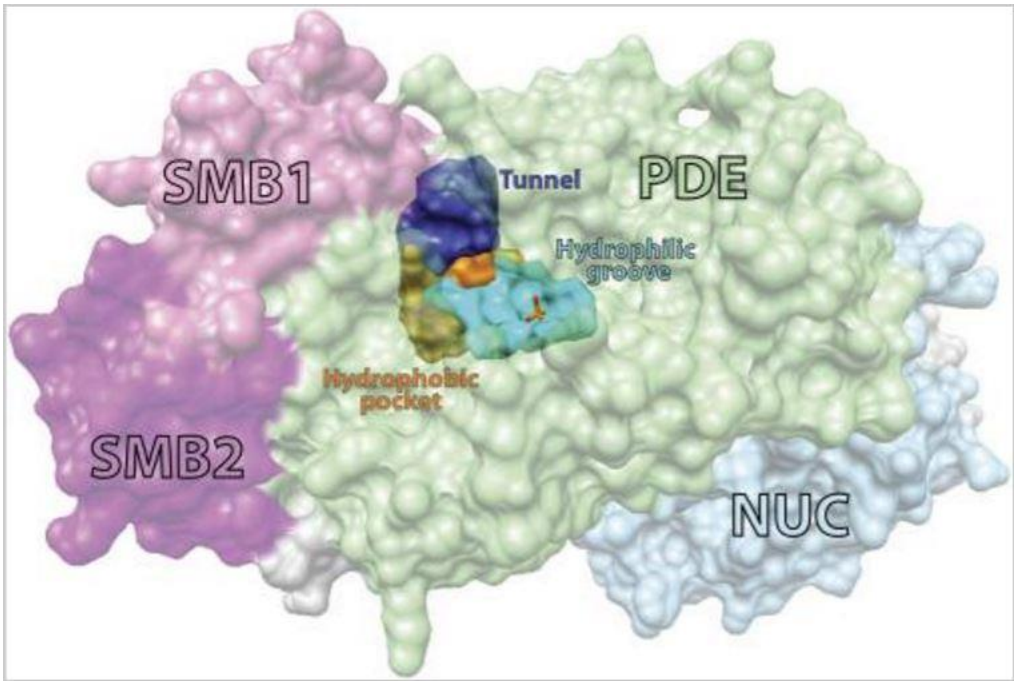

Figure 1.2 ATX structure

The ATX structure is shown as a semi-transparent surface. The dark and light magenta areas represent the two *N*-terminal SMB domains. The green section is the PDE domain. Lastly, the blue color covers the NUC domain. The estimated volumes of the shallow the open tunnel, groove, and the hydrophobic pocket are represented as dark blue, cyan, and orange solid surfaces, respectively (1).

1.3 LPA Signaling in Human Disease

ATX converts lysophosphatidylcholine (LPC) into LPA. The latter acts on specific G protein-coupled receptors (GPCRs) and activates numerous signaling pathways as shown in figure 1.3. The end result of LPA signaling depends on the patterns of LPA receptor (co-)expression as well as the tissue context. Cellular responses to LPA include survival, stimulation of cell migration, and proliferation. Many human diseases result from abnormal ATX and LPA signaling. Some of the major causes of harm to cardiac myocytes in myocardial infarction are ischemia and hypoxia. LPA tends to protect cells from hypoxia-induced apoptosis, especially mesenchymal stem cells, cardiac myocytes and renal cells (24-25).

Studies indicate that LPAR1 and LPAR3 enhance the hypertrophic response, which is achieved by the means of activating Gi and multiple downstream effectors. The effectors include PI3K/Akt, Rho, and NF-kB both in vivo and in-vitro (26, 27). LPA-mediated suppression of isoprenaline induces the cell shortening as a result of the stimulation of LPA1 and/or LPA3 in a PTX sensitive manner. Lipoprotein lipase (LPL) activity is also increased by LPA in cardiac myocytes (28).

Several scholars indicate that there is a strong correlation between genetic/biological factors and psychiatric disorders. LPA has the potential of contributing to disease progression of schizophrenia and bipolar disorder. It achieves this through its capacity to bring changes in glial cells and their progenitors as well as the physiology of neurons (29). LPA is also related to cancer. The first report to show that LPA can induce tumor cell invasion in vitro was made in 1993 (30). Since then, numerous studies have shown that LPA is involved in cancer etiology. These studies have been conducted using various tumor cell lines as well as on samples obtained from cancer patients. Angiogenesis is important in tumor growth, where it supplies oxygen and nutrition to support tumor growth. Vascular endothelial growth factor (VEGF) is known to promote angiogenesis. It is produced by tumor cells and the consequences of its inhibition are the suppression of tumor growth (31).

There is evidence showing that LPA signaling contributes to psychiatric disorders which indicates long-term spatial memory is related to LPA pathway (32). Additionally, the analysis of the concentration of LPA indicates that rat brains contain a significant amount of LPA (33). LPA

signaling pathway also controls neurite retraction and outgrowth which is required in the process of the rearrangement of synaptic connections to form neuronal plasticity (34).

LPA is also a key lipid in reproduction. Ovaries produce LPA1-4, and the expression of LPA4 in the ovary is greater than in any other human tissue examined. Autotaxin activity in ovaries increases after hormonal stimulation (35). The role of LPA signaling in reproduction is confirmed by the involvement of LPA/prostaglandin signaling in the development of the embryo and for sustaining pregnancy in sheep and pig (36, 37).

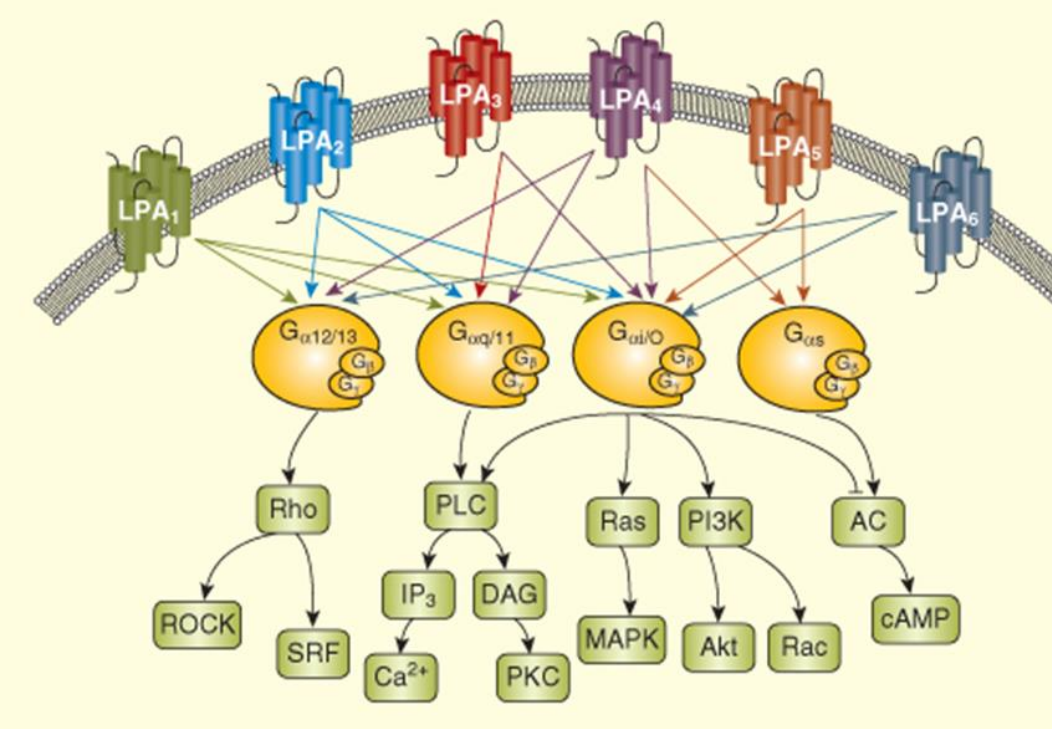

Figure 1.3, Signaling pathways stimulated by the 6 LPA receptors that have been confirmed (5).

In addition to the involvement of LPA in major organ systems and in many major diseases, LPA have been shown to associate with other disorders. Allergic asthma is a chronic inflammatory reaction associated with airway hyper-responsiveness and tissue remodeling of the airway structure. Numerous types of cells involved in asthmatic inflammation, which include lymphocytes, eosinophils, airway epithelial cells and macrophages, communicate within the microenvironment of the airway and airspace. LPA has a significant effect on cytokine synthesis and chemotaxis in lymphocytes (38-41), has been reported to affect contractility and proliferation of airway smooth muscle cells, and is known to modulate inflammatory signaling in bronchial epithelial cells (38-41), indicating its possible effect on the molecular pathogenesis of asthma**.** Taken together, we hypothesized that the ATX-LPA pathway plays an important role in the molecular mechanism of asthma.

1.4 Prostaglandin-Endoperoxide Synthase 2

In 1991, the Daniel Simmons laboratory at Brigham Young University discovered prostaglandin-endoperoxide synthase 2 (PTGS2 or COX-2) (45). In human beings, it is encoded by the *PTGS2* gene. Cyclooxygenase (COX) is responsible for the production of prostanoids from arachidonic acid, which is hydrolyzed from cell membrane phospholipids. Phospholipase A2 also participates in prostanoid production. Two isoforms of COX are known, including COX-1 and COX-2, and each encoded by different genes. The conventional symbols for the aforementioned genes are *PTGS1* and *PTGS2*, respectively. Finally, it has been found that COX-3 is a critical splice variant of COX-1 and predominates in the brain as well as the spinal cord (47).

It is thought that COX-1 is expressed constitutively and acts as a ‘housekeeping’ enzyme. On the other hand, COX-2 is believed to be either inducible or constitutive, depending on the tissue involved. COX-2 is associated with inflammation, and there are a number of cytokines and inflammatory mediators present in various inflammatory cells that can trigger its induction. In acute and chronic inflammatory states, the induction of COX-2 is an important pathway for the synthesis of prostanoids (figure 1.4). These prostanoid molecules play a key role in the pathology of many inflammatory conditions, including rheumatoid arthritis, cancer, respiratory disorders, and Alzheimer's disease.

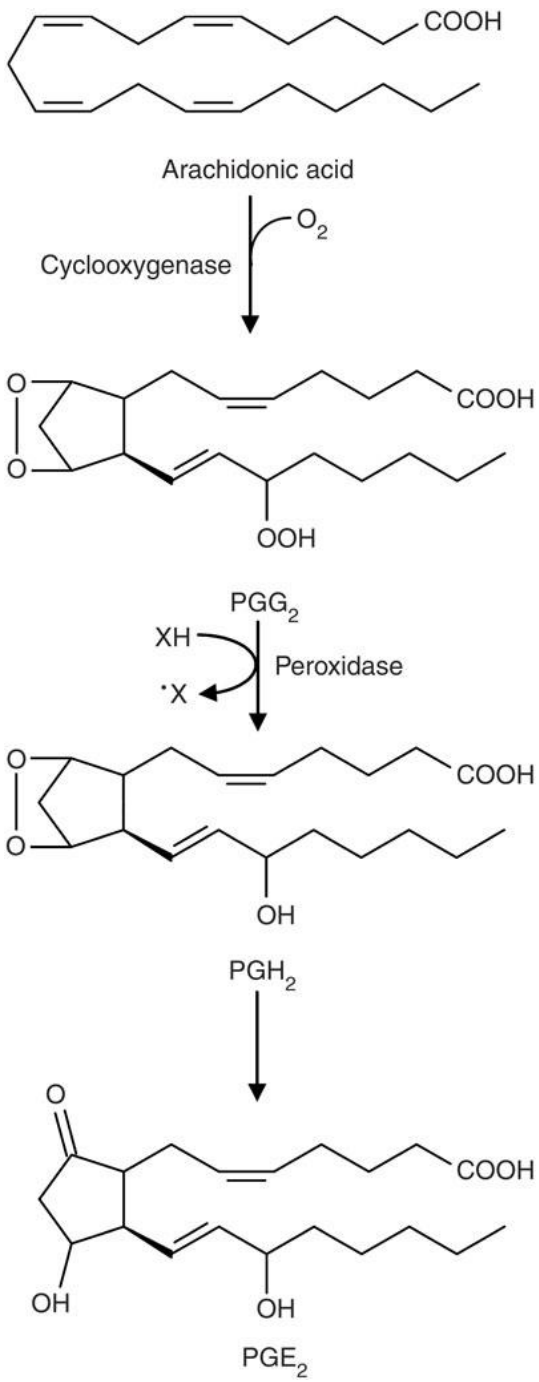

Figure 1.4 COX metabolites of arachidonic acid include prostaglandins, prostacyclin and thromboxanes. The COX enzyme acts as a catalyst for the formation of PGG_2 and PGH_2. PGH_2 can then form various bioactive products, including $PGF_{2\alpha}$, PGE_2, and PGI_2 (prostacyclin), in processes that sometimes involve enzymes and sometime occur spontaneously. Metabolites of PGH_2 include thromboxane A2 and B2 (46).

COX enzymes are membrane-bound proteins, which are located in the endoplasmic reticulum (ER). The three-dimensional structure of ovine COX-1 was first determined in 1994 followed by x-ray crystallographic analyses of human and murine COX-2. The COX-1 and COX-2 isoforms have considerable sequence homology (approximately 60%) and contain three main domains. These domains include a membrane binding domain (MBD), *N*-terminal epidermal growth factor (EGF)-like domain, and a large *C*-terminal globular catalytic domain. The large *C*-terminal globular catalytic domain contains the COX active site that can accommodate the substrate or the inhibitors as well as the peroxidase that has the heme cofactor.

The structures of COX-1 and COX-2 are shown in figure 1.5. Exchanging a valine at position 523, present in COX-2, for an isoleucine (Ile) residue as in COX-1, alters substrate specificity. This modification makes it possible to access an additional side pocket for COX-2. The swapping of Ile-434 for a valine in COX-2 allows the proximate residue phenylalanine-518 (Phe-518) to move away, resulting in further access to the side cavity. There is an arginine within the side pocket of COX-2 compared to a histidine-513 (His-513) in COX-1. The arginine can interact with polar moieties. These differences between the COX active sites are essential in their inhibitor selectivity (figure 1.6) (48).

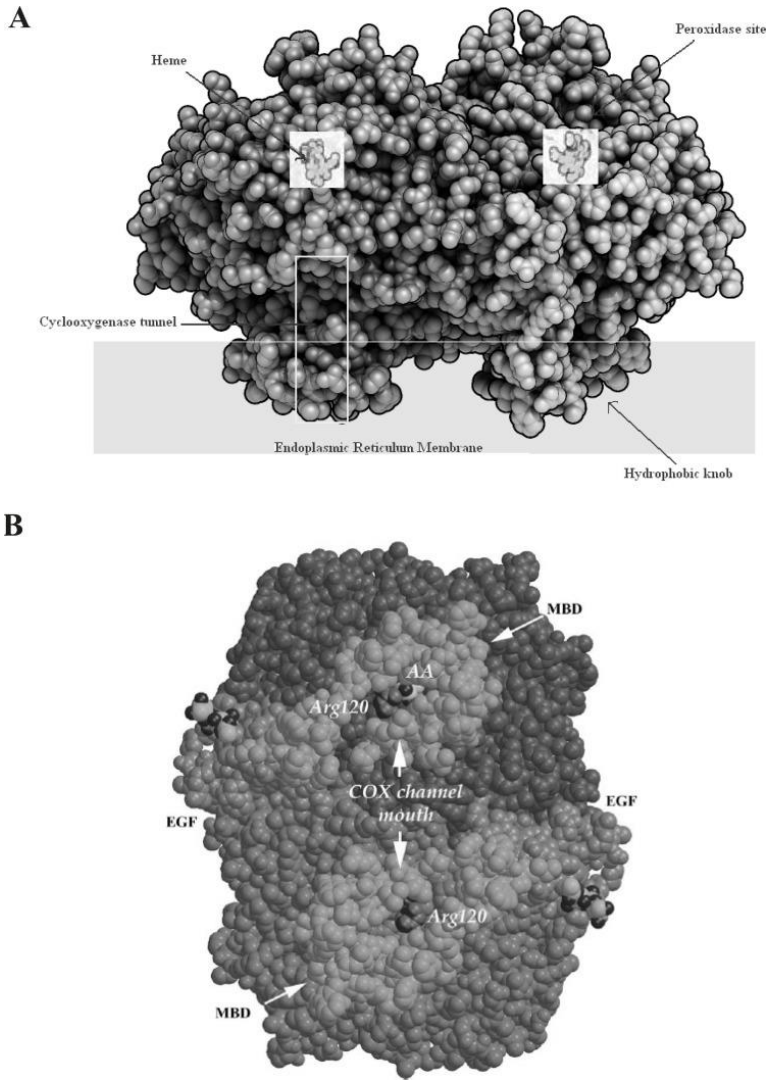

Figure 1.4 COX-1 and COX-2

A) Space-filling model of COX-2 and a simplified diagram showing sections of the enzyme. B) Space-filling model of the COX-1 dimer as seen from the plane of a membrane. (49).

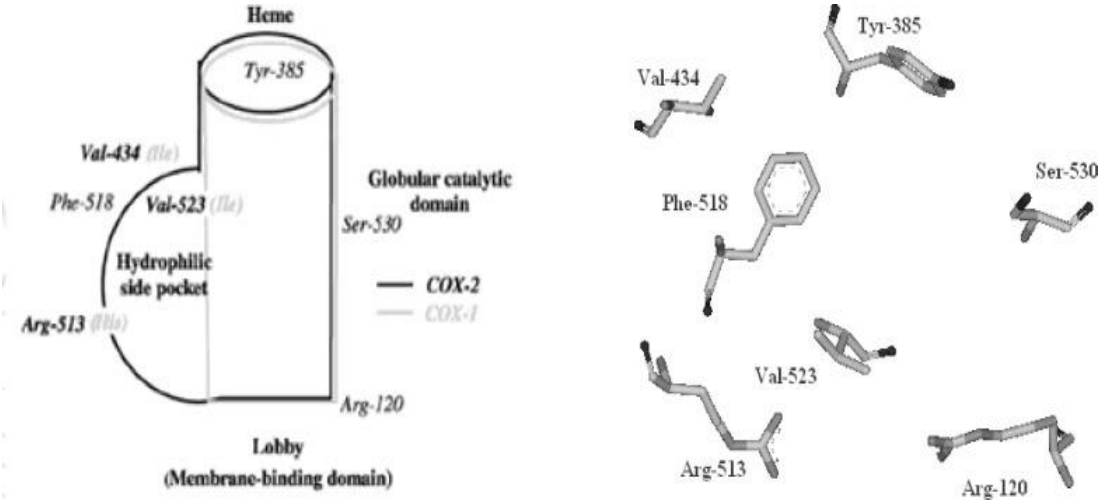

Figure 1.5 COX-2 active site

The COX-2 active site alongside its diagrammatic representation as drawn by Zarghi and Arfaei (49).

Studies indicate that there is an elevation of the amounts of COX-2 in premalignant as well as malignant tissues. The increased transcription and enhanced mRNA stability are the main reasons of overexpression of COX-2 (50, 51). The activation of PKC, as well as mitogen-activated protein kinases (MAPKs) are known to up-regulate COX-2. The additional factors that can effectively modulate the transcription of COX-2 in different types of cells as shown in figure 1.7 include nuclear factor interleukin-6 (NF-IL6), activator protein 1 (AP-1), nuclear factor of activated T-cells (NFAT), nuclear factor-kappaB (NF-kB), and polyomavirus enhancer activator 3 (PEA3).

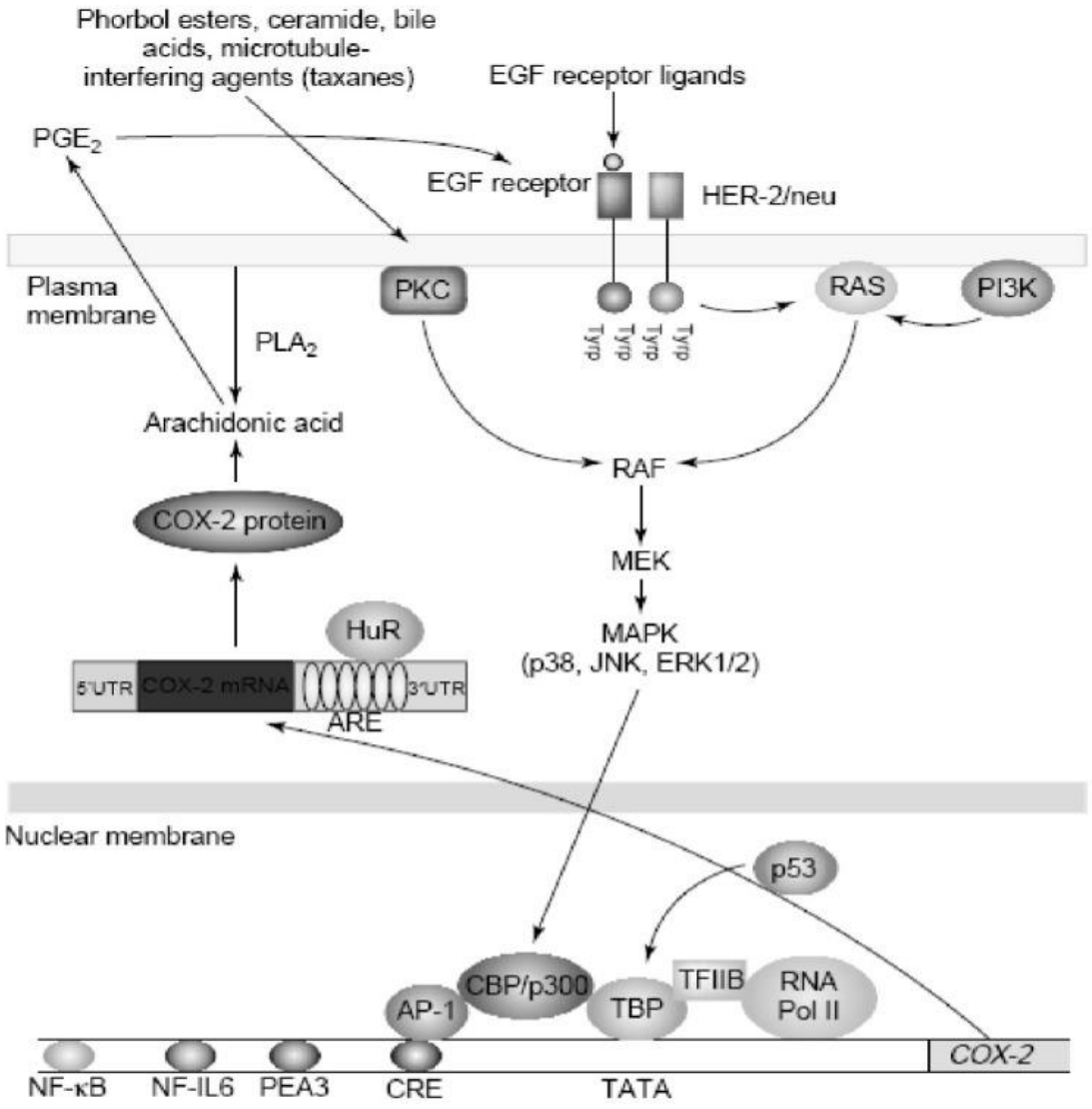

Figure 1.6 Cyclooxygenase 2 (COX-2) signal pathway in cancer

Activation of either RAS signaling or protein kinase C (PKC) facilitates the activities of mitogen-activated protein kinase (MAPK). Upon activation, MAPK stimulates the transcription of COX-2. The induction of COX-2 is mediated by numerous transcription factors that include including activator protein 1 (AP-1) and nuclear factor kB (NF-kB). Conversely, wild-type p53 inhibits transcription of COX-2 (52).

1.5 Prostaglandins

Prostaglandins are bioactive compounds that are made of lipids, containing hormone-like effects in the bodies of animals. Four major categories of prostaglandins have been identified and include prostaglandin (PG) E2 (PGE_2), prostacyclin (PGI_2), prostaglandin D2 (2) and prostaglandin F2α ($PGF_{2\alpha}$). Almost all types of cells produce these compounds. However, every type of cell generates only one or two dominant products. It is believed that prostaglandins are autocrine and paracrine lipid mediators whose main function in the body is to maintain local homeostasis. In case of an inflammatory response, the concentration and profile of prostaglandin production varies drastically. Prostaglandin production increases rapidly during an acute inflammation, before the recruitment of leukocytes and the infiltration of immune cells. These inflammatory cells are normally low in uninflamed tissues. Both COX-1 and COX-2 are known for their contribution toward the generation of autoregulatory and homeostatic prostanoids. However, COX-2, which is induced by inflammatory stimuli, growth factors, and hormones, is believed to be the most critical source of prostanoids in inflammation as well as in proliferative diseases (53).

The prostanoid receptor is a seven transmembrane spanning G protein-coupled receptor (GPCR) which is rhodopsin-like. The prostanoid receptor subfamily consists of eight members, including EP1 (E prostanoid receptor 1), EP2, EP3, and EP4 subtypes of the PGE receptor, PGD receptor (DP1), PGF receptor (FP), PGI receptor (IP), and TX receptor (TP). Prostanoid receptors couple to a variety of signaling pathways within cells and regulate the results of receptor activation on the activities of the cell. EP2, EP4, IP, and DP1 receptors are responsible for the activation of adenylyl cyclase via GPCRs, resulting in increasing the cyclic of adenosine monophosphate (cAMP) within the cells. EP1 and FP are responsible for the stimulation of phosphatidylinositol metabolism via Gq, leading to the production of inositol trisphosphate as a result of the mobilization of free calcium within the individual cells (54). In addition to signaling via Gq, the small G-protein Rho is also coupled to the FP receptor via a Gq-independent mechanism. See Table 1.1 below.

Table I Signal Transduction of Prostanoid Receptors

Class	Subtype	G-protein coupled	Second Messenger
TxA_2	TP_α, TP_β	G_q, G_{13}, G_h, $G_s(TP_\alpha)$, $G_i(TP_\beta)$	$\uparrow IP_3/DAG/Ca^{2+}$, RhoGEF $\uparrow\downarrow$cAMP
PGD_2	DP	G_s	$\uparrow$cAMP
	CRTH2	G_i	$\downarrow$cAMP, $\uparrow Ca^{2+}$
PGE_2	EP1	G_q	$\uparrow IP_3/DAG/Ca^{2+}$
	EP2	G_s	$\uparrow$cAMP
	EP3	G_i, G_{12}	$\downarrow$cAMP, $\uparrow Ca^{2+}$, Rho
	EP4	G_s	$\uparrow$cAMP
PGI_2	IP-IP	G_s	$\uparrow$cAMP
	IP- TP_α	G_s	$\uparrow$cAMP
$PGF_{2\alpha}$	FP_A, FP_B	G_q	$\uparrow IP_3/DAG/Ca^{2+}$, Rho

Prostaglandins play a significant role in the generation of the inflammatory response, and almost all animal species produce PGE_2 which involved in variety biological activities. PGE_2 takes part in a variety of biological activities under physiological conditions. Such functions include the control of immune responses, fertility, blood pressure, and gastrointestinal integrity. Unbalanced synthesis of PGE_2 or its degradation will result in a wide range of pathological conditions (55). PGE_2 play a key role in redness and edema. The main cause of redness and edema is the increased blood flow into the inflamed tissue (56). PGE_2 are also related to pain development through the effects on peripheral sensory neurons as well as on the central sites, which are located within the brain and the spinal cord (56). PGH_2 can be used as a substrate to synthesize PGE_2 by the enzymes include cPGES or mPGES-1 and mPGES-2 (57). The expression of cPGES is dominant in the cytosol of numerous body cells. Additionally, the cPGES requires glutathione (GSH), which is a necessary cofactor to enable it to produce PGE_2 (58). Mice with *cPGES* gene deletions cannot survive because of perinatal lethality (59). The mice that are deficient in mPGES-1 demonstrate the role of this enzyme in PGE_2 generation which is very important in the stimulation of inflammation.

In a model of collagen-induced arthritis (CIA), compared with wild-type mice *mPGES-1* knockout mice showed less incidence and reduced intensity of disorders (60). It was also found that macrophages migration induced by the peritoneal injection of thioglycollate was significantly reduced in *mPGES-1*-null mice compared to wild-type control (61). In conclusion, these reports indicate that deletion or inhibition *mPGES-1* can inhibit the inflammatory response.

mPGES-1-derived PGE_2 also plays a key role in inflammation during atherosclerosis. Atherogenesis in fat-fed hyperlipidemia mice model can be blocked by deleting *mPGES-1* (62). PGE_2 can bind to different EP receptors thereby producing both pro- and anti-inflammatory effects in a variety of cells, which include macrophages, dendritic cells, as well as T and B lymphocytes. PGE_2 controls the expression profile of cytokines in dendritic cells (DCs). Additionally, studies indicate that prostaglandin signaling promotes immune inflammation through Th1 cells (63), and PGE_2-EP4 signaling in DCs and T cells promote Th1 and IL-23-dependent Th17 differentiation (64). PGE_2 was also found to inhibit the differentiation of Th1, B cell functions, as well as allergic responses. Furthermore, PGE_2 has an anti-inflammatory effect on innate immune cells like neutrophils, NK cells, and monocytes (65).

PGD_2 is found in both the central nervous system (CNS) and peripheral tissues where it results in inflammation in these tissues (66). It was reported that PGD_2 also regulates sleep and pain perception (67). Mast cells, which are found in peripheral tissues, account for the production of most of PGD_2. Hematopoietic and lipocalin-type PGD synthases (H-PGDS and L-PGDS, respectively) have also been identified. PGD_2 induces IgE-mediated Type I acute allergic reactions in activated mast cells (68). PGD_2 levels detected in the bronchoalveolar lavage fluid can reach biologically active amounts within minutes which is at least 150-fold higher than pre-allergen levels in asthmatics (69). PGD_2 has been found to be produced by a variety of immune cells, which include antigen-presenting dendritic cells and Th2 cells. This is an indication that PGD_2 play a critical part in the establishment of antigen-specific immune system reactions (70). Bronchoconstriction and airway eosinophil infiltration in allergic asthma can be induced by PGD_2 challenge (71). Additionally, allergic response airway hyper-reactivity increased in a mouse model with increased PGD_2 generated by over-expressed lipocalin-PGD synthase (72).

Both DP1 and DP2/CRTH2 receptors regulate the pro-inflammatory effects of PGD_2. Furthermore, PGD_2 can activate multiple signaling pathways with varying effects by binding to both receptors with similar high affinity, which depend on how different types of cells express DP1 or DP2/CRTH2 receptors. The DP1 receptor, which is expressed on dendritic cells, plays an important role in initiating an adaptive immune response to foreign antigens. PGD_2 activation of the DP1 receptor following ovalbumin (OVA) challenge inhibits the migration of dendritic cells from the lung to lymph nodes, which leads to decreased antigen-specific T cells proliferation (73). PGD_2 produced by H-PGDS from inflammatory cells respond to the permeation of the vasculature in the context of inflamed intima (74). Furthermore, L-PGDS can be initiated by laminar sheer stress inside the vascular endothelial cells (75). PGD_2 was also reported to downregulate the expression of pro-inflammatory genes, such as iNOS and plasminogen activator inhibitor (76). Meanwhile, it was found that L-PGDS deficiency promotes atherogenesis (77).

PGI_2 has broad biological effect including vasodilation, inhibition of platelet aggregation, leukocyte adhesion and VSMC proliferation. The other critical observation is that $PGF_{2\alpha}$ binds Gq protein to increase the intracellular free calcium level.

In summary, prostaglandins play a critical role in the pathogenesis of many diseases and processes including inflammation, fever, reproduction, and Alzheimer's disease. A variety of

analytical methods have been developed and used to qualify and quantitate prostanoids. However, all these methods have certain limitations. Our laboratory has developed a method using UHPLC/MS/MS to quantitate PGE_2 and PGD_2 in biological fluids and tissues. UHPLC/MS/MS has distinct advantages when compared to the existing methods. Accordingly, it will contribute to research on the functions of prostaglandins in different diseases as well as in translational and clinical studies.

2. AUTOTAXIN PRODUCTION OF LYSOPHOSPHATIDIC ACID MEDIATES ALLERGIC ASTHMATIC INFLAMMATION

(Previously published as Park GY, Li Y and Christman JW (2013)
Autotaxin production of lysophosphatidic acid mediates allergic asthmatic inflammation, Am J Respir Crit Care Med. 2013,188(8):928-40.)

2.1 Introduction

Asthma is a chronic respiratory condition involving airways in the lungs. One of the major symptoms of the disease is difficulty in breathing. Asthma is brought about by a variety of cells, including lymphocytes, eosinophils, airway epithelial cells, and macrophages. These cells interact within the microenvironment of the airway and airspace and finally cause breathing difficulty. The airways of a patient suffering from asthma are always inflamed. They become even more swollen and the muscles around them tighten especially in circumstances where the symptoms are triggered. The swelling is known to bring about a temporary narrowing of the airways, which makes it difficult for air to move in and out of the lungs. The pathogenesis of asthma will cause symptoms such as coughing, wheezing, shortness of breath, and chest tightness. The studies indicate the existence of a nexus between genetic factors and an individual's predisposition to asthma. The genetic factors interact with the environment to bring about the condition, and the environmental influences may include timing and dose of allergen and co-exposure to infection (78). The interaction of local airway susceptibility factors and allergen-specific immune polarization have a very important effect on the initiation and subsequent expression of the disease phenotype (see figure 2.1).

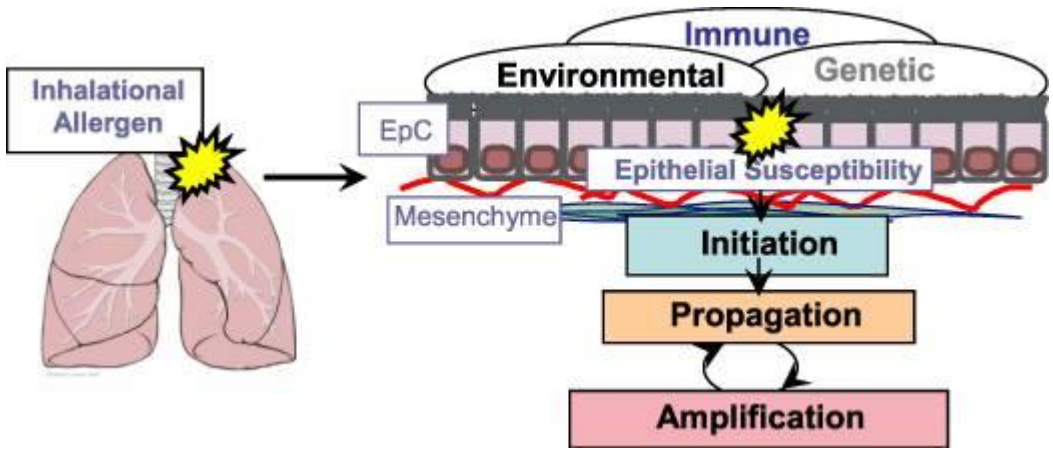

Figure 2.1 Gene environment interactions in asthma (79).

For a long time, fats have been construed as mere energy sources and a component of cell membranes. However, recent studies indicate that fatty acids and their derivative compounds are involved in an array of biological activities. For instance, bioactive lipids, spanning from simple saturated fatty acids to complex molecules, play an important role in homeostasis, regulation of inflammatory processes, and cell proliferation, among other functions.

Eicosanoids such as lysophospholipids (and their derivatives) are lipid mediators formed from arachidonic acid. There are several species including sphingosine-1-phosphate (S1P), lysophosphatidic acid (LPA), and endocannabinoids which belong to class 1 lipid mediators. LPA binds to receptors which take part in various biological processes, including brain development, embryo implantation, hair growth, and inflammation. LPA is a bioactive lipid mediator which is produced by the enzymatic activity of extracellular autotoxin (ATX) and might be involved in asthma pathogenesis. Additionally, LPA enhances the production of cytokine and chemotaxis in lymphocytes (80,81), which can lead to contractility, proliferation of airway smooth muscle cells, and changing inflammatory signaling in the epithelial cells of the bronchus (82,83). Together, these results indicate that LPA is involved in the molecular pathogenesis of asthma.

Our hypothesis is that the ATX-LPA axis plays a critical role in the pathogenesis of asthma and makes it an ideal target for an effective anti-asthma therapy. To test our hypothesis, a human model (an IRB-approved protocol for sub-segmental broncho-provacation with allergen, SBP-AG, to induce localized allergic inflammation in human volunteers), and a mouse model (mice subjected to a triple allergen) were used to explore the role of the ATX-LPA axis on the pathogenesis of asthma. To further explore the function of LPA in asthma, we used a transgenic mouse with ATX over-expression (ATX-Tg) to study the effect of triple allergen (house dust mite, ragweed and aspergillus allergen; DRA) challenge compared to that of wild type mice. LPA receptor 2 knock-out mice (LPA2-/-) were also used to provide further evidence to support our hypothesis.

2. 2 Material and Methods

2.2.1 Protocol for Sub-Segmental Bronchoprovocation with Allergen (SBP-AG)

Approval of this protocol was obtained from the Institutional Review Board of the University of Illinois (Chicago, IL). The U.S. Food and Drug Administration (FDA) provided an IND for bronchoscopic administration of allergens to volunteers. For the University of Wisconsin cohort, the protocol was approved by the University of Wisconsin Health Sciences Human Subjects Committee. All the participating subjects were asked to give their written consent before participating in the activity. The signing of the consent forms is an ethical obligation that is required this type of scientific inquiry. A summary of our clinical protocol is shown in figure 2.2.1.

Next, human subject recruits were screened for inclusion and exclusion criteria. This process entailed skin prick testing to dust mite, short ragweed, and cockroach allergens, and spirometry with bronchodilator reversibility and/or methacholine challenge. After enrolling in the study, subjects underwent bronchoscopy and bronchoalveolar lavage (BAL). The procedure began by the introduction of a four 40 ml aliquots of sterile saline, which was gently removed after each instillation with hand suction. The instillation was done with the purpose of recovering the lavage fluid (pre-challenge site). Sub-segmental bronchoprovocation with allergen **(**SBP-AG) was performed in a different sub-segment. The initial dosage in the process was 10-fold greater compared to the previously defined skin endpoint titration (SET) dose of allergen. After 4 minutes, 10 ml of saline was used to flush the segment before removing the bronchoscope. After 10 minutes, the same segment was subjected to a second challenge with a defined SET dose. 5 mL of a 100 BAU/mL or 1:2000 wt/vol concentration of allergen was used as the maximum challenge dose in the experiments. After 4 minutes, 10 ml of saline was used to flush the segment before removing the bronchoscope.

At the time point of 48 hours from initiating bronchoscopy, we collected BALs from three different sites, including the challenged segment of the challenged lobe (**Experimental site**), the unlavaged segment contralateral to the challenge site (**Contralateral site**) and the unchallenged segment adjacent to the challenged lobe (**Adjacent site**).

Table II Summary of clinical protocol for bronchoprovocation with allergen used for this investigation.

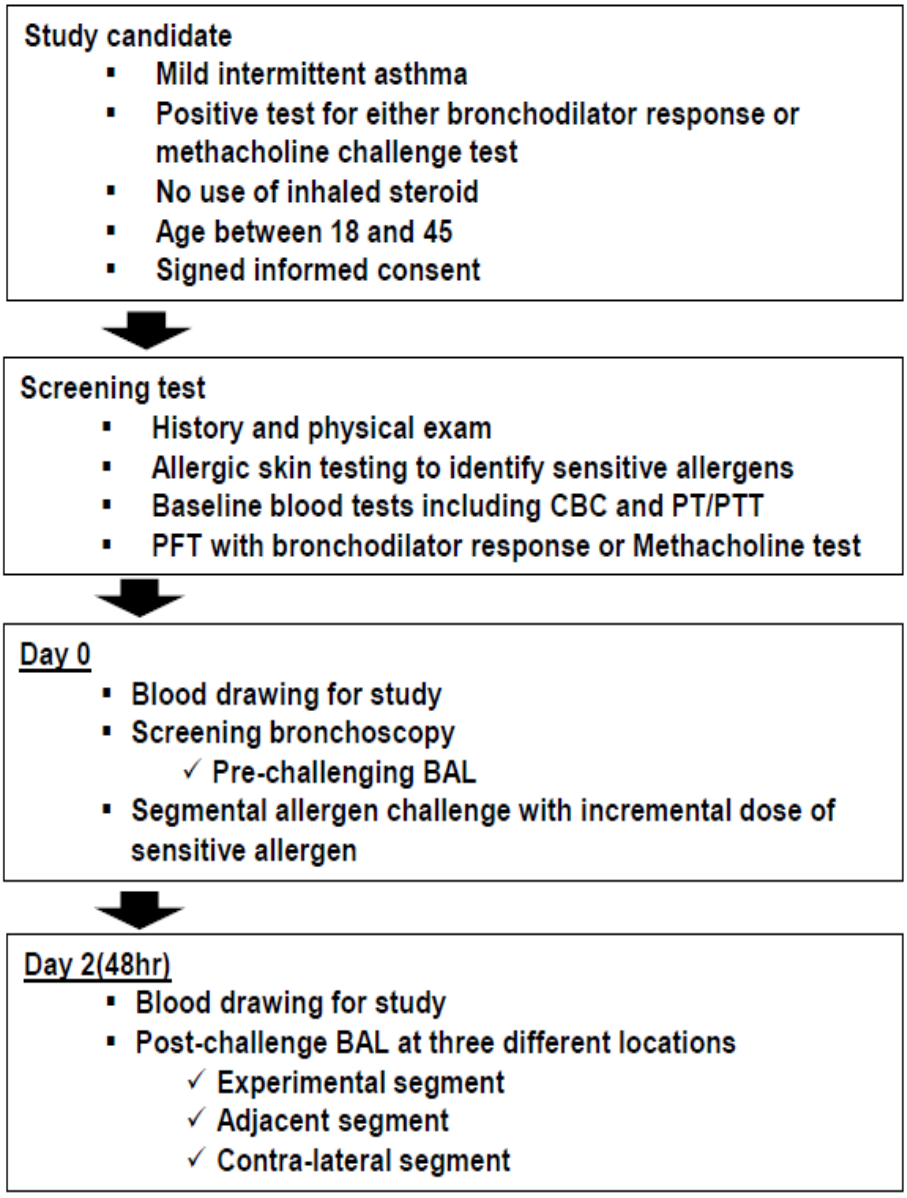

2.2.2 Mice

The mice used in the experiment were bred and housed in a pathogen-free barrier facility, which is under the management of the University of Illinois at Chicago, Biologic Resources Laboratory. The protocols used in all experiments were approved by the Institutional Animal Care and Use Committee of the University of Illinois (Chicago, IL) (IACUC approval numbers-14-122). The experiments used adult male mice which were 8- to 10-wk-old with an average weight of 20–25 g. The UIC animal facility successfully bred the breeding pairs of ATX-Tg and ATX heterozygous (ATX+/-) mice on the FVB background which were provided by Dr. Susan Smyth (University of Kentucky). Meanwhile, Dr. Chun (The Scripps Research Institute, La Jolla, CA) provided the LPA2-/- mice.

2.2.3 Reagents

Dr. Glenn D. Prestwich from University of Utah, Salt Lake City, Utah provided 4-(decanoylamino)benzyl]phosphonic acid, which is an ATX inhibitor GWJ-23 (figure 2.2). GWJ-23 was dissolved in 1% DMSO and injected into the intra peritoneum at a dose of 10 mg/kg. Meanwhile, the control groups were administered at the equivalent dose of DMSO carrier only.

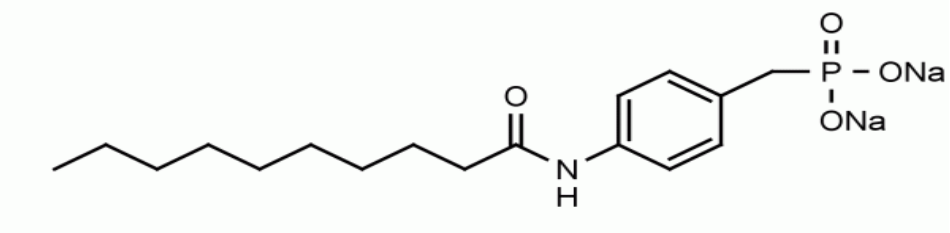

Figure 2.2 Structure of 4-(decanoylamino) benzyl]phosphonic acid (GWJ-23)

2.2.4 DRA Triple Allergen Asthma Model

The triple allergen (DRA)-induced allergic mice asthma model of Goplen *et al*. (84) was used with minor modifications in order to repeat the pathophysiologic features of SBP-AG of human asthmatics. On the first and fifth days, we sensitized the mice with the DRA antigens and gave the intranasal challenge on days 12, 13 and 14. On day 15, the sensitized mice were sacrificed once we collected their bronchiole alveolar lavage (BAL) fluids for analyzing cellularity and pro-inflammatory cytokines. Meanwhile, lung tissues were collected to assess allergic inflammation and cytokine production. Triple antigen (DRA) challenge can significantly stimulate eosinophils and macrophages infiltrating into alveolar spaces, aggravate the peribronchial and perivascular inflammation and increase Th2 cytokines production.

2.2.5 Lung Tissue Preparation

We used pressurized low melting agarose to prepare mouse lung tissue after sacrifice. Briefly, pressurized low melting agarose was prepared by boiling 0.5% w/v low melting point agarose at 60°C and then keeping it at 42°C in a water bath. After tracheostomy, we infuse the 0.5% melted agarose through the tracheostomy tube from a height of 28 cm H_2O so that agarose could be pressurized equally over the lung fields. Thereafter, the tracheostomy tube was tied while the lung tissue was placed into a formalin container which was refrigerated overnight in order to facilitate solidification and fixation.

2.2.6 Morphometric Analysis and Digital Pathology

The Genie System (Aperio Technologies, Vista, CA, US), specially designed to automatically classify tissue in whole slide images, was used in the study. In this system, users outline tissue regions of interest to be analyzed and quantified. These outlined regions are submitted to the server, and all these data can be used to build a data pool and develop an image processing algorithm that can effectively differentiate between the defined tissue classes. Actually a "black box" to analyze unknown images, the user does not need to know the exact algorithm applied by the Genie System to successfully and reproducibly differentiate the chosen tissue classes. For this study, we defined several training regions as 4 groups: inflammation, bronchus, alveoli, and a blank. Overall training accuracy for all the regions was 96.18%.

In order to quantitate the Periodic acid–Schiff (PAS) staining, we use a Vectra 1.0 system

(PerkinElmer, Waltham, MA, USA) to image the entire lung field. We manually selected all microscopic fields containing bronchus. Vectra version 2.0 system was applied to identify the bronchus tissue class and segment nuclei. A manually set threshold was applied to define PAS staining for each "nucleus" as positive or negative. The same threshold setting was applied on the entire lung field. The final measurement was the percentage of PAS positive nuclei in the bronchial epithelial cells. The pathologist doing the analysis was blinded by the treatment group information.

2.2.7 Western Blot

We used the same amounts of BAL fluid drawn from each lung segment of pre-challenged and post-challenged SBP-AG human subjects to do electrophoresis and immunoblotting using lysophospholipase D (autotaxin) polyclonal antibody (10005375, Cayman Chemical). In order to verify the specificity of the autotaxin band, a specific ATX blocking peptide, lysophospholipase D blocking peptide (10007193, Cayman Chemical) was used to pre-absorb the antibody as per the manufacturer's instructions.

2.2.8 Measurement of Cytokines and Total IgE

Cytokine levels in BAL fluids and lung homogenates were analyzed using of multiplexed bead-based Milliplex system (EMD Millipore, Billerica, MA, USA). Total serum IgE levels were analyzed using a mouse IgE kit (eBioscience, San Diego, CA, USA), as per the manufacturer's instructions.

2.2.9 Immunohistochemistry and Immunofluorescent Staining

We used formalin-fixed and paraffin-embedded sections of lung specimens for immunohistochemistry (IHC) and cytospin slides from BAL samples for immunofluorescence (IF). This study applied several primary antibodies including anti-MBP1 (kindly provided by Dr. James J. Lee, Mayo Clinic Arizona, Scottsdale AZ) and anti-ATX (10005375, Cayman Chemical). For IHC, a commercialized kit was used (Daco). A Zeiss LSM 710 confocal microscope (Carl Zeiss, Germany) was used to photograph fluorescent images.

2.2.10 Statistical Analysis

All data were statistically analyzed by the statistician at the UIC Center for Clinical and Translation Science, Design and Analysis Core (DAC). In summary, we examined the normality for all data using the Kolmogorov-Smirnov test and Q-Q plots. For normally distributed data, we

used the paired two-sample t test to compare two group with equal variance or unequal variance assumptions. For data with non-normal distribution, a non-parametric method (signed rank test) was applied to compare two paired samples. All data were analyzed using the SAS statistical package (version 9.2, SAS Institute, Cary. NC).

2.3 Results

2.3.1 ATX Protein Level Increased in BAL Fluid of Asthma Subjects Following Allergen Challenge and in Lung Tissue of Mice Following a Triple Allergen Challenge

Total and differential cells were counted in BAL fluid recovered from the subjects with mild asthma enrolled in the SBP-AG protocol. The data showed that the total cell count, which primarily consists of eosinophils and macrophages, increased ~8-fold in the BAL fluid drawn from the allergen-challenged sub-segment compared with the negative control group. The eosinophil cell count in the adjacent segment only mildly increased and did not increase in the contralateral segment, strongly suggesting that the allergic reaction was confined to the experimental site following with allergen challenge, and that there was minimal spill over to adjacent segments (figure 2.3). We then used Western blot to quantitate the ATX protein level within BAL fluid acquired before and after allergen challenge from three different segments. These data indicated ATX expression significantly increased in the allergen-challenged site compared with the pre-challenged or contra-lateral post challenge sites (figure 2.4). In addition, we found a significantly lower level of ATX in the adjacent sub-segment to the allergen challenged site (figure 2.4).

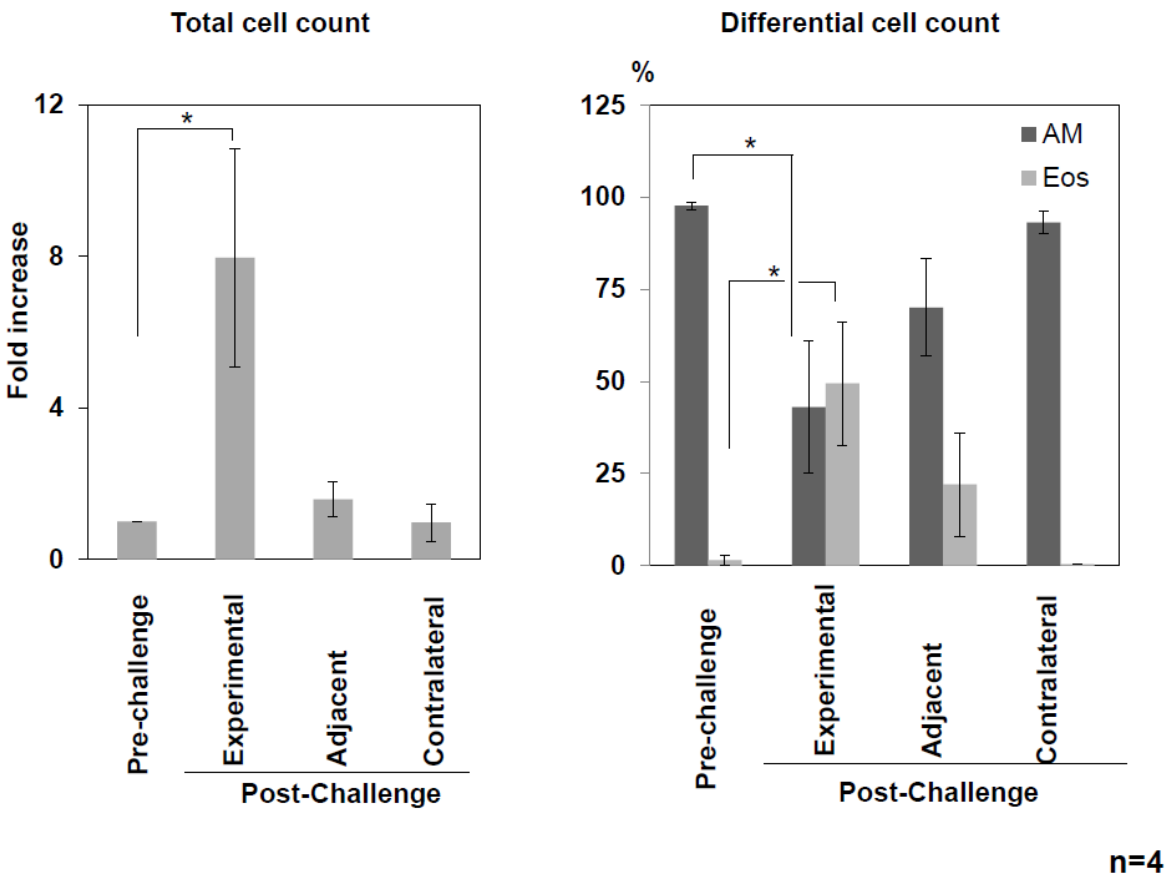

Figure 2.3 Total cell and differential counts of BAL fluid recovered from subjects with mild asthma enrolled in the SBP-AG protocol. The total cell count increased approximately 8-fold in the BAL fluid from the allergen-challenged subsegment and consisted primarily of eosinophils (Eos) and alveolar macrophages (AM). There was only a mild increase in the eosinophil count in the adjacent segment and no increase in the contralateral segment, indicating that the allergic reaction was confined to the experimental site, with minimal spillover to adjacent segments.

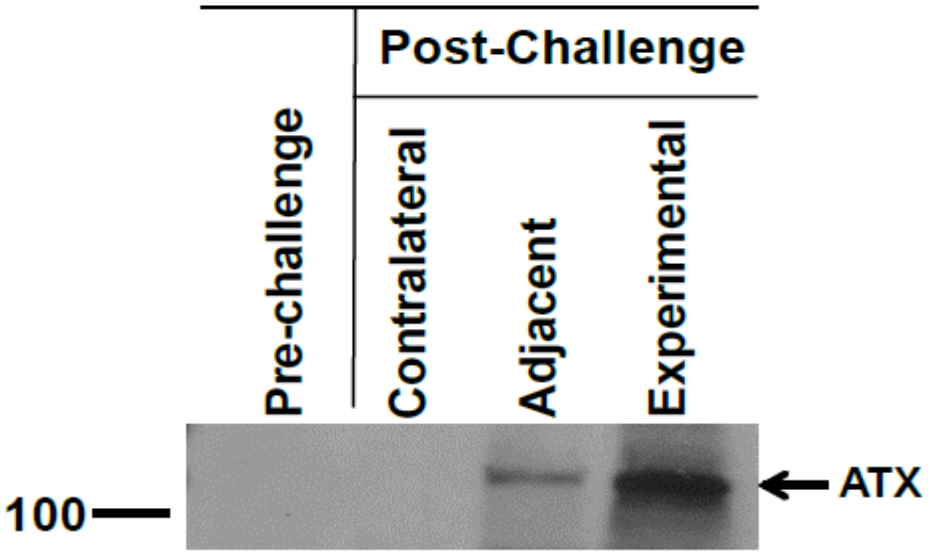

Figure 2.4 Western immunoblot for ATX in BAL fluid samples obtained from human subjects pre- and post-allergen challenge in the SBP-AG protocol.

In order to further confirm our results, we applied an antibody neutralizing peptide in the experiments (figure 2.5). The results showed that neutralizing peptide diminished the bands obtained after the allergen-challenge. These results indicated that the antibody neutralizing peptide specifically bound to the specific ATX band and confirmed that ATX expression upgraded after allergen challenge. In response to allergen challenge, ATX was shifted to a perinuclear localization from the cytoplasm of alveolar macrophages where ATX was located before allergen challenge.

Bone marrow-derived murine macrophages (BMDMs) instead of human alveolar macrophages were used to test weather allergen challenge affect ATX expression because it is very difficult to culture and harvest enough human alveolar macrophages. Western blot was used to quantify the ATX expression level in BMDMs which were treated with IL-4. The results showed that IL-4 can induce ATX expression, and ATX was found to be secreted into the culture medium (figure 2.6).

Mice were subjected to sensitization and challenge with a combination of house dust mite, ragweed and aspergillus allergen (triple allergen DRA), as previously described with minor modifications (84), including two of the major allergens used for human SBP-AG. H & E staining and Diff-Quik staining showed that the triple allergen DRA model induced abundant eosinophilic allergic lung inflammation (figure 2.7). In the model, we found ATX protein expression in lung tissue, especially in terminal bronchial epithelial cells and alveolar macrophages by immunostaining, whereas there was minimal ATX staining in type 1 pneumocytes endothelial cells and eosinophils (figure 2.8 A and B).

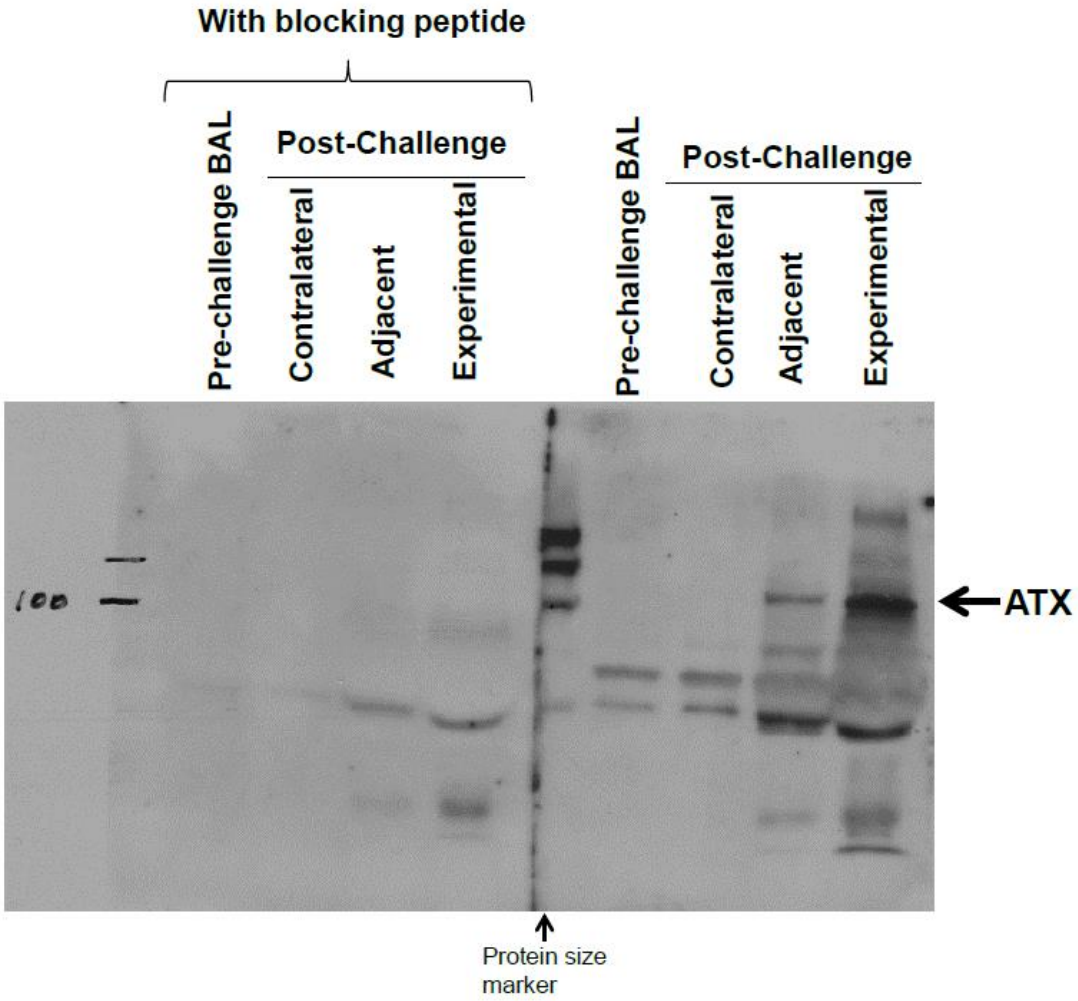

Figure 2.5 Western immunoblot for ATX in BAL fluid samples obtained pre- and post-allergen challenge in the SBP-AG protocol with or without blocking peptide.

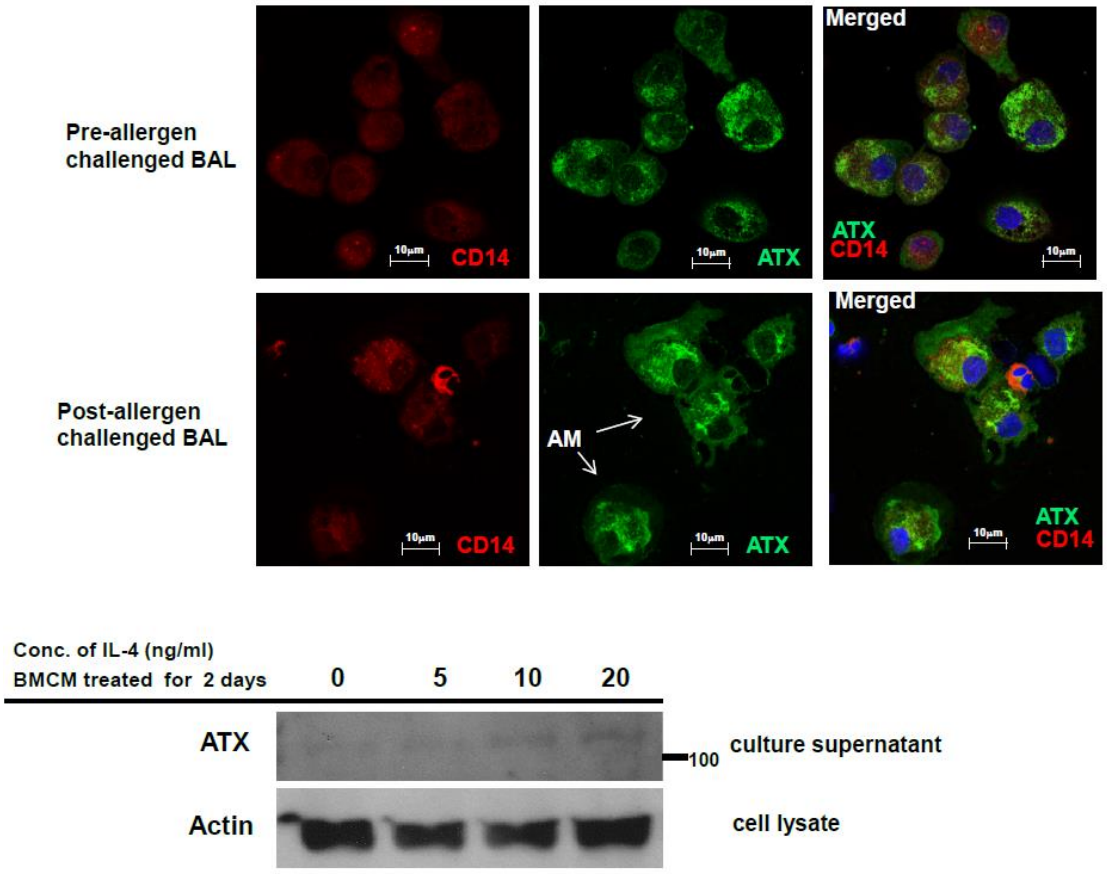

Figure 2.6 Immunofluorescent staining for ATX in BAL cells recovered from an SBP-AG protocol subject pre- and post-allergen challenge. Cytospin slides of BAL cells from a SBP-AG asthma subject were prepared from the allergen-challenged sub-segment before and after allergen challenge and stained by immunofluorescence for CD14 and ATX. Anti-CD14 (red) was used a biomarker for alveolar macrophages. The anti-ATX antibody was conjugated with GFP (green). In the bottom panel, murine bone marrow derived macrophages (BMDM) were treated with various concentrations of IL-4 (0-20 ng/ml) for 48 hours and the culture supernatants were analyzed by Western blotting for ATX; a dose-response relationship was demonstrated for the IL-4 induced secretion of ATX by BMDM.

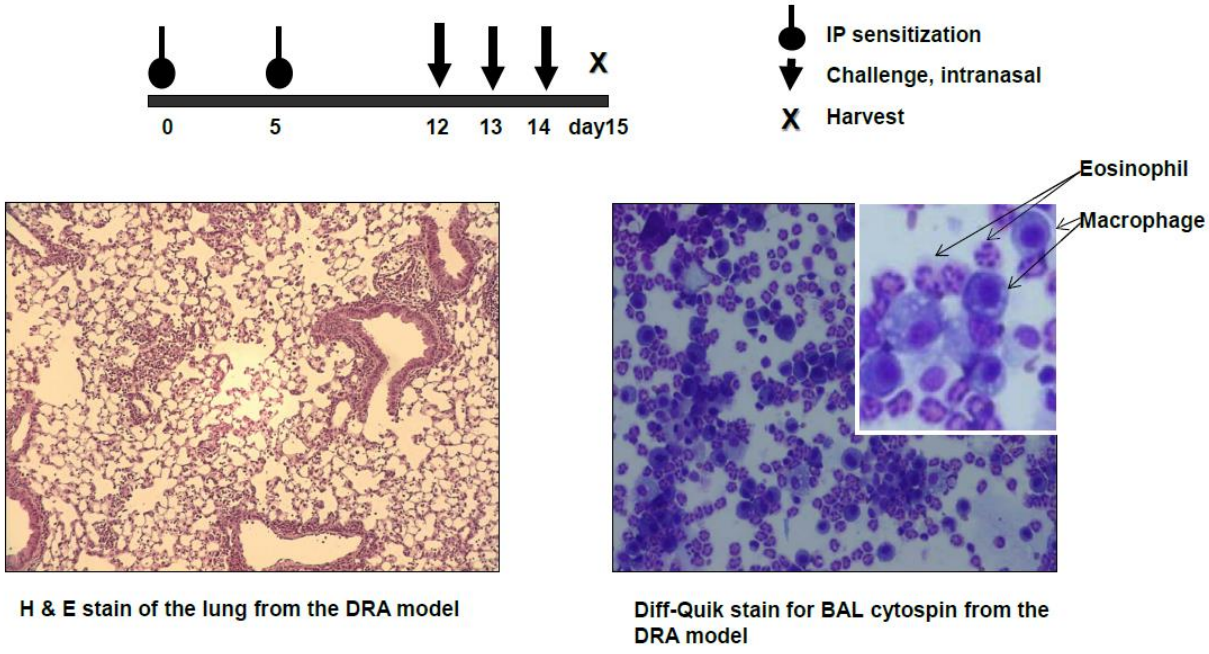

Figure 2.7 Summary of triple antigen (house dust mite, ragweed and aspergillus allergen) DRA-induced acute allergic mouse model. The mice developed an intense peribronchial inflammatory response (left panel), and the BAL cells were predominantly resident macrophages with a pronounced eosinophilic infiltration.

A

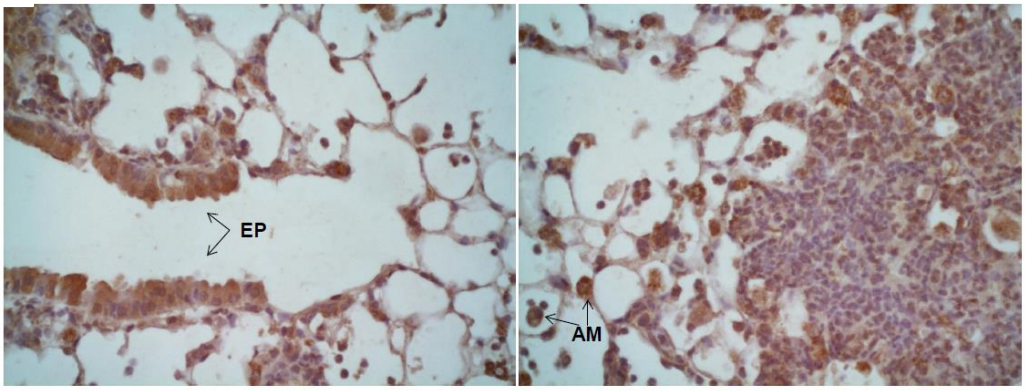

EP: bronchial epithelial cells
AM: alveolar macrophages

B

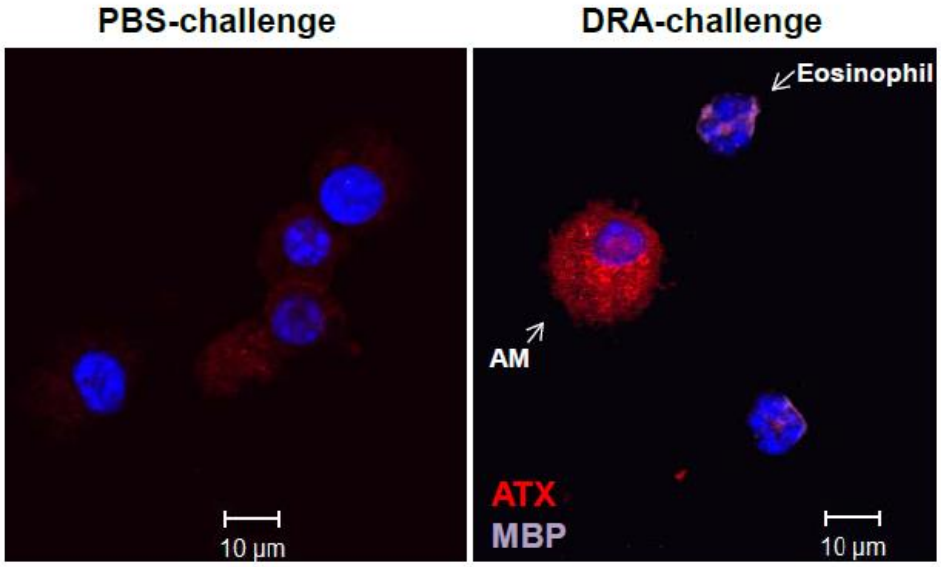

Figure 2.8 Immunohistochemistry for ATX expression in allergic lung inflammation induced by the triple allergen DRA mouse model. A) Autotaxin was highly expressed in distal airway epithelial cells in the distal airway, mostly on the luminal side, as well as by alveolar macrophages; while B) expression by endothelial cells, eosinophils and type1 pneumocytes was significantly lower or minimal.

2.3.2 Over-Expression of ATX Accentuates Allergic Lung Inflammation in Mice

A strong association was observed between allergen challenge and ATX protein expression in BAL fluid from allergen challenged asthmatics subjects. In order to investigate the role of the ATX/LPA axis in the pathophysiology of asthma, we used genetically modified mice to furtherly test our hypothesis. First of all, transgenic mice with ATX (ATX-Tg) over-expression was subjected to triple allergen DRA, the result showed that ATX-Tg mice produced more inflammatory cells, mostly eosinophils, and more protein in lung homogenate in response to triple allergen DRA challenge than wild type mice (figure 2.9), but there was no significant difference in the percentage of differential cell counts between two groups. Total serum IgE level increased equally in both groups of mice following DRA sensitization (figure 2.10). In the DRA model, ATX-Tg mice generated significantly higher levels of IL-4 and IL-5 in lung homogenates and BAL fluid (figure 2.11) compared with wild type mice (WT-FVB), whereas IFN-γ showed no significant difference between the two groups (figure 2.12). We used automated digital morphometric analyses to evaluate the severity of allergic lung inflammation in cross sections of the entire lung field which indicated that there was a greater degree of lung inflammation in ATX-Tg mice than wild type mice (WT-FVB) in response to DRA challenge (figure 2.13). ATX-Tg mice also had a greater degree of goblet cell metaplasia compared to wild type mice (WT-FVB) in response to DRA challenge (figure 2.14).

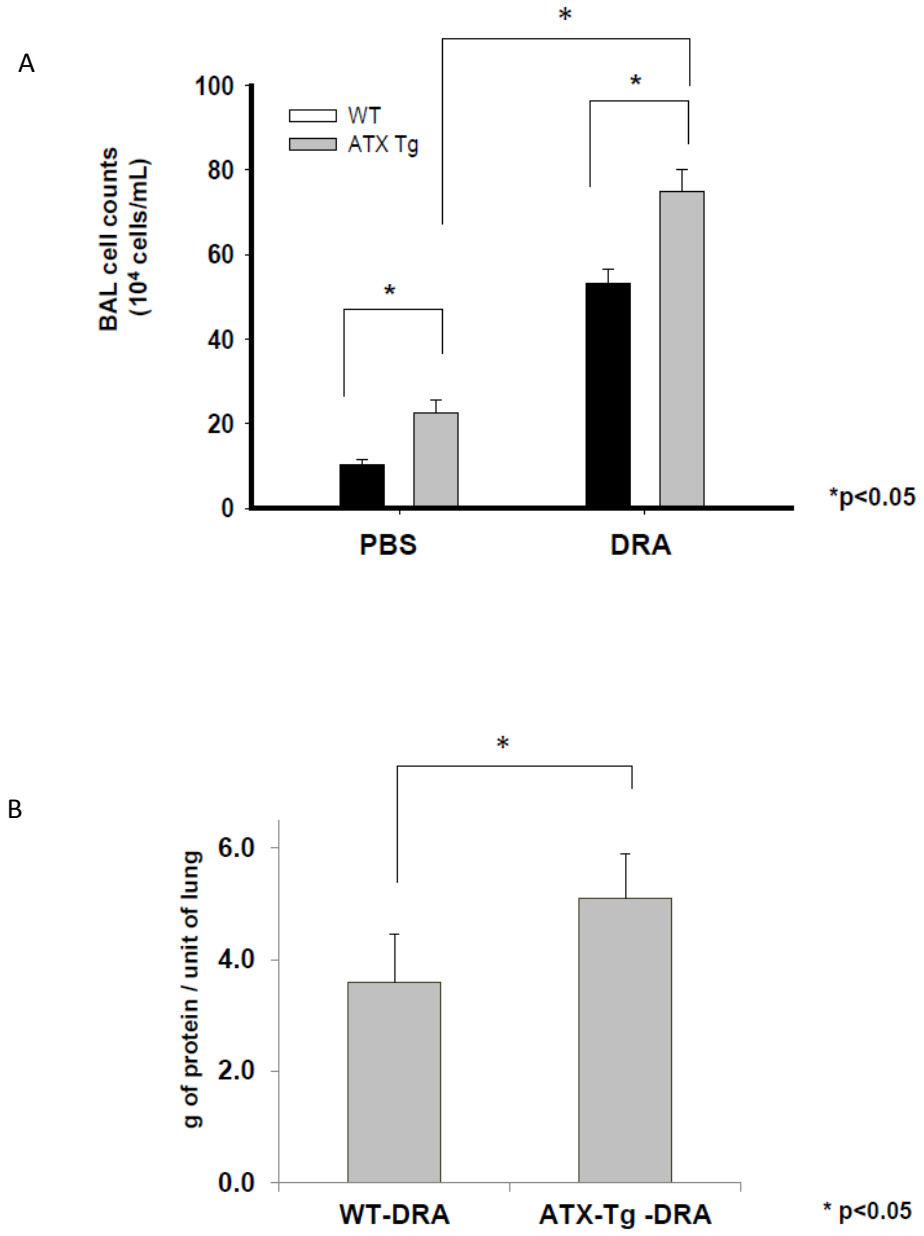

Figure 2.9 A) Total cell counts in BAL fluid of ATX-overexpressing transgenic mice. ATX-Tg mice had more BAL cells before and following allergen challenge, compared with WT mice of the same background. B) Concentration of total protein of lung homogenates in wild type vs. ATX-Tg mice as induced by DRA triple allergen protocol. The protein concentration of lung homogenates of ATX-Tg was higher than that of wild type mice, following DRA allergen challenge.

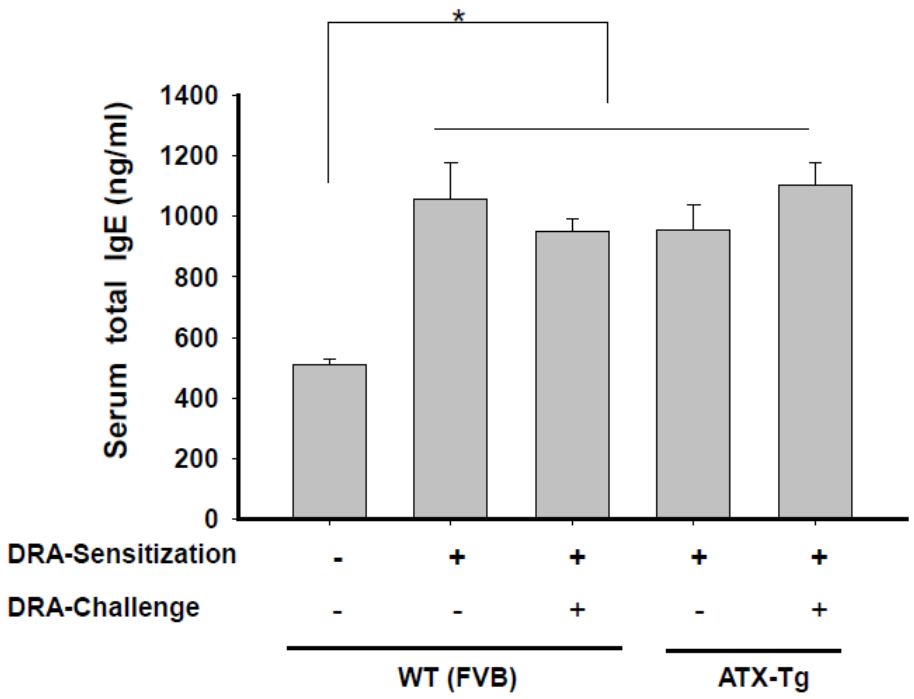

Figure 2.10 Total serum IgE concentrations in wild type vs. ATX-Tg mice as induced by the DRA triple allergen model. Total serum IgE levels were measured by ELISA.

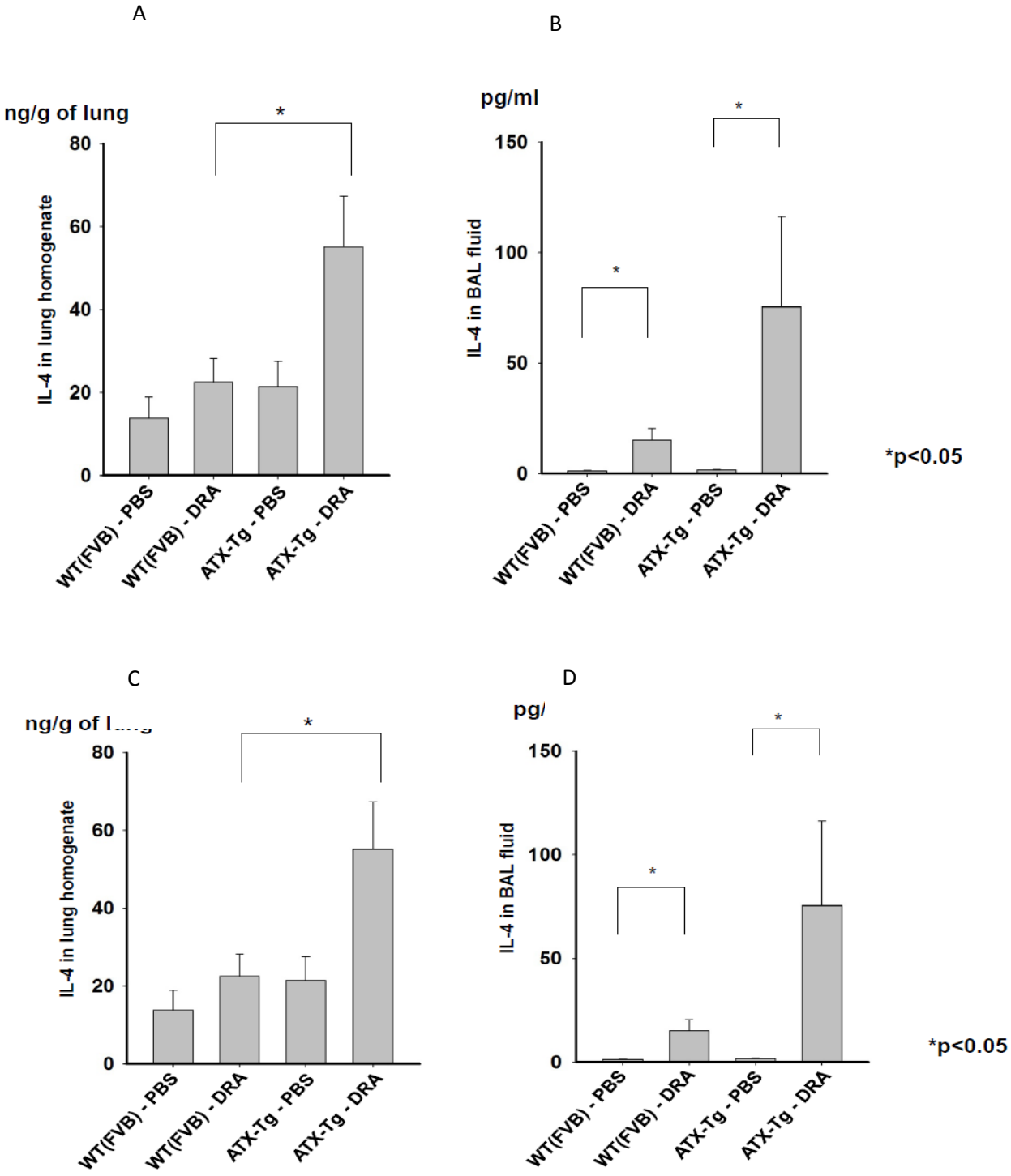

Figure 2.11 Concentration of IL-4 in lung homogenates (A) and BAL fluids (B) of ATX-Tg vs. and wild type (WT-FVB) mice induced by the DRA triple allergen model. Concentration of IL-5 in lung homogenates (C) and BAL fluids (D) of ATX-Tg and wild type (WT-FVB) mice induced by the DRA triple allergen model. $n \geq 5$

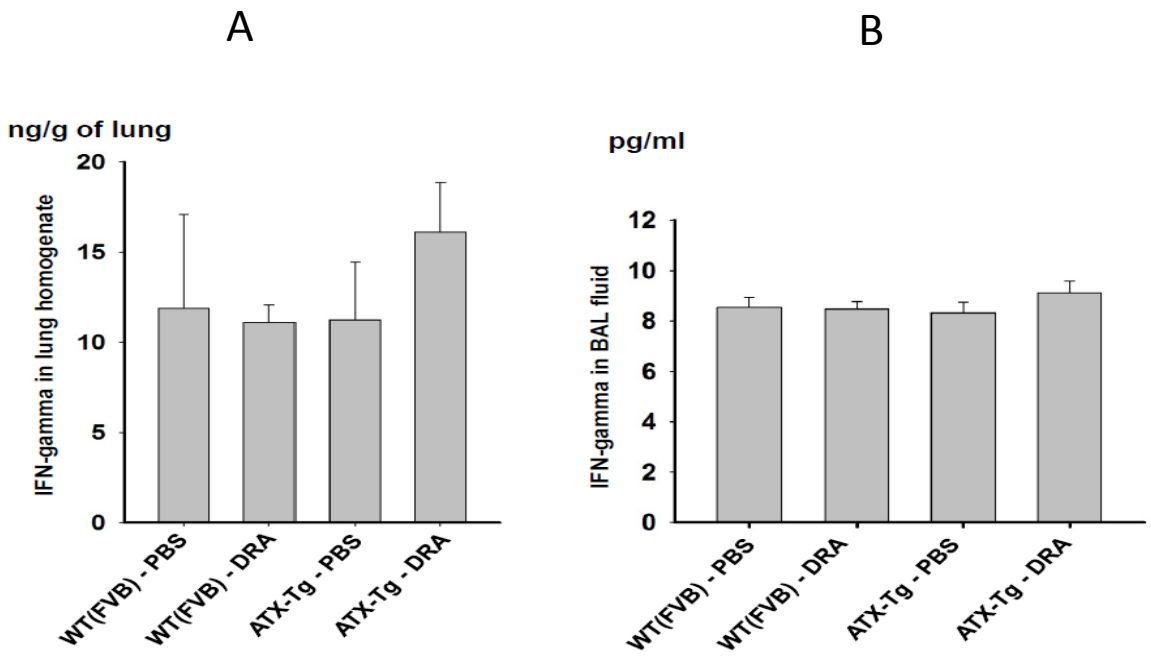

Figure 2.12 Concentration of IFN-γ in lung homogenates (A) and BAL fluids (B) of ATX-Tg vs. and wild type (WT-FVB) mice induced by the DRA triple allergen model.

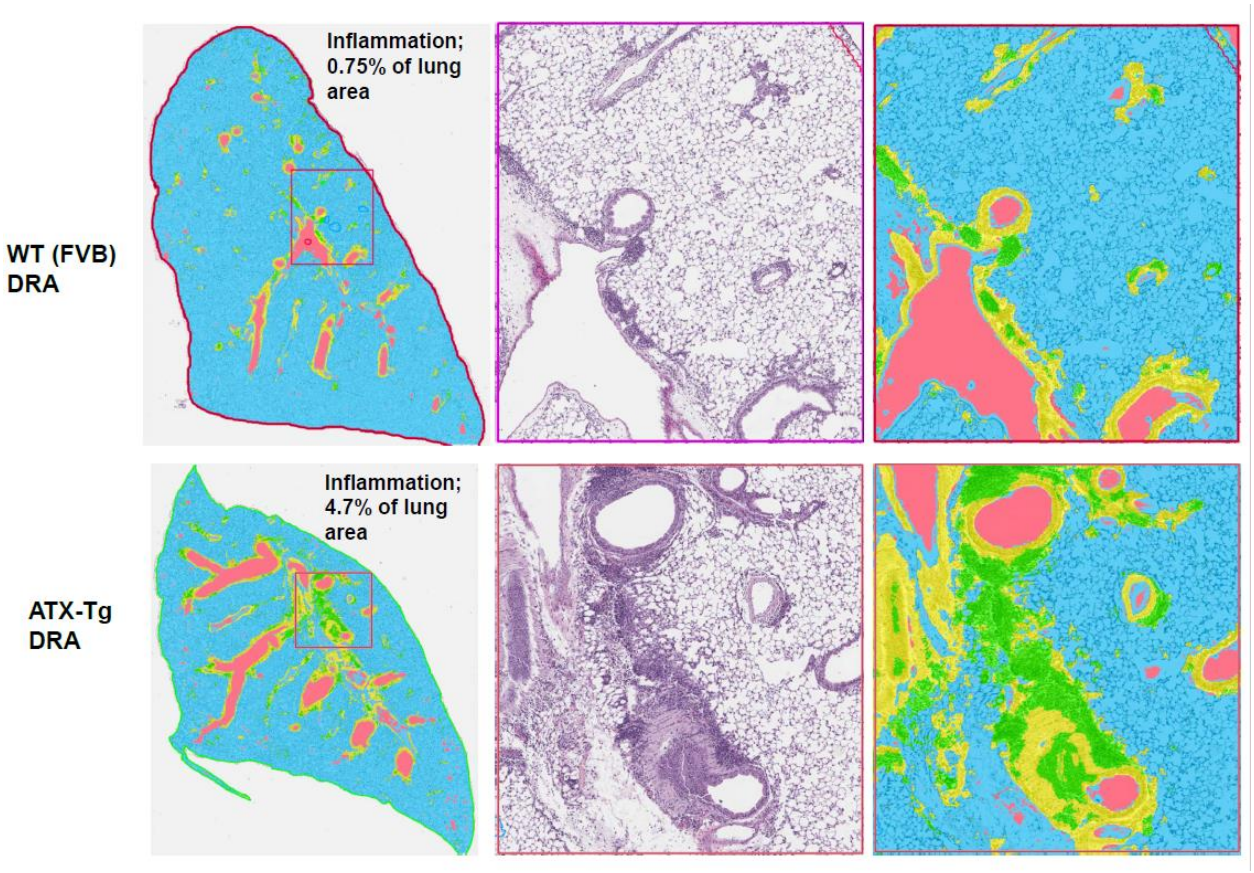

Figure 2.13 The pathologic severity of allergic lung inflammation in ATX-Tg vs. wild type (WT-FVB) mice induced by the DRA triple allergen model. Total lung inflammation was quantified using digital morphometry software systems as described in Materials and Methods section. Whole lung fields were scanned and analyzed to classify regional involvement of inflammation in a blinded fashion. The numeric values correspond to the percentage of the regional area of lung inflammation. The analysis was repeated at least twice with similar results. The color codes represent the following: green-inflammation, blue-alveolar space, yellow-structural tissue, and pink-void area.

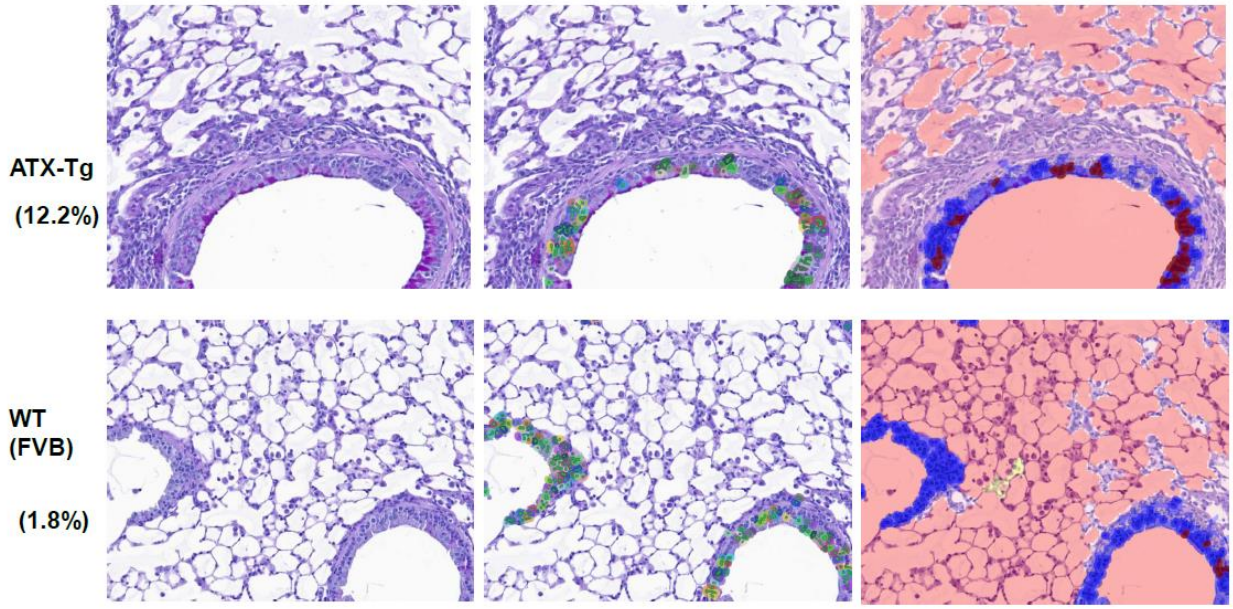

Figure 2.14 Quantitation of goblet cell metaplasia in ATX-Tg vs. wild type (WT-FVB) mice induced by the DRA triple allergen model. Using the digital morphometric software system described in the Materials and Methods section, bronchial epithelial cells were automatically identified. PAS staining was assessed using the same threshold setting for the whole lung field. The left figure shows the raw PAS staining, the middle figure shows the identification of individual bronchial epithelial cells, and the right figure identifies the PAS positive goblet cells using digital signal threshold as described in the Materials and Methods section. The numeric values represent the percentage of PAS positive cells of total bronchial epithelial cells. The analysis was repeated at least twice with similar results.

2.3.3 Blocking the ATX/LPA Axis Attenuates Allergic Lung Inflammation

Secondly, we investigated the hypothesis that blocking ATX-LPA axis could alleviate allergic inflammation induced by triple allergen DRA in mice. LPA receptor 2 (LPA2) has been reported to be expressed in the lung tissue as well as many other cell types (84). Our preliminary data indicated that eosinophils highly expressed LPA2 mRNA. Therefore, LPA2 knock-out mice (LPA2-/-), which had lost the LPA2 receptor signaling pathway (86), were used to study the function of ATX-LPA in allergic lung inflammation. Our results showed that in comparison with wild type mice with the same genetic background (WT-129SV), LPA2-/- mice subjected to DRA challenge have fewer inflammatory cells in BAL fluid (figure 2.15) and alleviated DRA challenging induced increase of IL-4 and IL-5 level in both lung tissue and BAL fluid (figure 2.16). Meanwhile, IFN-γ showed no significant difference between the two groups which was similar to the previous results (figure 2.17). A lesser degree of inflammation with the triple allergen DRA challenge model in LPA2-/- mice was shown by quantification of lung pathology (figure 2.18).

Since total knockdown of ATX (ATX -/-) was embryonically lethal, we then tested our hypothesis by using another transgenic mice with conditional knockout of ATX (ATX +/-). The ATX protein level decreased 50% in the heterozygote mice compared with their wild type counterparts (87). In order to completely prevent the enzyme activities of ATX, GWJ-23, a novel chemical inhibitor of ATX was used to evaluate the role of ATX in the imitation of asthma in mice (88). The protocol of GWJ-23 experiments is described in figure 2.19. Our result showed that the ATX (+/-) mice had reduced levels of IL-4 and IL-5 in BAL fluid induced by triple allergen DRA challenge compared with wild type mice. The level of IL-4 and IL-5 in BAL fluid was furtherly reduced by pre-treatment with the ATX inhibitor GWJ-23 (figure 2.20). These results proved that the ATX/LPA axis was critical to induce asthmatic inflammation and indicated that the ATX/LPA axis was a possible novel target for therapeutic intervention in severe asthma.

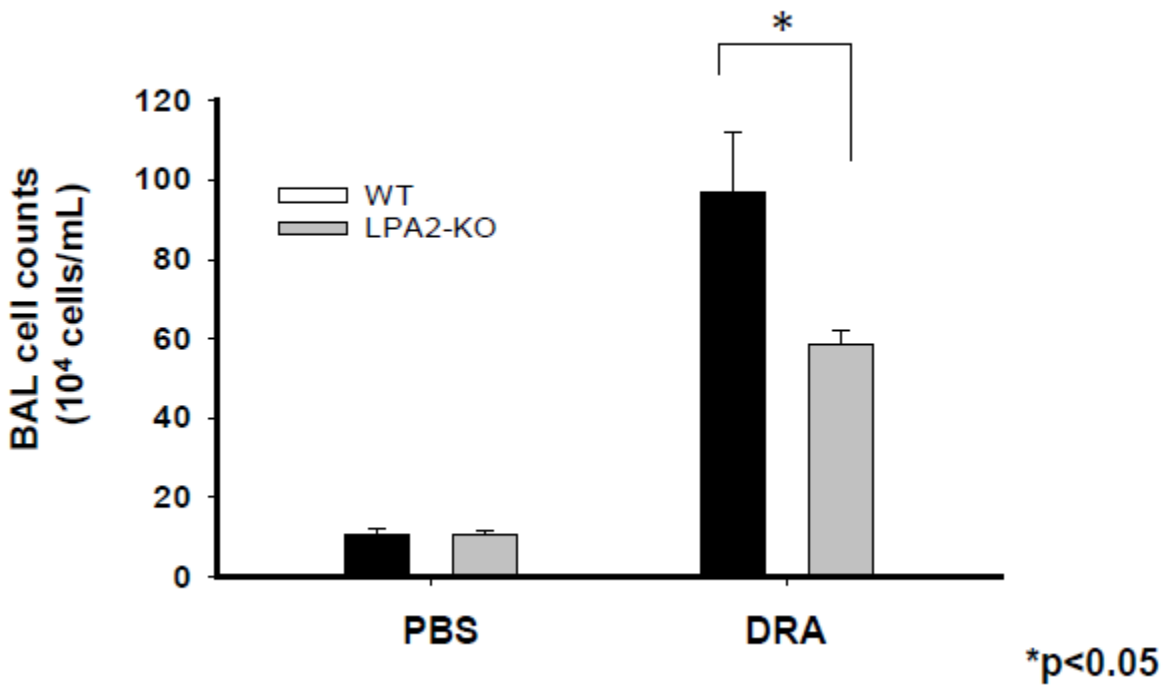

Figure 2.15 Total cell counts in BAL fluid of wild type vs. LPA2-/-. LPA2-/- mice induced by the DRA triple allergen model. LPA2-/- mice had a lower number of total cells in BAL fluid following allergen challenge, compared with wild type mice of the same background (WT-129SV). $n \geq 5$ mice per group. *$p<0.05$

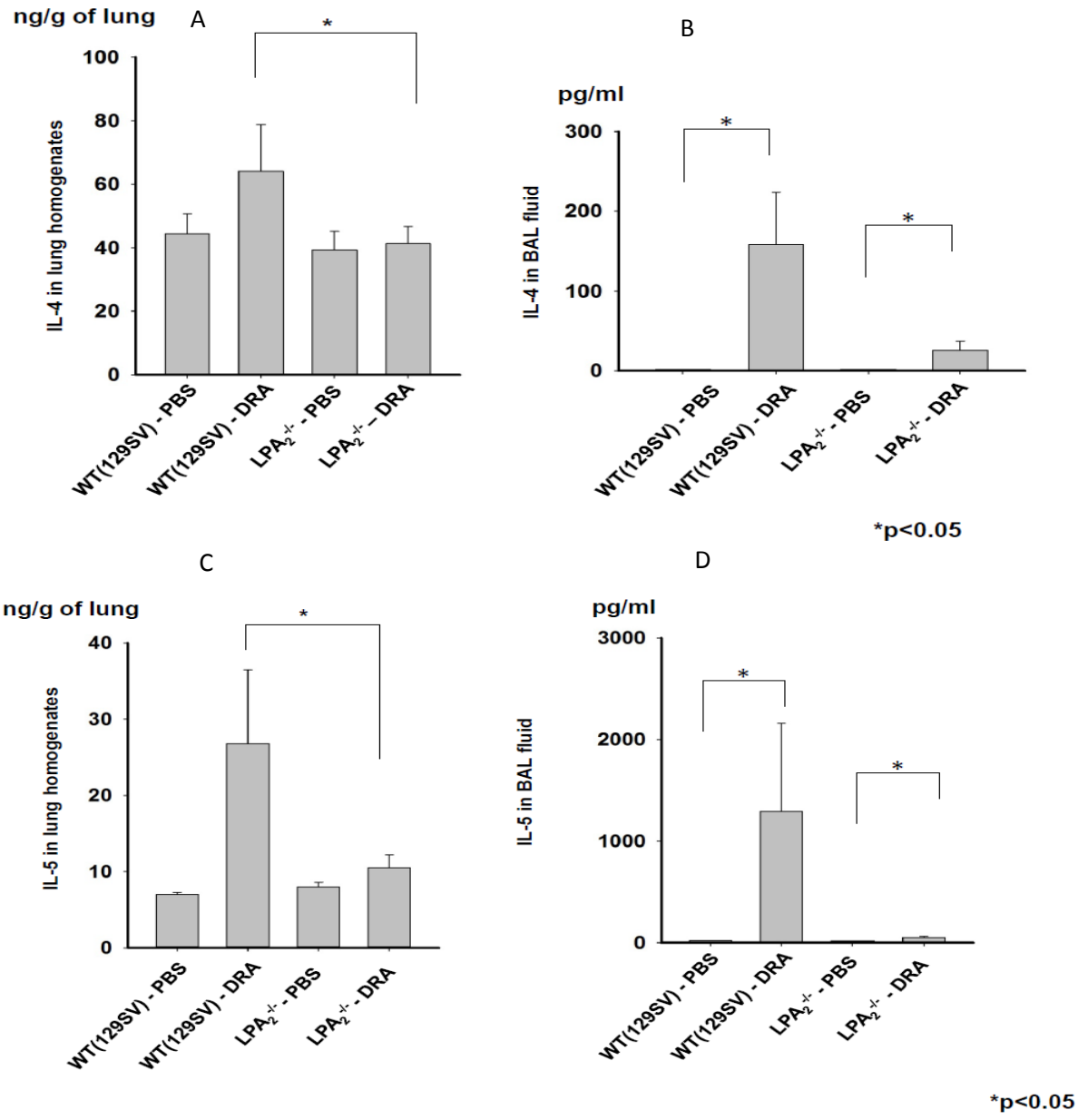

Figure 2.16 Concentrations of IL-4 in whole lung homogenates (A) and BAL fluids (B) of the LPA2-/- vs. wild type (WT-129SV) mice induced by the DRA triple allergen model. Concentration of IL-5 in whole lung homogenates (C) and BAL fluids (D) of LPA2-/- vs. wild type (WT-129SV) mice induced by DRA triple allergen. Experiments were carried out at least twice with similar results. n ≥ 5 mice per group. *p<0.05.

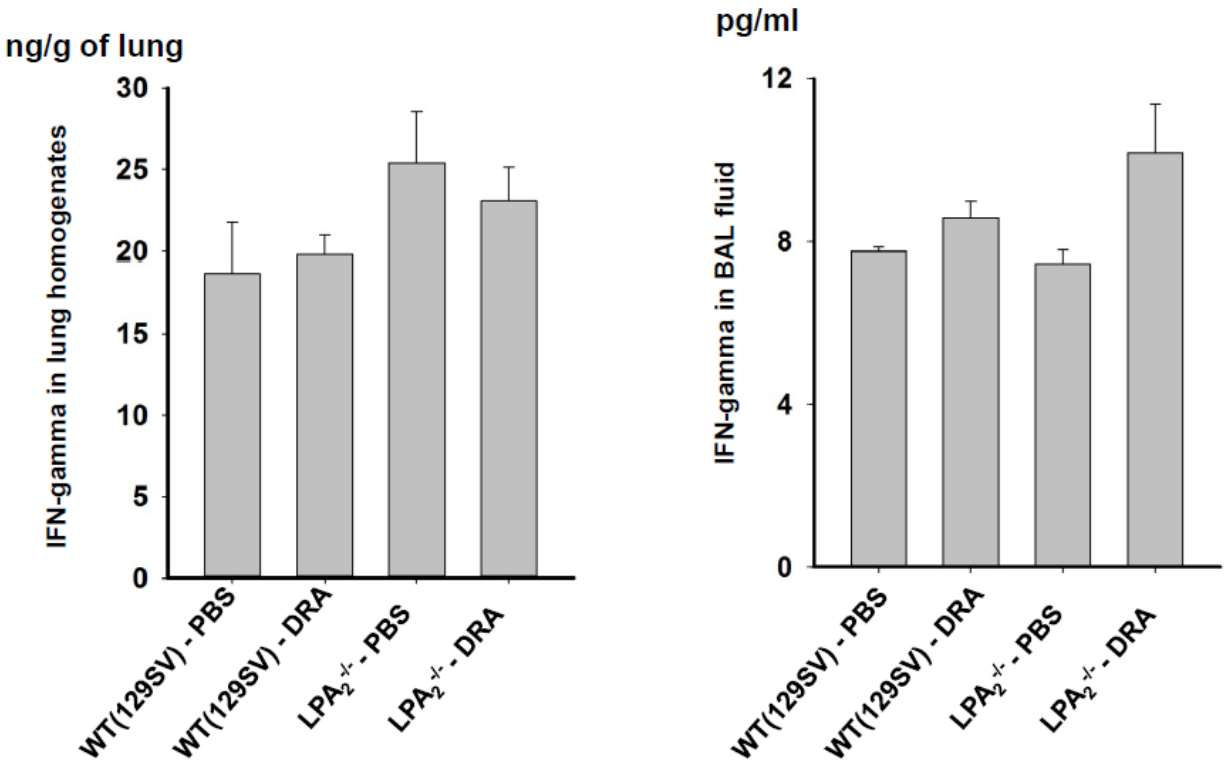

Figure 2.17. Concentration of IFN-γ in lung homogenates and BAL fluid of LPA2-/- vs. wild type (WT-129SV) mice sensitized with DRA and challenged either with PBS or DRA in the DRA allergic asthma model. $n \geq 5$ mice per group

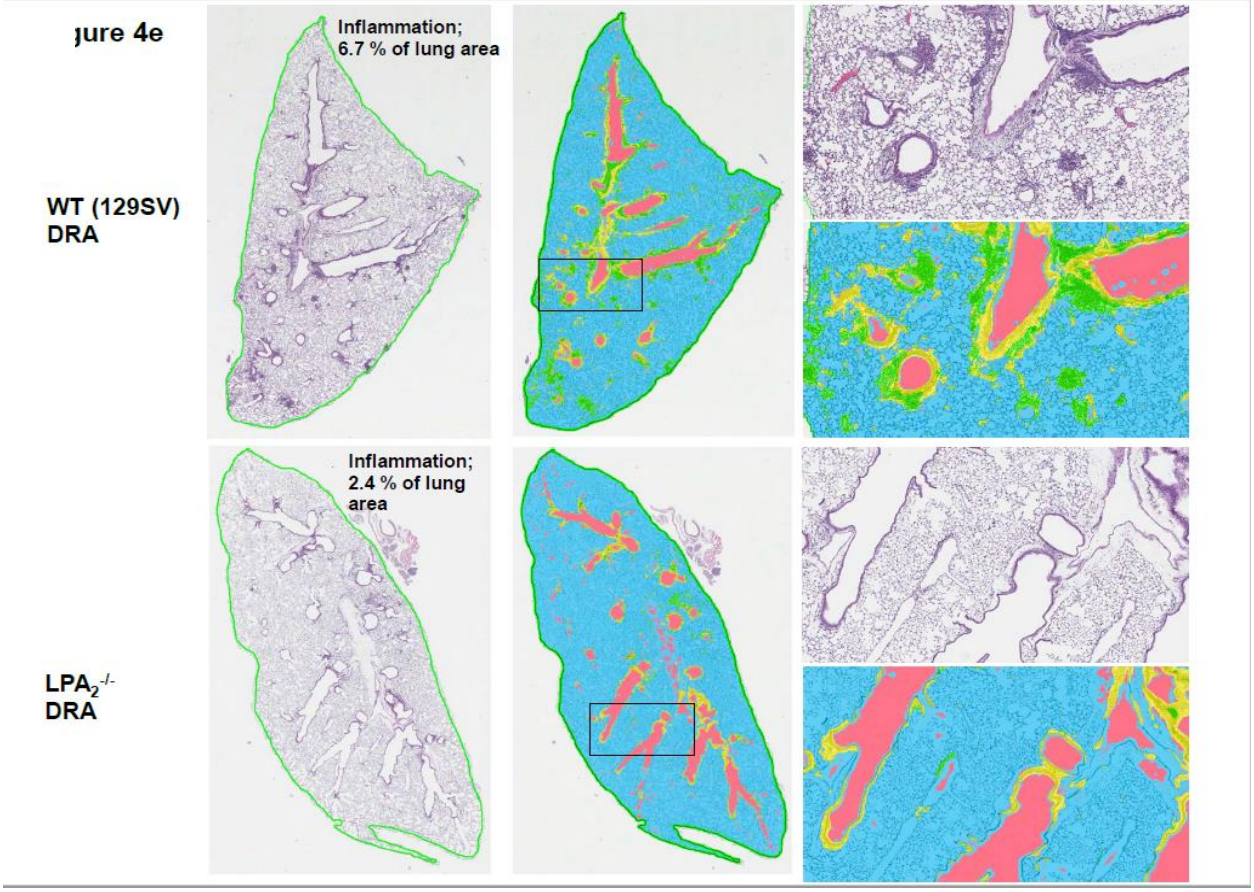

Figure 2.18 Pathologic severity of allergic lung inflammation in LPA2-/- vs. WT(129SV) mice in the DRA triple allergen model. The whole lung field was scanned and analyzed as described in the Materials and Methods section. The numeric values represent the percentage of regional area of lung inflammation. The analysis was repeated at least twice with similar results. The color codes represent followings: green-inflammation, blue-alveolar space, yellow-structural tissue, and pink-void area.

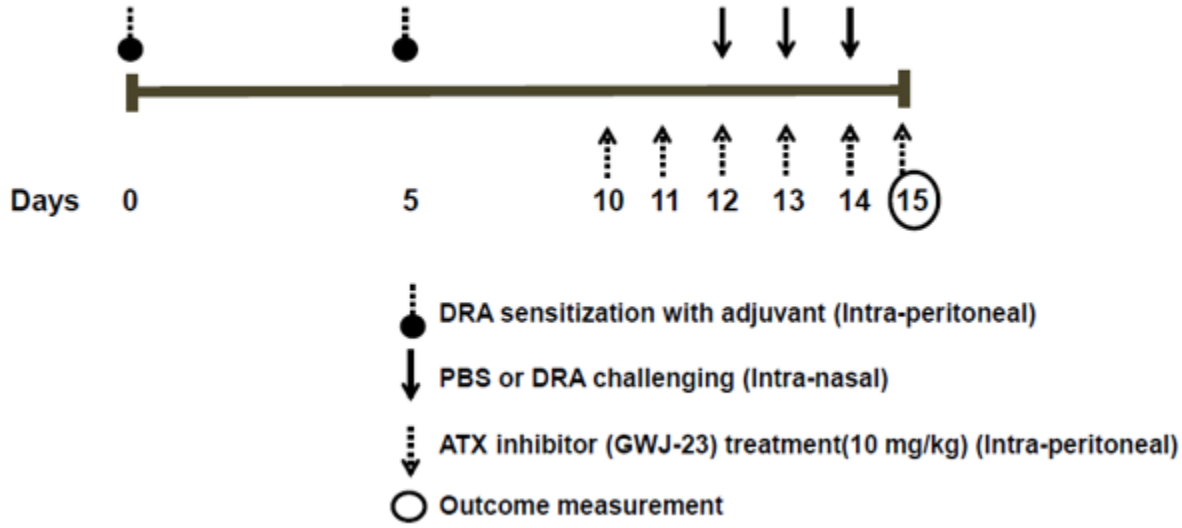

All mice received either GWJ-23 (ATX inhibitor) or equivalent dose of the vehicle (DMSO).

Figure 2.19 Diagram of the experimental design used for the ATX inhibitor, GWJ-23 in WT and ATX (+/-) mice in the DRA triple allergen model.

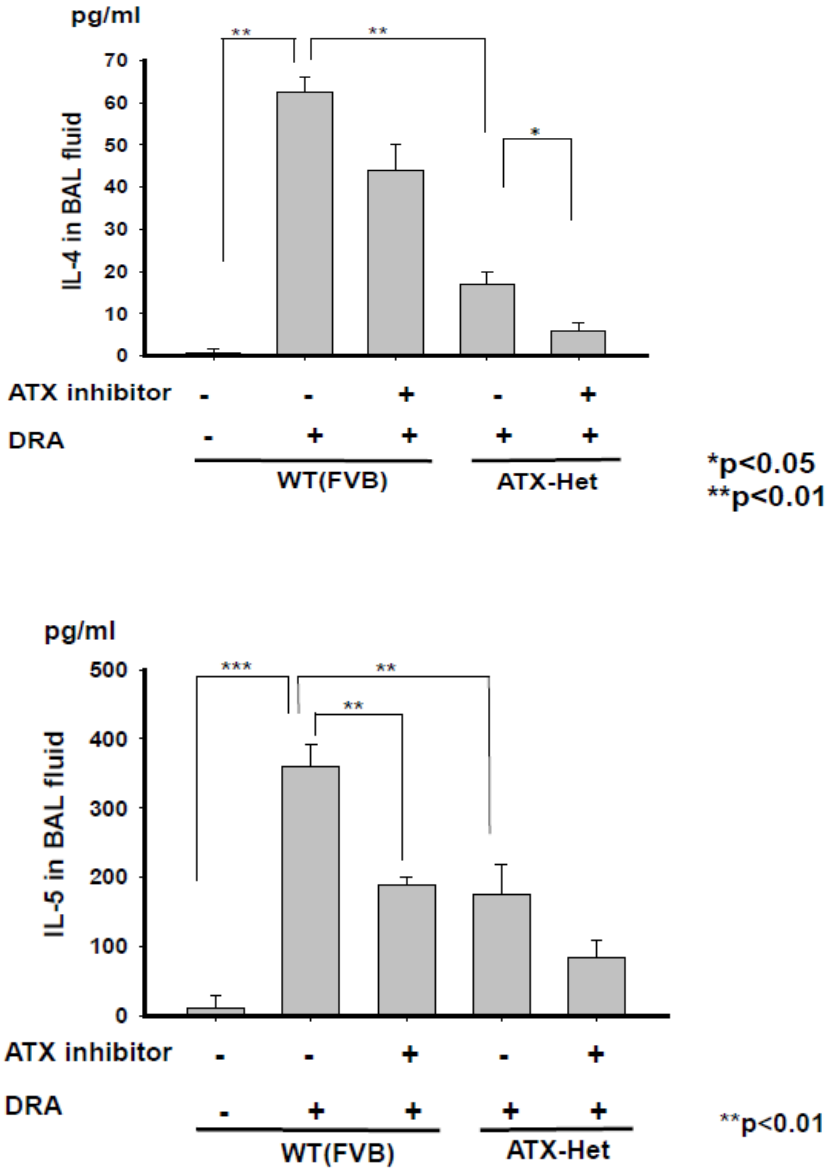

Figure 2.20 Concentration of IL-4 (A) and IL-5 (B) in BAL fluids of ATX-het vs. WT mice induced in the DRA triple allergen model. ATX-heterozygous and WT mice were sensitized and challenged by DRA, with and without treatment using an ATX enzyme inhibitor (GWJ-23).

2.4 Discussion and Conclusion

Asthma is a common chronic inflammatory disorder of airways of the lungs which is caused by a combination of complex and incompletely understood gene-by-environment interactions. Although researchers have proposed a variety of asthma pathogenic mechanisms, few have been successfully translated into effective treatments of asthmatic patients. There are various inflammatory protein mediators which involved in the pathophysiology of asthma including various lipid mediators, chemokines, cytokines, cytokines, as well as growth factors (89). Bioactive lipid mediators such as prostaglandins are also believed to have a significant effect on the pathogenesis of asthma (90). In our study, the data showed that LPA, a classic bioactive lipid mediator, plays a critical role in pathogenesis of asthma through experiments which explored a human model of asthmatic lung inflammation and a triple-allergen-induced model (DRA) of lung inflammation in gene knockout mice.

First, our clinical data indicated that the levels of ATX protein were elevated in airway spaces of patients with mild asthma following subsegmental bronchial allergen challenge in both a discovery and verification cohort of subjects. Secondly, we confirmed our previous findings according to results from the DRA murine asthma and human asthmatic SBP-AG subjects. Thirdly, the result of a gain-of-function study indicated elevation of ATX level in mice accentuates allergic lung inflammation and the asthma phenotype in terms of Th2 cytokine production. Fourthly, the result of the loss-of-function study showed that the combined genetic (ATX +/-) and pharmacologic (GWJ-23, an ATX enzyme inhibitor) inhibition of the ATX-LPA axis significantly suppressed both Th2 cytokine production and inflammatory response in the mouse DRA model. Additionally, LPA_2 receptor knockout mice were resistant to the development of asthmatic lung inflammation induced by triple allergen DRA challenge. The somatomedin B (SMB) domains of ATX are homologous to the SMB domain of vitronectin, both of which can bind to integrins (91). The interaction between integrin and SMB domain of ATX leads to produce LPA in the area of activated integrins expression. The biological function of LPA is believed to mediate by binding to the LPA_2 receptor in our mice allergic asthma model, but the role of LPA receptors on human inflammatory and airway cells have not been tested yet. Above all, we can conclude that ATX/LPA signaling pathway plays a very critical role in the pathophysiology of asthma and could be a novel therapeutic target of asthma.

3. DEVELOPMENT OF AN ULTRAFILTRATION LC-MS PLATFORM FOR AUTOTAXIN

3.1 Introduction

Belonging to the small enzyme family of ectonucleotide pyrophosphatases and phosphodiesterases, autotoxin (ATX) is an extracellular enzyme that hydrolyzes lysophosphatidyl cholines (LPCs) into lysophosphatidic acids (LPAs) (figure 3.1). LPAs are simple lipid mediators that bind selectively to cell surface receptors and activate intracellular responses. ATX-LPA signaling has been implicated in vascular development (92), various human cancers (93), lymphocyte homing and chronic inflammation (94), fibrotic diseases (95), thrombosis and cholestatic pruritus (96) and urethral obstructive disease (97). Given its role in human disease and the fact that ATX is an extracellular enzyme, ATX is a promising target for therapy.

The development of sensitive, efficient and high throughput methods to study the ligand-enzyme binding affinity and their potential to inhibit ATX activity are essential to identify novel ATX inhibitors. ATX can hydrolyze LPC into two products, choline and LPA, and both can be used to measure ATX activity. Previously, several other in vitro biochemical assays have been developed and used to screen compounds for potential ATX inhibition including a radiometry method (98,99) and a fluorescence method (100-102), which are designed to test one compound at a time for binding or inhibition. Liquid chromatography-tandem mass spectrometry (LC-MS/MS) also can be used to measure LPA (103,104), but most of the LCMS based methods were used to detect naturally occurring LPA in biological fluids (i.e. plasma, bronchoalveolar lavage).

Although not yet applied to ATX inhibitors screening, mass spectrometry-based bioassays have been useful in the discovery of protein ligands and enzyme inhibitors. For example, pulsed ultrafiltration (PUF) liquid chromatography-mass spectrometry (LCMS) based methods (figure 3.2) (105,106), invented in our laboratory, have been used for screening of combinatorial library mixtures and natural product extracts in order to identify ligands for a wide variety of macromolecular targets including quinone reductase-2 (107), cyclooxygenase-2 (108,109), estrogen receptors (110), and the retinoid X receptor (111). The main advantages of PUF-LCMS based screening over optical or radioactive detection methods are high throughput, low cost, and

less false positives, and the fact that there is no need to modify either the ligand or the targets by attaching a radiolabel, a chromophore and a fluorophore, etc.

When the macromolecular target is soluble such as a cytosolic or extracellular protein, PUF-LCMS screening is particularly useful because the target protein is maintained in solution during the screening process. During PUF-LCMS, potential ligands in combinatorial library mixtures or natural product extracts are allowed to bind to the target protein, ultrafiltration is used to separate the protein-ligand complexes from unbound small molecules, and then the retained ligands are released by denaturing the target protein for analysis using LC-MS. To the best of our knowledge, no screening assays have been reported previously for the discovery of ATX inhibitors from complex mixtures. Since ATX is an extracellular soluble enzyme, the application of a solution-phase screening technique such as PUF-LCMS is ideal for the discovery of small molecule ATX ligands contained in complex matrixes such as botanical extracts. Subsequent to detection during PUF-LCMS, high resolution tandem mass spectrometry may be used to facilitate the characterization and identification of each ligand by high resolution accurate mass measurement.

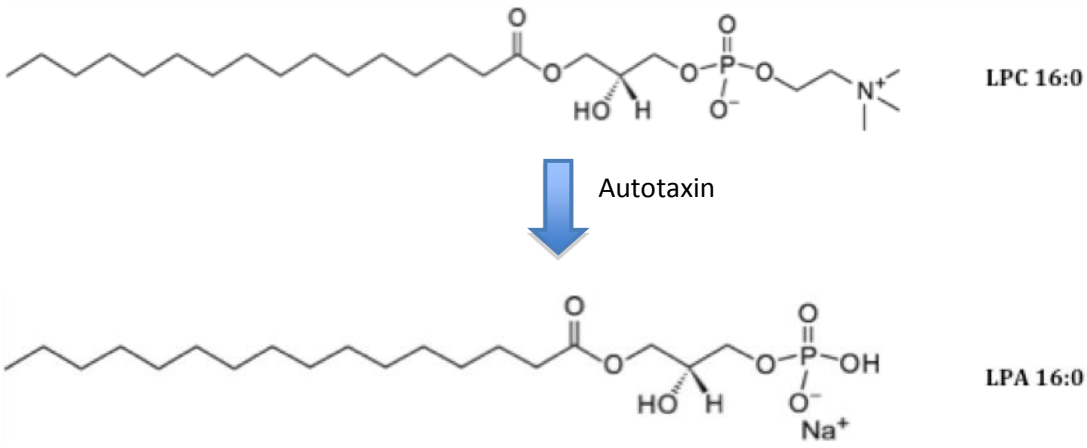

Figure 3.1 Conversion of 16:0 LPC to 16:0 LPA by autotaxin

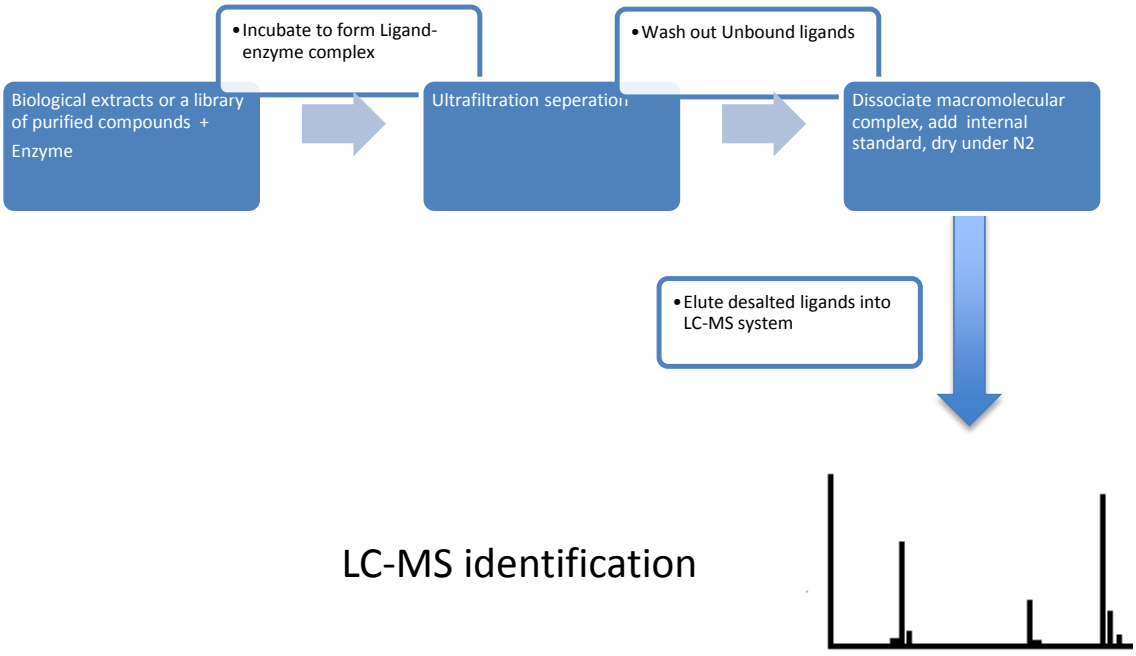

Figure 3.2 Conceptal diagram of PUF-LCMS

3.2 Materials and Methods

3.2.1 Chemicals and Reagents

All solvents were HPLC grade or better and were purchased from Fisher (Hanover Park, IL). Recombinant human ATX, PF-8380 and S32826 were purchased from Cayman Chemical (Ann Arbor, MI). GWJ-23 and BrP-LPA were purchased from Echelon Bioscience (Salt Lake City, UT), and centrifugal ultrafiltration filters (Microcon YM-30) were purchased from Millipore (Bedford, MA) (see chemical structures in figure 3.3). Methanol extracts of *Glycyrrhiza glabra* and *Glycyrrhiza uralensis* were provided by the UIC/NIH Botanical Center for Dietary Supplements Research, and glabridin (see chemical structures in figure 3.4) was purchased from Sigma-Aldrich (St. Louis, MO). C16:0 LPC, C16:0 LPA and C17:0 LPA were purchased from Avanti Polar Lipids (Alabaster, AL). Dulbecco's Modified Eagle Medium was purchased from Gibco (Grand Island, NY). All organic solvents were HPLC grade or better and were purchased from Thermo Fisher (Hanover Park, IL). High purity water was prepared using a Millipore (Bedford, MA) Milli-Q system.

3.2.2 Sample Preparation

Ultrafiltration separations were carried out using centrifugation with a Millipore (Billerica, MA) vial system (MWCO 30 kDa) for screening pooled compound libraries and extracts of botanical extracts. A library of purified natural products and synthetic compounds was prepared from compounds isolated in-house at the UIC/NIH Center for Botanical Dietary Supplements Research or purchased from multiple vendors. The purity and identity of each compound was verified using LC-MS. Stock solutions were prepared by the dissolution of powdered material in dry DMSO and then stored at -20 °C. Botanical extracts were obtained as organic solutions and were also stored at -20 °C until use. A standard stock solution of pooled samples was prepared containing ~100 compounds in DMSO at an equimolar concentration of 100 µM. Working solutions of the pooled ligands were prepared by diluting the DMSO standard stock solution with 50 mM ammonium acetate buffer (pH 8.0) containing 100 mM NaCl to produce final incubation concentrations between 2.5-4 µM. The volume of DMSO in the final incubations was less than 3%.

The assay protein concentration of 1 µM was selected for the detection of ligands with

dissociation constants of 50 μM or lower, which included the natural ligand glabridin (K_d ~1 μM) and a wide range of potential ligands with lower affinity. The concentration of autotaxin within each incubated solution was calculated using the molecular mass of 125 kDa. Genistein was used as an internal standard for all incubations, and a stock solution of 100 μM genistein in DMSO was prepared from powdered material.

3.2.3 Ultrafiltration Screening Conditions

For PUF-LC-MS screening for ligands of ATX, 10 μM compounds (individually or in mixtures) or 0.5 mg/mL of botanical extract was incubated with 1 μM of human recombinant ATX or denatured human recombinant ATX (negative control) in 150 μL of 50 mM Tris buffer (pH 8.0) containing 140 mM NaCl, 25 mM KCl, 1 mM $CaCl_2$, and 1 mM $MgCl_2$ at 37 °C for 1 h. After incubation, each compound, compound mixture or extract was filtered through a 30,000 Da molecular weight cutoff ultrafiltration membrane by centrifugation at 13, 000x*g* for 10 min at 4 °C. To remove unbound compounds, the ATX-ligand complexes were washed three times with 150 μL aliquots of 50 mM ammonium acetate (pH 7.5) followed by another centrifugation at 13,000x*g* for 10 min. The ligands were dissociated from ATX using 300 μL of methanol. Then the ultrafiltrate containing ligands was evaporated to dryness under a stream of nitrogen.

After reconstitution in 100 μL 50% aqueous methanol, the ultrafiltrates containing ATX ligands were characterized using LC-MS. Identical incubations using denatured ATX were used to control for nonspecific binding; and LC-MS peaks that increased in area in the experiments relative to the control containing denatured ATX indicated specific binding. A hit was defined as an LC-MS peak area response that is at least 5 times higher than the response of the negative control containing denatured ATX. A hit meeting these criteria was re-tested for binding to the active site of ATX by adding 10 μM PF-8380 as a competitive inhibitor of binding to the ATX active site to the test solution and then repeating the PUF-LCMS screening process. If signal of the potential hit was attenuated or eliminated in the presence of 10 μM PF-8380, then the potential ligand was confirmed to bind to the ATX active site. If binding was not attenuated by competition with PF-8380, then the ligand would be determined to be binding to another site on ATX.

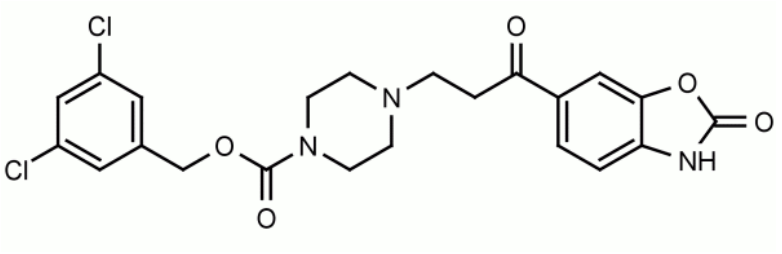

PF-8030

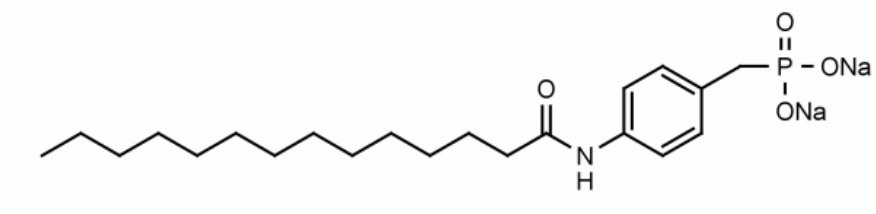

S32826

Figure 3.3 Structures of ATX inhibitors: PF-8380 and S32826

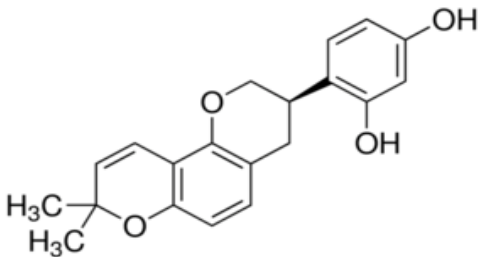

Figure 3.4 Structure of glabridin

3.2.4 LC-MS Conditions for the Proof of Principle Assay

Each reconstituted ultrafiltrate was analyzed using either a Shimadzu (Kyoto, Japan) LCMS-8050 triple quadrupole mass spectrometer (for library compounds such as PF-8380) or a Shimadzu ion trap/time-of-flight (IT-TOF) high resolution mass spectrometer (for botanical extracts) equipped with a Shimadzu Nexera UPLC system. For the analysis of ultrafiltrates from incubations with discreet compounds, the triple quadrupole mass spectrometer was used with selected ion monitoring and polarity switching. The injection volume was 10 µl, and separations were carried out using a Waters (Milford, MA) Acquity UPLC BEH C_{18} column (130Å, 1.7 µm, 2.1 mm x 100 mm) with a 5 minute linear gradient from 25% to 95% acetonitrile in 0.1% aqueous formic acid, followed by isocratic 95% acetonitrile for 1.5 minutes. The flow rate was 400 µl/min, and the column was re-equilibrated at least 2.5 minutes between analyses. For detection of protonated or deprotonated molecules of PF-8380 and S32826, the ions of *m/z* 477.60 (positive mode), *m/z* 396.4 (negative mode), *m/z* 338.1 (negative mode), and *m/z* 405.4 (negative mode) were monitored, respectively. For the analysis of ultrafiltrates from incubations with complex natural product mixtures such as botanical extracts, 40 µl aliquots were analyzed on the high resolution mass spectrometer equipped with a Waters (Milford, MA) Xterra C_{18} column (150 x 2.1 mm, 3.5 µm). After 5 minutes at 95% methanol in water containing 0.1% formic acid (v/v), a 95 minute linear gradient was used from 5% to 100% methanol. Mass spectra were recorded over the mass range *m/z* 180 to 750 or from *m/z* 740 to 1500 using electrospray with polarity switching (±) for a total duty cycle of 1.72 seconds at a normalized collision energy for collision induced dissociation of 90%, ion accumulation time of 10 ms, and an activation q value of 0.210. The ion source parameters for tandem mass spectrometry included a capillary voltage of -3.5 kV, source block temperature 300°C, desolvation line temperature 200°C, and a nebulizer gas flow of 2.5 l/min. External calibration using a solution of sodium trifluoroacetate provided mass accuracy within 5 ppm. Genistein at 50 nM was used as an internal standard for all incubations, and a stock solution of 100 µM genistein in DMSO was prepared from powdered material.

3.2.5 LC-MS Conditions for Screening of Natural products for Binding to Autotaxin

The reconstituted ultrafiltrate solution was injected (40 µl) onto a Waters Xterra 150 x 2.1 mm 3.5 µm C_{18} column connected to Shimadzu (Columbia, MD) LC20ADXR enhanced pressure tolerance HPLC system coupled with an IT-TOF mass analyzer. A universal LC-MS method for

all sample types was developed allowing for an uncomplicated batch setup and data processing workflow of large sample sets. The aqueous mobile phase (A) was water containing 0.1 % v/v formic acid and the organic mobile phase B was acetonitrile. The gradient was 5% B from 0 to 5 minutes and then from 5% to 100% B from 5 to 100 minutes for a slope of 1 % B per minute, isocratic 100% B for 2 minutes, re-equilibrate at initial condition for 5 minutes. A total run time of 120 minutes proved to be sufficient to elute all compounds and eliminate run to run carry over. The Shimadzu IT-TOF HRMS was scanned from *m/z* 180 to 750 and from *m/z* 740 to 1500 using electrospray ionization with both positive and negative polarities for a total duty cycle of 1.72 seconds. Pure methanol was analyzed as a blank. Operating parameters were defined as follows: Vcap = +4500 V or -3500 V, heating block and curved desolvation line set to 300°C, nitrogen drying gas flow 2.5 l/min. A total of four events with two assigned for each polarity were employed to cover the desired mass range *m/z* 100-1500 with a total cycle time of 500 ms.

3.2.6 LC-MS Based ATX Functional Assay

To a microcentrifuge tube containing C16:0 LPC (193 µl of a 40 µM in Dulbecco's Modified Eagle Medium) and test compound (5 µl of various concentrations), 2 µl of a 2 µM ATX solution in storage buffer (final concentration 20 nM) was added, and the reaction mixture was incubated at 37°C for 60 minutes. The reaction was stopped by adding 400 µl methanol followed by 10 µl of a 2 µM solution of C17:0 LPA in methanol as an internal standard. Samples were centrifuged at 13,000x*g* for 10 minutes, and supernatants were analyzed using LC-MS/MS. Control experiments were performed in parallel using an identical procedure except that the test compound was omitted. All the functional assays were performed in duplicate and analyzed twice.

The concentration of C16:0 LPA (the enzymatic product of ATX conversion of C16:0 LPC) in each sample was measured using LC-MS/MS, and the percent of ATX inhibition by each test solution was determined by comparing the amount of C16:0 LPA produced in the experiment with that produced in the negative control incubation. Measurements were carried out using LC-MS/MS with selected reaction monitoring on the Shimadzu LCMS-8050 triple quadrupole liquid chromatograph mass spectrometer. A 5 µl aliquot of each supernatant was injected onto a Supelco (Sigma-Aldrich) Ascentis Express C_8 HPLC column (2.1 x 75 mm; 2.7 µm particle size). A 5-minute linear gradient was used from 25% to 95% acetonitrile/chloroform (80:20, v/v) with a counter solvent of methanol/water/formic acid (60:39.5:0.5, v/v/v) containing 5 mM ammonium

formate followed by an isocratic hold for 1.5 minutes. The flow rate was 400 µl/minute, and the column was re-equilibrated at least 2.5 minutes between analyses. The selected reaction monitoring transitions that were measured were *m/z* 496 to *m/z* 184 (positive mode) for 16:0 LPC, *m/z* 409 to *m/z* 152.9 (negative mode) for 16:0 LPA, and *m/z* 423.1 to *m/z* 152.9 for the internal standard 17:0 LPA. Polarity switching was used, and the dwell time was 10 milliseconds per transition.

For IC_{50} value determination, 8 different concentrations of each inhibitor were assayed twice. The IC_{50} value of each inhibitor toward ATX was determined by plotting and analyzing the inhibition curve data using GraphPad Prism 5.0c software (Mountain View, CA). Using 8 concentrations of C16:0 LPC from 0 to 300 µM, the initial rates of formation of C16:0 LPA were determined for ATX using LC-MS/MS. From these data, Michaelis-Menten curves were plotted, and the Km values were determined using GraphPad Prism 5.0c software (Mountain View, CA).

3. 3 Results

3.3.1 PUF-LC-MS Screening Assay

To verify that this new PUF-LCMS assay could detect ATX ligands, the known ligands PF-8380 and S32826 were screened (figure 3.5). Using denatured ATX as a negative control, LC-MS analysis of the ultrafiltrates after incubation, washing, and release of the same known ATX ligands indicated that these compounds exhibited little or no non-specific binding to denatured ATX or the PUF apparatus. Based on the LC-MS peak enhancement for the known ligands of ATX relative to the corresponding peaks in the negative controls, all of the ligands produced signals indicative of positive hits in the PUF-MS/MS assay (figure 3.5). All of these compounds were tested at the same concentration of 10 μM, and as expected, PF-8380 had the highest peak enhancement compared with the negative control.

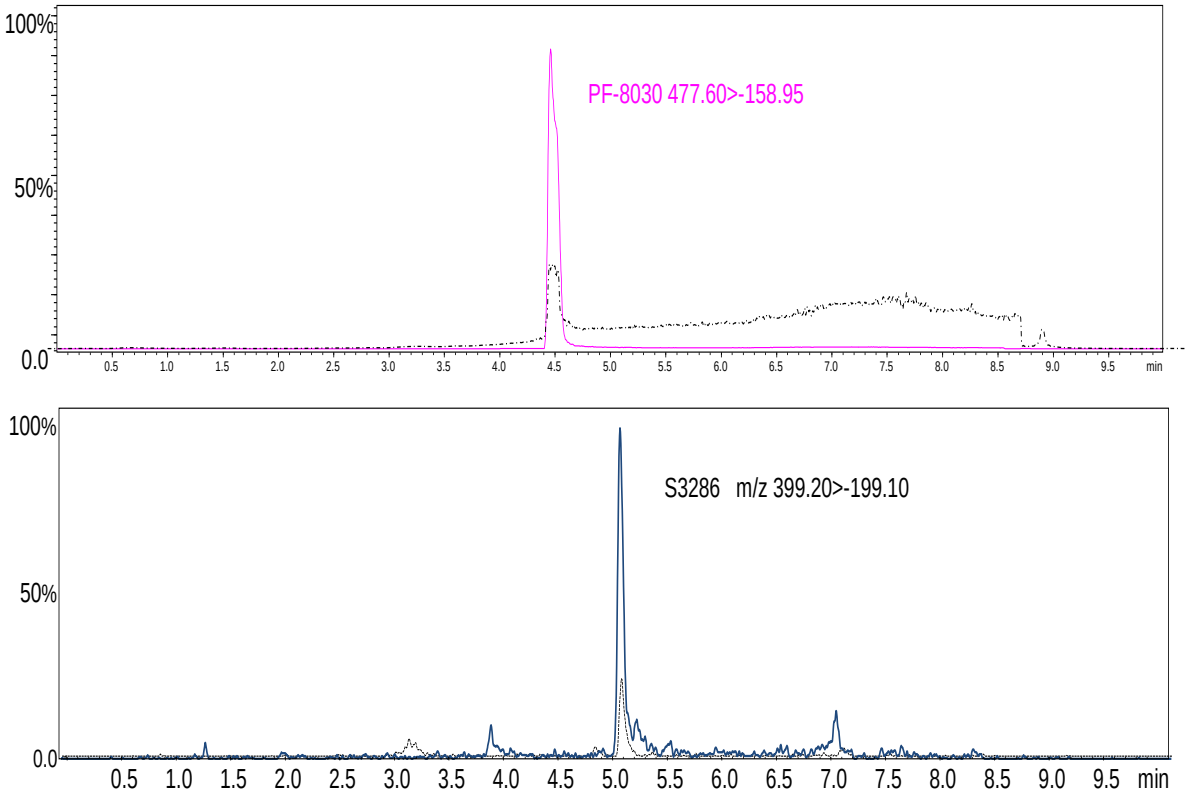

Figure 3.5 PUF-LCMS Chromatography of PF-8380 and S32826

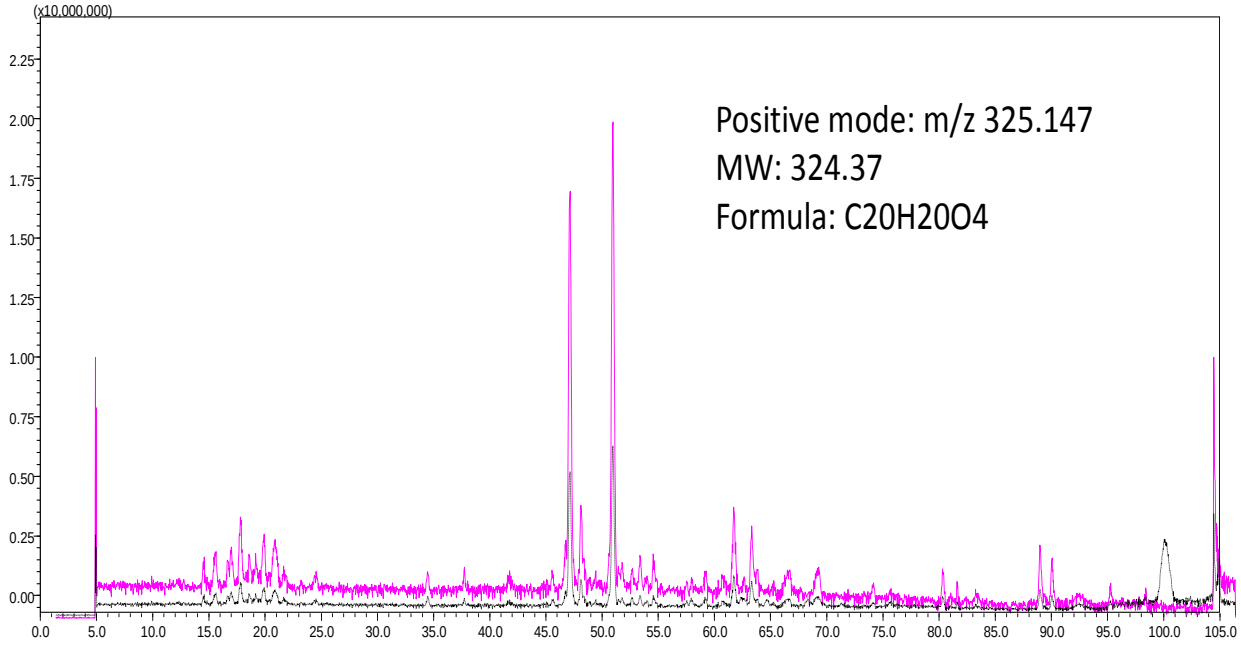

Figure 3.6 PUF-LCMS total ion chromatogram of ultrafiltrate obtained following the incubation of a *G. glabra* extract with ATX. Note the hit at a retention time of 51.5 minutes.

After confirming that PUF-LCMS screening can be used to detect known ligands/inhibitors of ATX including PF-8380 and S32826, this approach was used to screen a series of botanical extracts including the licorice roots, *Glycyrrhiza uralensis* and *Glycyrrhiza glabra*, for new natural product ligands of ATX. As shown in the PUF-LCMS chromatograms in figure 3.6, a hit was detected in the extract of *G. glabra*, eluting at 51.5 min. Enhancement of the peak was more than 20-fold compared to the control containing denatured enzyme, which indicated significant specific binding of the ligand to ATX. Based on the high resolution accurate mass measurement of the protonated molecule of this hit of *m/z* 325.147 (figure 3.7), the elemental composition was determined to be $C_{20}H_{20}O_4$ (-1 ppm, theoretical mass of glabridin). Based on this elemental composition and comparison with the known compounds of *G. glabra*, the isomeric licorice compound glabridin was obtained for comparison. Based on identical retention times (figure 3.8), elemental composition, and tandem mass spectra (figure 3.9), this PUF-LCMS hit was identified as glabridin (see structure in figure 3.4).

To verify that the ligand glabridin was bound to the active site of ATX, PF-8380 was added to the incubation mixture as a competitive inhibitor, and the PUF-LC-MS screening process was repeated. As shown in the computer-reconstructed mass chromatograms in Figure 3.10, the signal for glabridin of *m/z* 325.147 was attenuated or eliminated in the presence of 10 μM of the high-affinity ATX ligand PF-8380. These results confirmed that the *G. glabra* compound glabridin binds to the active site of ATX.

3.3.2 ATX Functional Assay

To assess the ability of glabridin to inhibit ATX, a functional ATX enzyme activity assay was developed and validated based on LC-MS/MS quantification of the reaction product, C16:0 LPA formed from the enzymatic release of choline from C16:0 LPC. The unnatural phospholipid, C17:0 LPA, was used an internal standard. Because the chemical structures (Figure 3.11) and retention times of C16:0 LPA and C17:0 LPA were nearly identical (retention times 2.25 min and 2.26 min respectively (Figure 3.12), the internal standard could be added to the sample before extraction to control for errors during sample preparation as well as for fluctuations in mass spectrometer response. The SRM transitions for analytes and internal standard during electrospray MS/MS with collision-induced dissociation for 16:0 LPC were *m/z 496* to *m/z 184* in positive mode and in negative ion mode were *m/z* 409.0 to *m/z* 153.1 for 16:0 LPA and *m/z* 423.0 to *m/z* 153.1

for the internal standard 17:0 LPA (I.S.). For fragmentation sites in these molecules, see figure 3.12.

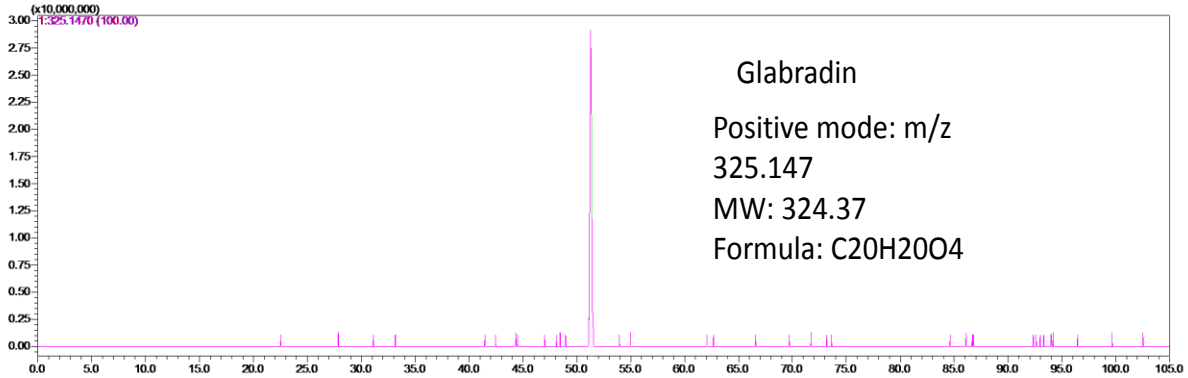

Figure 3.7 High resolution accurate mass measurement of the protonated molecule of this hit of *m/z* 325.147

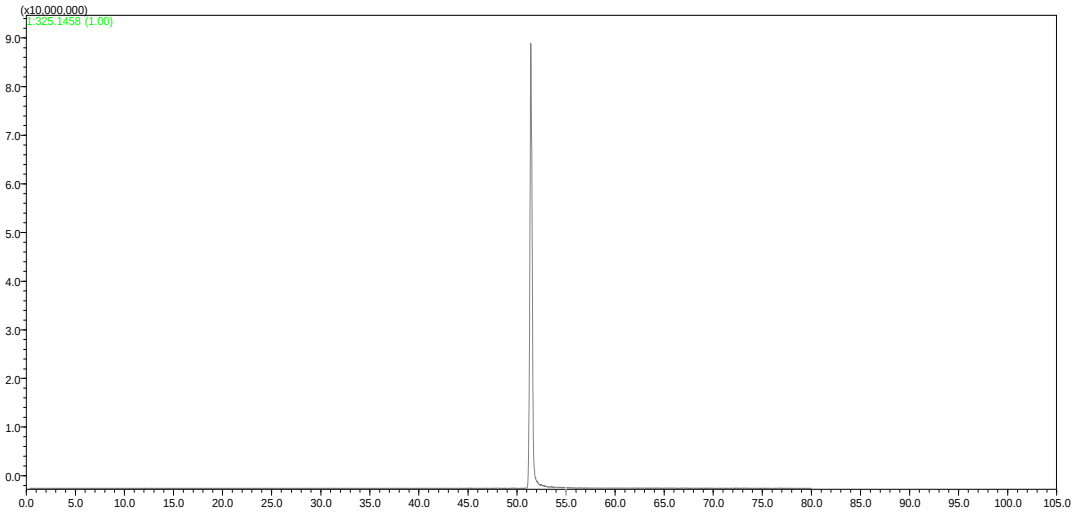

Figure 3.8 LC-MS of 10 μM standard of glabridin

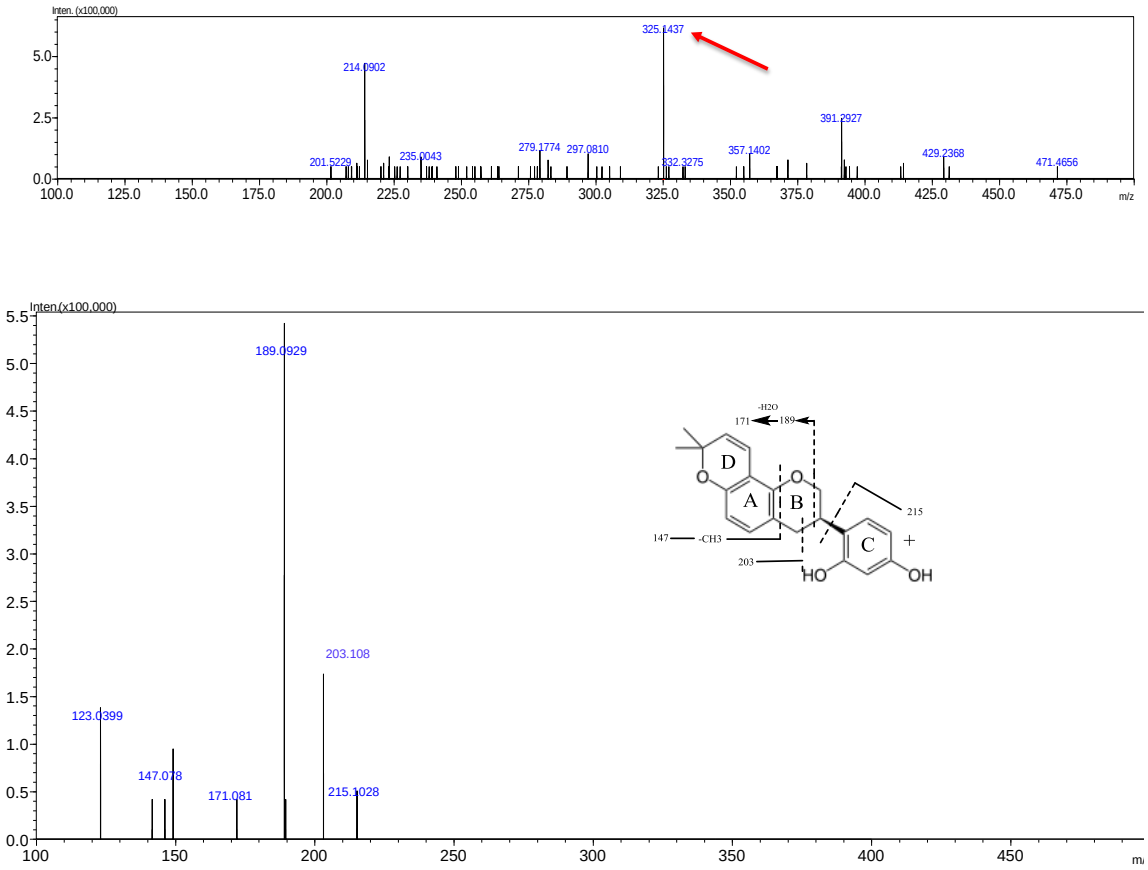

Figure 3.9 High resolution positive ion electrospray mass spectrum of the protonated molecule of glabridin (top) and collision-induced dissociation product ion tandem mass spectrum (bottom)

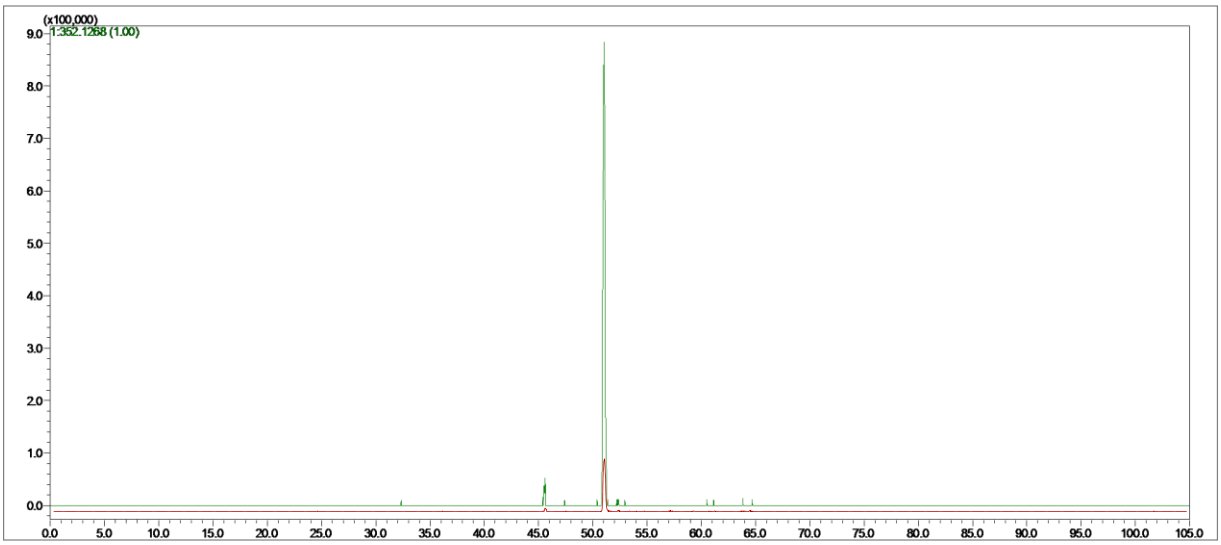

Figure 3.10 PF-8380 (Green solid line) was added to the incubation mixture as a competitive inhibitor glabridin *m/z* 325.147 attenuated or eliminated (Red dot line) in the presence of 10 μM of the high-affinity ATX ligand PF-8380

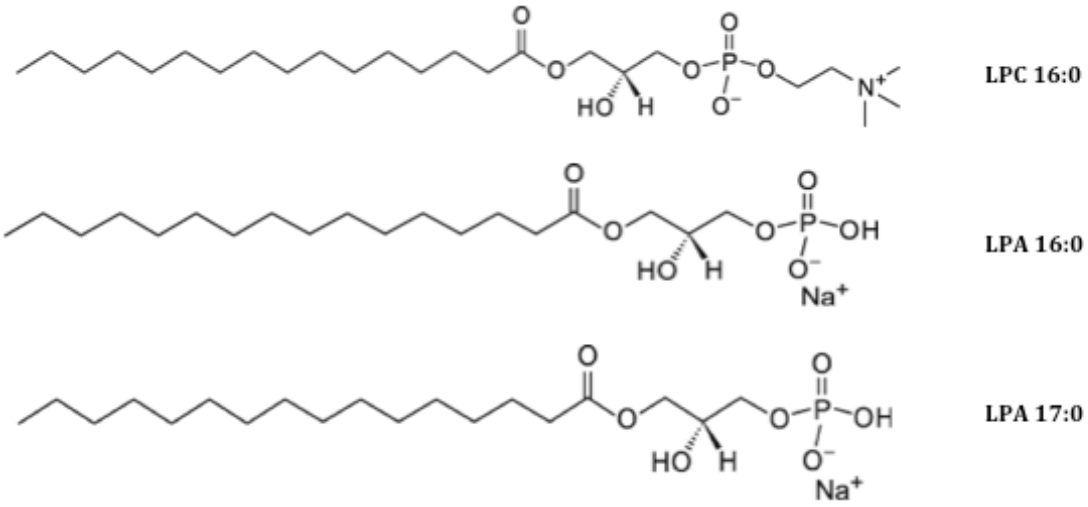

Figure 3.11 Chemical structures of 16:0 Lyso PA, 16:0 Cyclic LPA and 17:0 Lyso PA

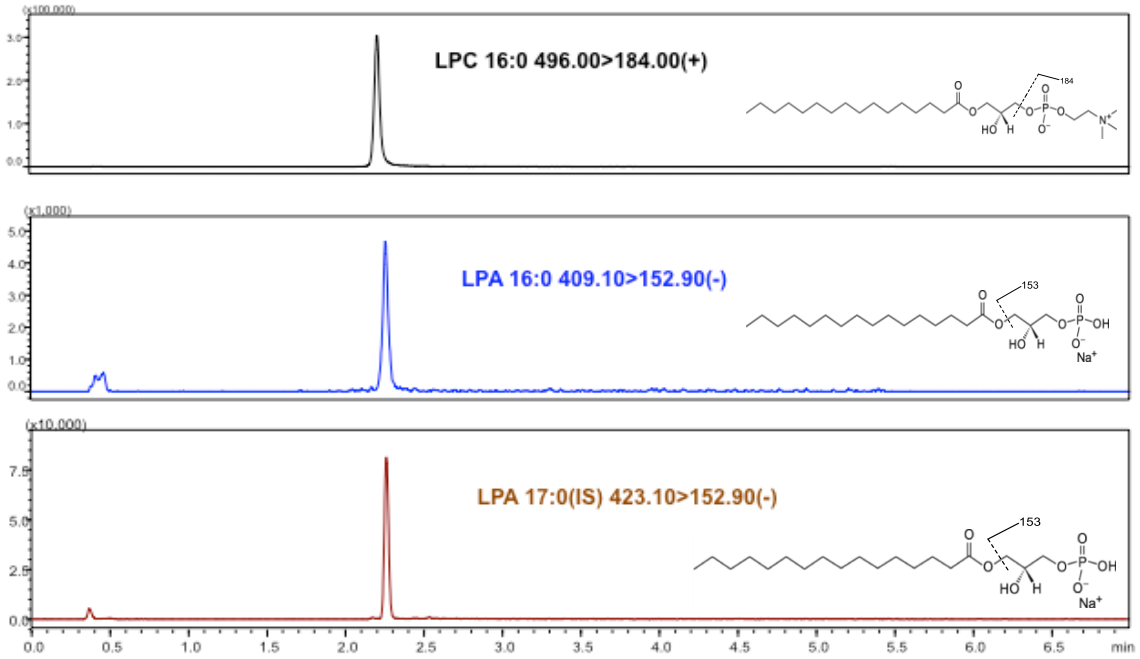

Figure 3.12 LC-MS/MS selected ion chromatograms and fragmentation patterns of 16:0 Lyso PA, 16:0 Cyclic LPA and 17:0 Lyso PA

Beginning with the ATX incubation conditions as above, multiple parameters were optimized including the ATX enzyme level, the substrate concentration and the incubation time. This experimentally determined Km of ATX was in the range reported previously of 100 to 260 μM (112-114) and was within the normal range of LPC in plasma (115). Based on this information, the concentration of the substrate, 150 μM C16:0 LPC, used in the enzymatic reaction was selected based on kinetics studies that indicated the Km value of human recombinant ATX for LPC was 150 μM.

In order to select the incubation time for the functional assays, control experiments (without inhibitors) were carried out for various times (0, 30, 60, 90 and 120 minutes). A reaction time of 60 min was determined to be optimal, as C16:0 LPA formation was linear up to 60 minutes after which the reaction rate declined (Table 3.1). The calibration curve for the measurement of C16:0 LPA was linear (r2>0.998) over the range 10 pg/ml to 10 μg/ml, and the limit of detection (LOD) and limit of quantitation (LOQ) were 10 pg/ml and 50 pg/ml, respectively. The intraday and interday accuracies of C16:0 LPA measurement were from 97.4 to 102.3%, and the precision was within 4.5% for concentrations of 10 pg/ml to 10 μg/ml.

To develop a dose-response curve, additional functional experiments were carried out with various concentrations ranging from 0.01 to 10 μM PF-8380, S32826, GWJ-23 and BrP-LPA against 1 μM ATX enzyme at 37°C. Quantification of C16:0 LPA by using LC-MS/MS. The percent inhibition of the reaction product C16:0 LPA was calculated using the following equation: 100(A0 - A)/A0, where A0 was the amount of C16:0 LPA (reaction product) formed when no inhibitor was present and the C16:0 LPA concentration in the presence of respective inhibitor. The IC_{50} values of PF-8380, S32826, GWJ-23 and BrP-LPA were calculated by nonlinear regression analysis using sigmoidal dose-response curve fitting. The regression square value of the dose-response curve was 0.995, and the IC_{50} values for the inhibition of ATX by PF-8380, S32826, GWJ-23 and BrP-LPA are shown in Table 3.2.

Table III 16:0 LPA Formed in Control Experiments Performed at Incubation Times 0, 30, 60, or 90 min

Incubation time (min)	16:0 LPA μM
0	0.513 ± 0.03
30	5.429 ± 0.05
60	14.162 ± 0.02
90	12.839 ± 0.07

*Control experiments were carried out without inhibitor

Table IV IC_{50} values for the inhibition of ATX by PF-8380, S32826, GWJ-23 or BrP-LPA

ATX inhibitors	IC50
PF-8380	2.8nm
S32826	9nm
GWJ-23	18nm
BrP-LPA	100–200 nM

ATX inhibitors	IC50 for ATX
PF-8380	4.1nm
S32826	12.7nm
GWJ-23	29.3 nm
BrP-LPA	180 nM

Glabridin is the first ATX inhibitor known to occur in plants. The natural source of glabridin, the licorice species *G. glabra*, has long been used to treat a variety of diseases including peptic ulcers, hepatitis C, and pulmonary and skin diseases and exhibits a wide range of pharmacological properties including antiinflammatory, antiviral, antimicrobial, antioxidative, anticancer, immunomodulatory, hepatoprotective, and cardioprotective effects (116). Since its initial isolation and structure determination from *G. glabra* in 1976, glabridin (117) and standardized licorice extracts have had an increasingly significant impact on the food, dietary supplements and cosmetic markets. The inhibition of ATX by glabridin probably accounts for some of the anti-inflammatory properties of *G. glabra.* Although in comparison with PF-8380 (IC_{50} 2 nM) and other published ATX inhibitors, glabridin was a weaker inhibitor ($IC_{50} > 0.5$ μM), it represents a new scaffold for the development of more potent inhibitors of ATX that may overcome some of the limitations of these previously reported compounds in terms of their safety and efficacy (118).

3.4 Conclusion

We developed a PUF-LCMS based binding assay for ligands of the enzyme ATX and validated it using the known ATX inhibitors PF-8380 and S32826. The assay was successfully applied to the screening of botanical extracts, and the natural product glabridin, from *G. glabra*, was identified through dereplication. As with PUF-LCMS assays reported for other targets, complex botanical extracts can be screened and hits characterized and dereplicated much faster than is possible using the conventional bioassay-guided fractionation approach. Even if a natural product hit is a novel structure and cannot be identified through dereplication, the use of high-resolution accurate mass measurement and tandem mass spectrometry during the assay provide insight into the structure of the hit. As the chromatographic retention time of the hit is known, this can be a starting point for isolation of the natural product for additional structural characterization.

To complement the screening assay, a functional ATX inhibition assay was developed and validated based on the LC-MS/MS measurement of the enzymatic conversion of C16:0 LPC to C16:0 LPA. This sensitive assay uses small amounts of enzyme that are comparable to those required for optical-based commercial kits. The assay is also fast and requires less than 5 min per sample.

4. FIBROBLAST-SPECIFIC DELETION OF VON HIPPEL-LINDAU PROTEIN PROTECTS AGAINST BLEOMYCIN-INDUCED PULMONARY FIBROSIS IN A HIF-INDEPENDENT PATHWAY

4.1 Introduction

Idiopathic pulmonary fibrosis (IPF) is a chronic and ultimately fatal disease characterized by a progressive loss of lung function without clear etiology. Recent approvals of Ofev (Nintedanib) and Esbriet (Pirfenidone) by the U.S. Food and Drug Administration (FDA) as novel orally antifibrotic available drugs indicated for IPF marked a milestone for an effective therapies of IPF (119). Although both agents are "First-in-class" products which offer the promising option to slow down the progression IPF, the therapeutic effects of these medications are rather modest and were only tested in a very short time period. Therefore, there is an urgent need to explore novel strategies to enlighten the management of IPF patients.

The von Hippel-Lindau protein, also known as pVHL, is a protein expressed in human and is encoded by the *VHL* gene. Researchers first identified Von Hippel-Lindau protein (pVHL) as a tumor suppressor since the mutation of VHL gene has a strong association with tumors via activation of hypoxia-inducible factor (HIF) (120-124), however, more emerging evidence indicates that VHL also plays an important role in alveolar epithelial function epithelial cilia maintenance (124), extracellular matrix assembly, cell proliferation(124-132) and cytoskeleton dynamics through HIF-independent functions. Although the role of VHL in human diseases is mostly illustrated in a loss-of-function model (133), recent published results show that VHL protein is overexpressed in patients with IPF (134, 135) and chronic obstructive pulmonary disease (COPD).

Our previous data showed that lungs from patients with IPF overexpressed VHL protein in fibroblastic foci (135). Bleomycin treatment also induced increased VHL expression in mouse lung fibroblasts, but not increased in alveolar type II cells (135). We believe that overexpression of VHL may lead to increased lung fibroblast proliferation, induction of collagen, fibronectin and fibronectin receptor α5 integrin subunit, and increased activation of focal adhesion kinase (FAK) (135). Furthermore, suppression of VHL expression prevented the proliferation of mouse embryonic fibroblasts induced by TGF-β1 (135). These results suggest that overexpression of

VHL causes the activation of integrin/FAK signaling pathway, fibroblast proliferation, and fibrosis, aberrant expression of fibronectin and collagen.

In this study, we obtained novel evidence that fibroblast-specific pVHL (Fsp-VHL) plays a critical role in the blelomycin-induced mouse fibrosis model. We generated novel strains of fibroblast specific knockout or knockdown mice to identify whether suppression of pVHL in fibroblasts prevents bleomycin-induced pulmonary fibrosis independent of HIF activation. Paradoxically, we found that pVHL is only involved in pulmonary fibrosis but is not affected by bleomycin-induced lung injury and inflammation. Moreover, suppression of pVHL blocks the activation of Wnt and promotes the antifibrotic PGE signaling. Together, our data suggest that pVHL is essential for the development of pulmonary fibrosis in bleomycin-induced mouse fibrosis model.

Previously we reported that von Hippel-Lindau protein (pVHL) expression is elevated in human and mouse fibrotic lungs and that overexpressed pVHL stimulates fibroblast proliferation. We sought to determine whether loss of pVHL in fibroblasts prevents bleomycin-induced injury or fibrosis *in vivo*. We generated heterozygous fibroblast specific pVHL knockdown mice (Fsp-VHL+/-) and homozygous fibroblast specific pVHL knockout mice (Fsp-VHL$^{-/-}$by crossbreeding *vhlh* 2-lox mice (VHL$^{+/+}$) with Fsp-Cre mice. We found that Fsp-VHL$^{-/-}$ but not Fsp-VHL$^{+/-}$ mice had elevated red blood cell counts, hematocrit, and hemoglobin content, an indicator of HIF activation. To examine the role of pVHL in bleomycin-induced lung injury and fibrosis *in vivo*, we administered PBS or bleomycin to age-, sex- and strain-matched 8 week-old VHL$^{+/+}$, Fsp-VHL$^{+/-}$ and Fsp-VHL$^{-/-}$ mice. In Fsp-VHL$^{+/-}$ and Fsp-VHL$^{-/-}$ mice, bleomycin-induced collagen accumulation, fibroblast proliferation, differentiation, matrix protein dysregulation was prevented. Suppression of pVHL also decreased bleomycin-induced Wnt signaling and PGE2 signaling. Loss of pVHL decreased inflammation 21 days after administration of bleomycin. Taken together, these results suggest that pVHL plays a critical role in bleomycin-induced pulmonary fibrosis, possibly via HIF-independent pathway.

4.2 Methods and Procedures

4.2.1 Mice.

Homozygous *vhlh* 2-lox mice (provided by Dr. Volker Haase from Vanderbilt University) and homozygous (Fsp)-Cre mice (provided by Dr. Anthony J Trimboli from laboratories of Dr. Gustavo Leone and Michael C. Ostrowski from the Ohio State University) were crossbred to generate mice with fibroblast-specific knockout of VHL (18, 19). Tail DNA from their offspring was tested by PCR to identify the genotypes with the primers listed in Table 4.1 on a Mastercycler epgradient S model (Eppendorf, Hamburg/Germany) (136, 137). Animal studies were done following the procedures from the National Institutes of Health and experimental protocols were approved by the University of Illinois at Chicago Institutional Animal Care and Use Committee.

4.2.2 Chemical and Reagents

PGE2, PGD2, d4-PGE2, and d4-PGD2 were purchased from Cayman Chemicals (Ann Arbor, MI). Citric acid and bleomycin were purchased from Sigma-Aldrich (St. Louis, MO). Butylated hydroxytoluene (BHT) was purchased from Thermo Fisher Scientific (Rockford, IL), and formic acid was purchased from EMD Chemicals (San Diego, CA). Purified water was prepared using an ELGA (Saint Maurice Cedex, France) PURELAB Ultra purification system. All organic solvents were HPLC grade or better and were purchased from Thermo Fisher Scientific (Rockford, IL), and all other chemicals and solvents were ACS reagent grade, unless stated otherwise.

4.2.3 Delivery of Bleomycin and PBS to Mice Lungs.

50 µl of saline or bleomycin (50 µl, 0.045 units) dissolved in saline was delivered intratracheally as described previously (17, 20). Briefly, mice were sedated and secured. We used a flexible metal wire to guide the placement of angiocath and then administered bleomycin by direct instillation into the angiocath (two 25 µl aliquots 2 minutes apart) using a Hamilton syringe.

4.2.4 Isolation and Culture of Mouse Lung Fibroblasts.

Mouse lung fibroblasts were isolated from mice following published procedures (135). The identification of mouse lung fibroblasts was done basing on the morphology and expression of vimentin and collagen. Finally, the viability of cells was analyzed by Trypan blue exclusion assay.

4.2.5 Histological Analysis.

The mouse lungs have were removed *en bloc*, fixed in 10% paraformaldehyde, embedded in paraffin and sectioned. These lung sections were used for staining with H&E and Masson's Trichrome staining (135).

4.2.6 Bronchoalveolar lavage (BAL) Analysis

BAL fluid were collected through a 20-gauge angiocath ligated into the trachea as described (138). 1 ml PBS/mouse were injected to collect the BAL. 200-µl aliquot of the BAL fluid will be placed in a cytospin and used for Wright staining to determine cell counts and cell differential analysis. The supernatant of remaining BAL fluid were used for the measurement of BAL protein (Bradford) (135).

4.2.7 Sircol Assay

Mouse lungs were homogenized and aliquots of lung homogenates were assayed for total lung collagen levels using the Sircol collagen dye binding assay (Bicolor Ltd., Northern Ireland, UK) according to the manufacturer's directions.

4.2.8 Measurement of PGD2 and PGE2 by Mass Spectrometry

Quantitative analysis of PGD2 and PGE2 were carried out by UHPLC-MS/MS as described previously (139). UHPLC separations were performed using a Shimadzu (Columbia, MD) Nexera UHPLC system equipped with a Waters (Milford, MA) Acquity ultra performance liquid chromatography (UPLC) BEH C_{18} (2.1 mm × 50 mm, 1.7 µm) analytical column. An isocratic mobile phase consisting of acetonitrile/aqueous 0.1% formic acid (40:60, v/v) was used at a flow rate of 1.2 ml/min. The UHPLC column temperature was 50°C. The operating pressure was 0.690 mBar (10,000 psi), and the sample injection volume was 5 µl. The UHPLC system was interfaced to a Shimadzu LCMS-8040 triple quadrupole mass spectrometer, and prostanoids were

detected using negative ion electrospray. The ion source conditions were as follows: 350°C interface temperature, 3,500 V interface voltage, 250°C DL temperature, 400°C heat block temperature, 3 l/min nebulizer gas, and 15 l/min drying gas. The UHPLC-MS/MS system was controlled using Shimadzu LabSolutions 5.41.239 software. During MS/MS, argon was used for collision-induced dissociation, and the Q1, Q3 pre bias and collision energy were optimized for each analyte. The selected reaction monitoring (SRM) dwell time was 15 ms, and the switching time between SRM transitions was 1 ms. Isomeric PGD2 and PGE2 were measured using a SRM transition of *m/z* 351 to *m/z* 271, and the SRM transition of *m/z* 355 to *m/z* 275 was selected for the internal standards d4-PGE2 and d4-PGD2.

Stock standard solutions of the 6 prostanoids (PGE_2 and PGD_2) and 2 internal standards (d_4-PGE_2, and d_4-PGD_2) were prepared in methanol at a concentration of 100 µg/ml each. Working standard mixture solutions of the 2 analytes and 2 internal standards at 10 µg/ml each were prepared by dilution of the stock solutions in methanol/water (50:50, v/v). All stock solutions and working solutions were stored at -20°C in the dark. PBS was spiked with calibration standards containing 2 analytes at concentrations of 0.05, 0.1, 0.5, 1, 2, 5, 10, 20, 50, 100, 200, 500, 800, and 1000 ng/ml to make a final volume of 500 µl for each solution. Samples for quality control (QC) were prepared by spiking appropriate aliquots of the working solution into PBS at concentrations of 0.1, 4, 400, and 750 ng/ml. The spiked samples were treated as the same as BAL.

4.2.9 Quantitative Real-Time RT-PCR and Microarray Analysis.

Total RNA was extracted using the miRNeasy mini kit (Qiagen, Valencia, CA) and quantified with Nanodrop 2000 Spectrophotometer (Thermo Scientific., Waltham, MA). Synthesis of complementary DNA (cDNA) was performed using the ABI High Capacity cDNA Reverse Transcription Kit (Applied Biosystems, Foster City, CA). Quantitative real-time RT-PCR (qRT-PCR) was carried out on the ABI StepOnePlus real-time PCR system using the ABI SYBR Green PCR master mix (Applied Biosystems). The amplification of the genes was normalized to the amplification of the mitochondrial ribosomal protein L19 (RPL19). The sequences of the primers used in the real time qRT-PCR are shown in Table 4.1. We overexpressed pVHL in N12 human fibroblast by infection of pAd-VHL-HA (pAd-GFP was used as control infection) (135), extracted the total RNAs, and performed microarray analysis with Affymetrix GeneChip Human Genome U133 Plus 2.0 Array. Data was analyzed in Partek Genomics statistical package from

Partek, (St. Louis, MO). Hybridization signal intencyties were normalized by quantiles and summarized using the Robust Multi-array Average (RMA) (140).

4.2.10 Measurement of TGF-β1 in BAL fluid

Levels of TGF-β (R&D Systems, Minneapolis, MN) were measured using an ELISA kit following the manufacturer's protocol. The optical density of each well was read using a GloMax-Multi Detection System (Promega, Madison, WI) set to 450 nm with wavelength correction set to 540 nm.

4.2.11 Statistical Analysis.

Results were presented as mean (± SEM). First we used one way analysis of variance (ANOVA) to analyze data. Then once the ANOVA showed a significant difference, the Bonferroni correction post-test was performed to compare all individual groups. The statistical significance level was set at 0.05 level.

4.3 Results

4.3.1 Fibroblast Specific Knockout of pVHL and Activation of HIF.

Previously, we have shown that VHL is upregulated in fibroblasts in fibrotic tissues and overexpression of VHL induces fibroblast proliferation (135), indicating that pVHL may involve into the development of IPF. To test our hypothesis, we investigated whether loss of VHL can prevent pulmonary fibrosis. Strains of fibroblast specific VHL knockdown (Fsp-VHL$^{+/-}$) and knockout mouse (Fsp-VHL$^{-/-}$) were generated by crossbreeding the homozygous *vhlh* 2-lox (VHL$^{+/+}$) mice (provided by Dr. Volker Haase of Vanderbilt University) with homozygous Fsp-Cre mice (provided Dr. Gustavo Leone of the Ohio State University) (figure 4.1A) (136, 137). Two *loxP* sites which develop normally flank the *VHL* promoter and the first exon in *vhlh* 2- lox mice. In Fsp-Cre mice, the fibroblast specific protein-1 (Fsp-1; also known as S100A4) promoter (137, 141) drives the Cre expression. In lung, fibroblasts but not macrophages or ATII cells express Fsp-1 and Fsp-1 expresses in procollagen positive cells, suggesting that in lung Fsp-1 is also fibroblast relatively specific (142). We confirmed the genotypes of Fsp-VHL$^{fl/fl}$, Fsp-VHL$^{+/-}$ and Fsp-VHL$^{-/-}$ mice by analyzing the DNA samples obtained from mouse tails using the PCR technique (figure 4.1B). Mouse lung fibroblasts (MLF) from these mice were also isolated and pVHL mRNA from MLF were analyzed. We confirmed that the level of pVHL mRNA in Fsp-VHL$^{+/-}$ and Fsp-VHL$^{-/-}$ mice were graded knockdown (figure 4.1C). Two commercial pVHL antibodies were used to detect pVHL proteins in MLF; however, no bands were showed in neither of them even in wild-type MLFs, indicating a limited application of pVHL antibodies on MLFs. pVHL is a known E3 ligase which aims at HIFα for proteosome degradation and loss of pVHL results in increased HIF activity (133, 143). As expected, Fsp-VHL$^{-/-}$ mice showed elevated levels of hematocrit (HCT), red blood cells (RBC) and hemoglobin (HGB), suggesting HIF activation (figure 4.1D-4.1F). However, levels of RBC, HCT, and HGB from Fsp-VHL$^{+/-}$ mice showed no significant difference with levels from wild type mice (figure 4.1D-4.1F), suggesting that knockdown of VHL is not sufficient to activate HIF pathway.

Furthermore, elevated mRNA levels of HIF downstream genes, vascular endothelial growth factor(VEGF), erythropoietin (EPO), and glucose transporter (Glu) 1 were shown in MLFs isolated from Fsp-VHL$^{-/-}$ mice, but not Fsp-VHL$^{+/-}$ mice (figure 4.1G-4.1I). These results indicated that the HIF pathway was activated in Fsp-VHL$^{-/-}$ mice, but not Fsp-VHL$^{+/-}$ mice. Thus,

Fsp-VHL$^{+/-}$ and Fsp-VHL$^{-/-}$ mice are an ideal model to explore the HIF-dependent and HIF-independent functions of pVHL during pulmonary fibrosis. To measure the percentage of Fsp-1-positive population in MLFs, we labeled MLFs isolating from Fsp-VHL$^{fl/fl}$ mice with Fsp-1 antibody, and analyzed them by using fluorescence-activated cell sorting test. This result showed that 93.97 (3.84) % (mean [±SEM]) of MLF were Fsp-1 positive **(Figure 4.1J)**. In comparison, 96.21% of pooled MLF, which isolated from five Fsp-VHL$^{-/-}$ mice were Fsp-1 positive. These data indicated that knockout of pVHL does not change the population of Fsp-1-positive MLF.

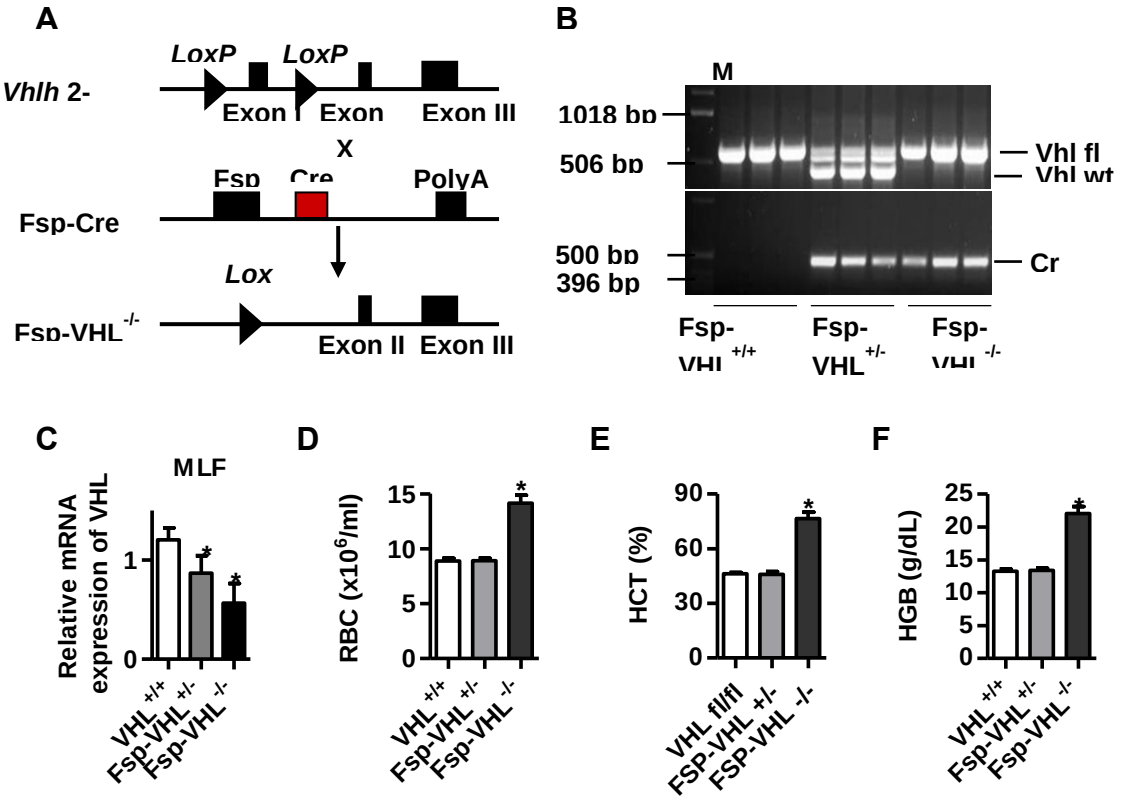

Figure 4.1 The figure shows conditional knockout of VHL in fibroblasts**.** A) Schematic illustration of the generation of heterozygous fibroblast specific VHL knockout mice (Fsp-VHL$^{+/-}$) as well as homozygous VHL knockout mice (Fsp-VHL$^{-/-}$). This is achieved by crossbreeding *vhlh* 2-lox (VHL$^{fl/fl}$) mice with Fsp-Cre mice. B) Genotypes of these mice were confirmed by PCR using DNAs obtained from the tails of mice. C) Mouse lung fibroblasts (MLF) were then isolated from these mice where they were used to measures the mRNA levels of VHL. D-F) The mice were anesthetized and the blood was drawn to measure the amounts of hematocrit (HCT), red blood cells (RBC), and hemoglobin (HGB). n≥5; *, P<0.05; **, p<0.01.

4.3.2 Suppression of Fibroblast-Specific pVHL Prevents Bleomycin-Induced Pulmonary Fibrosis *in Vivo*.

To test the hypothesis that VHL plays a key role in bleomycin-induced pulmonary fibrosis, we delivered bleomycin (0.045 units dissolved in 50 μl saline)/mouse intratracheally to $VHL^{+/+}$, Fsp-$VHL^{+/-}$, and Fsp-$VHL^{-/-}$ mice for 21 successive days. We used mice administered with the same volume of PBS as control. 21 days after successive administration, the lung tissues of these mice were harvested and the collagen contents which is a hallmark of fibrosis were measured. As shown in figure 4.2A, despite Fsp-$VHL^{-/-}$ mice exhibited a slight elevation of basal collagen expression, both Fsp-$VHL^{+/-}$ and Fsp-$VHL^{-/-}$ mice displayed an increased collagen expression in bleomycin-administrated mice. Meanwhile, Fsp-$VHL^{+/-}$ and Fsp-$VHL^{-/-}$ mice also showed an increase of the mRNA levels of col1a1 and col1a2 (figure 4.2B and 4.2C). Furthermore, the results of Masson's Trichrome staining confirmed our observation (figure 4.2D). Above all, these results indicate that pVHL has a HIF-independent function in the development of pulmonary fibrosis.

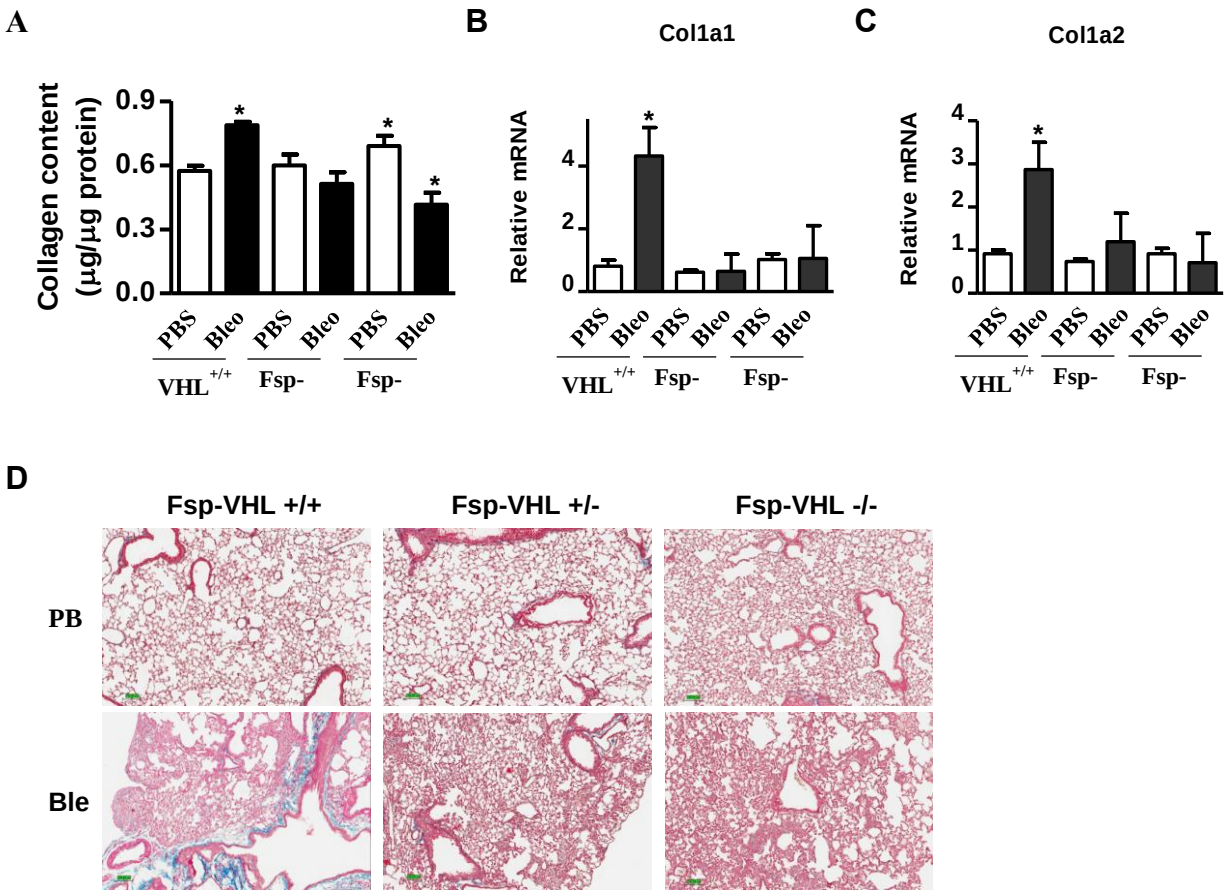

Figure 4.2. Suppression of fibroblast-specific pVHL prevents bleomycin-induced fibrosis *in vivo*. Wild type ($VHL^{+/+}$) mice and Fsp-$VHL^{+/-}$ and Fsp-$VHL^{-/-}$ mice were administered with PBS or Bleomycin intrachacheally. 21 days later, the lungs of these mice were collected and used for collagen analysis by the Sircol assay (A), real time qRT-PCR (B-C), and Masson's Trichrome staining (D). RPL19 gene was used as internal control for qRT-PCR. n≥5; *, P<0.05; **, p<0.01.

4.3.3 Suppression of Fibroblast-Specific pVHL Prevents Bleomycin-Induced Pulmonary fibroblast Proliferation, Differentiation, and Matrix Protein Dysregulation *in Vivo*

As we know, pulmonary fibrosis is related with fibroblast proliferation, differentiation, and ECM protein dysregulation. To address whether inhibition of VHL can prevent pulmonary fibrosis via suppression of fibroblast proliferation *in vivo*, we measured the levels of mouse proliferating cell nuclear antigen (PCNA) in lung tissues collected from the $VHL^{+/+}$, Fsp-$VHL^{+/-}$, and Fsp-$VHL^{-/-}$ mice which were administrated PBS or bleomycin for 21 successive days. Our results showed that the expression levels of bleomycin-induced PCNA were decreased in Fsp-$VHL^{+/-}$ and Fsp-$VHL^{-/-}$ mouse lungs (figure 4.3A). Our results also suggested that suppression of VHL decreased the level of bleomycin-induced α-SMA (Acta2) (figure 4.3B). Above all, we concluded that suppression of fibroblast-specific VHL prevents fibroblast proliferation and differentiation.

Expression of ECM proteins is dysregulated in the pathogenesis of pulmonary fibrosis. Previously our data indicated that overexpression of VHL upregulates the expression of Fn (fibronectin) and integrin α5β1 and activates FAK in lung fibroblasts, resulting in fibroblast proliferation (135). Our results showed that suppression of VHL in fibroblasts inhibited the expression of integrin α5β1 (figure 4.3C). MMP2 and MMP9 regulate the dysregulation of ECM during fibrosis (144, 145). Although suppression of VHL had little effect on the expression of bleomycin-induced MMP2 in the $VHL^{+/+}$, Fsp-$VHL^{+/-}$, and Fsp-$VHL^{-/-}$ mice, the expression level of MMP9 decreased in these mice (figure 4.3D and 4.3E). These data suggest that VHL may play an important role in ECM deposition in fibroblast via a MMP9-specific pathway.

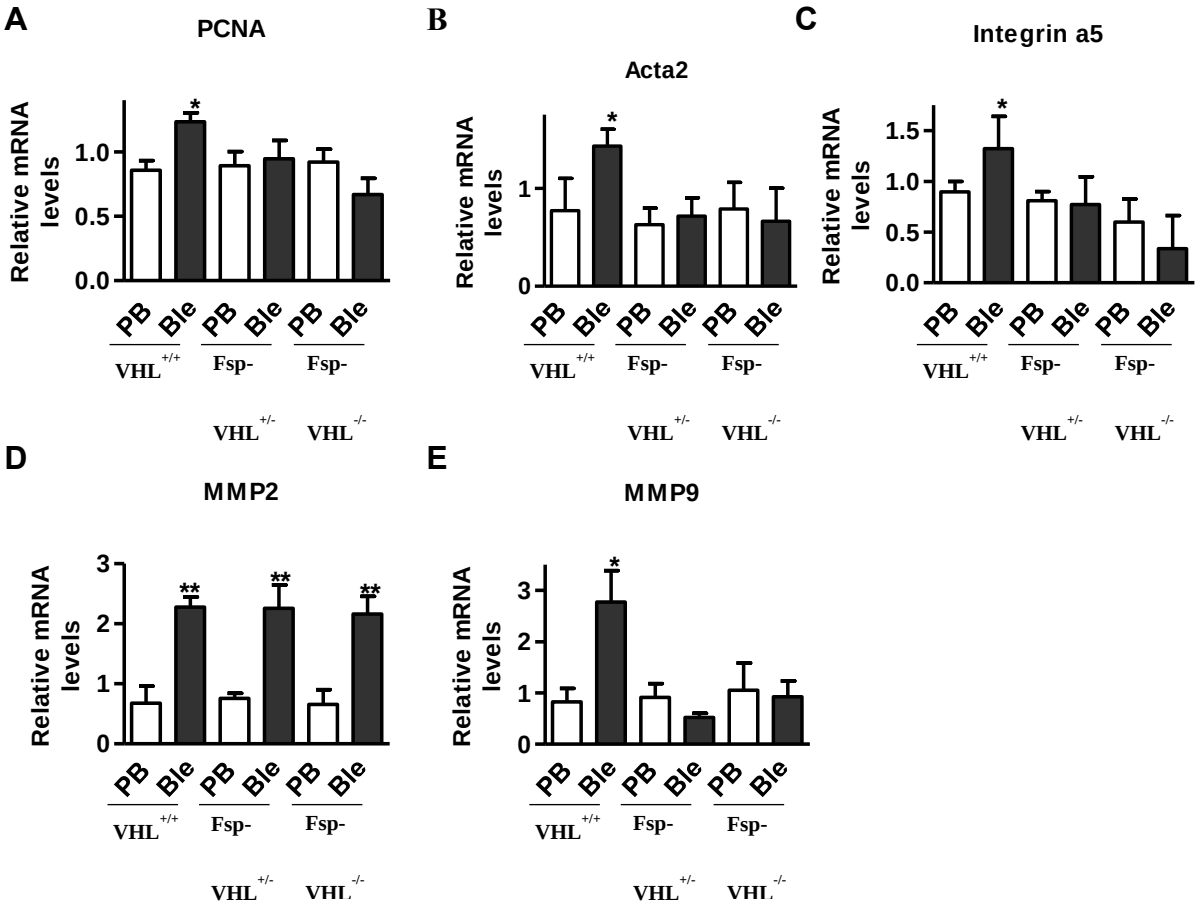

Figure 4.3. Suppression of fibroblast-specific pVHL prevents bleomycin-induced fibroblast proliferation, differentiation, and matrix protein dysregulation *in vivo*. We harvested lungs of $VHL^{+/+}$, Fsp-$VHL^{+/-}$, and Fsp-$VHL^{-/-}$ mice 21 days after administration of PBS and bleomycin. Mouse lungs were homogenized and used to extract total RNA for the measurement of mRNA levels of mouse PCNA (A), α-SMA (Acta2) (B), integrin α5 (C), MMP2 (D), and MMP9 (E) by real time qRT-PCR. RPL19 gene was used as internal control for qRT-PCR. n≥5; *, $p<0.05$; **, $p<0.01$; n.s, no significance. * and ** compare the difference between PBS and other groups. n.s. compares the difference between the high dose AD vector group and the bleomycin group.

4.3.4 Expression of VHL Correlates with the Wnt/Frizzled Pathway

Previous reports indicated that Wnt signaling plays a critical role in IPF (146-149). The levels of Wnt-2B, 5B and Frizzled (Fz)-related protein were found to be elevated in patients with IPF, and we know that β-catenin targets play an important role in promoting pulmonary fibrosis or proliferation (150-152). Wnt signaling pathways share the same essential elements in classical Wnt signaling through stabilizing β-catenin and translocating to the nucleus, however they have different ligands. To investigate whether VHL correlates Wnt signaling, overexpressed VHL in N12 fibroblast was used to do microarray analysis, the result showed that overexpression of VHL led to upregulation of Wnt signaling (figure 4.4A). In Fsp-VHL$^{+/-}$ and Fsp-VHL$^{-/-}$ mice, we found that bleomycin-induced expression of Wnt5b and Wnt16 decreased (figure 4.4B and 4.4C). Although bleomycin had no direct effects on lipoprotein receptor-related protein 6 (Lrp6) expression, Lrp6 expression was inhibited by suppressing VHL in the mice treated with bleomycin (figure 4.4D). These data indicated that Wnt signaling correlated with VHL expression.

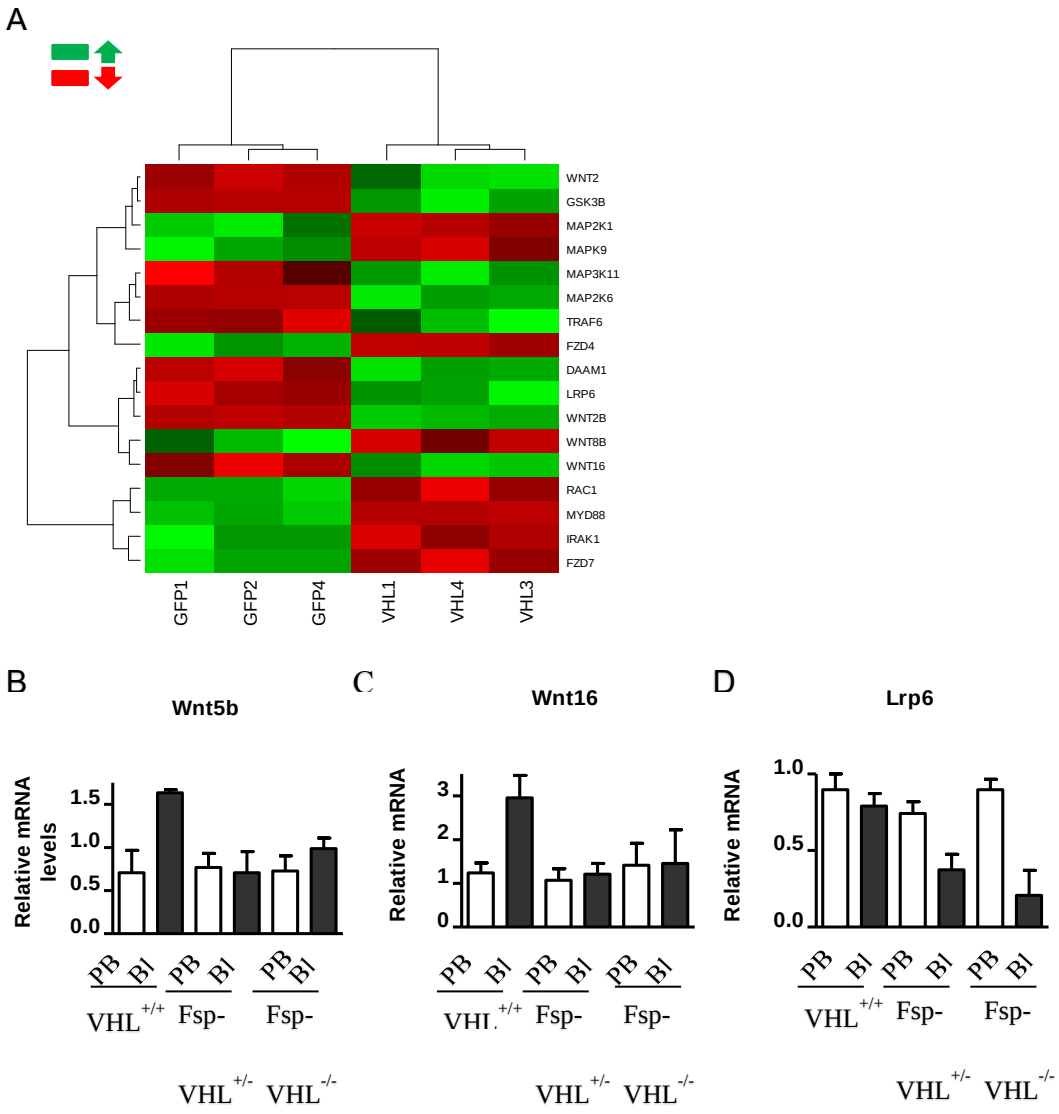

Figure 4.4. Expression of VHL correlates with the Wnt/Frizzled pathway. A) N12 cells infected with Ad-GFP or Ad-VHL-HA were used for microarray analysis with Affymetrix GeneChip Human Genome U133 Plus 2.0 Array. The overexpression of pVHL was validated in our previous publication (17). ANOVA test were used to calculate significance of the differential expression. Microarray expression data was analyzed by Pathway Studio® to represent all known relationships and potential interactions between the differentially expressed genes. The color of each cell denotes its log2 signal intensity. Black is the median of all signal intensities on the heat map. Green and red indicates the up- and down-regulated genes respectively. B-D) We measured the mRNA levels of Wnt5b (B), Wnt16 (C), Lrp6 (E) in lungs of $VHL^{+/+}$, Fsp-$VHL^{+/-}$, and Fsp-$VHL^{-/-}$ mice administered with PBS and bleomycin by real time qRT-PCR. RPL19 gene was used as internal control for qRT-PCR. n≥5; *, $p<0.05$; **, $p<0.01$; n.s, no significance. * and ** compare the difference between PBS and other groups. n.s. compares the difference between the high dose AD vector group and the bleomycin group.

4.3.5 Suppression of VHL Protects Bleomycin-Mediated Suppression of PGE2 and PGD2 in the Fibrotic Stage

Emerging data suggested that the loss of production of prostaglandins (PGs), including PGE_2, plays a critical role in the pathogenesis of IPF (153-155). Pulmonary fibrosis can be inhibited by PGE_2 signaling through inhibiting lung myofibroblast differentiation and migration (155, 156). Our results showed that PGE_2 levels decreased in the lungs collected from bleomycin-treated mice, whereas PGE_2 and PGD_2 levels showed no significant change in Fsp-$VHL^{+/-}$ and Fsp-$VHL^{-/-}$ mice treated with bleomycin (figure 4.5A-4.5B), indicating that pulmonary fibrosis in mice can be prevented by knockdown or knockout of VHL which can retain the homeostasis of PGE_2 signaling.

PGE_2 is converted from PGH_2 through the catalyzation of prostaglandin synthase enzymes (e.g., PGE synthases) (155,157). PGH_2 is synthesized by arachidonic acid (AA) and the conversion is catalyzed by cyclooxygenase (COX)-1 or COX-2 enzymes (155, 158). During pulmonary fibrosis PGE_2 exerts its anti-fibrosis effect via E-prostanoid (EP) receptors, particularly EP2 and EP4 (155, 159). To study the mechanism of restoring PGE2 signaling in Fsp-$VHL^{+/-}$ and Fsp-$VHL^{-/-}$ mice, we harvested lung tissue samples in these mice and quantitated the gene expression of COX-1, COX-2, PGE synthase1, 2, 3 and EP2 and EP4 by qRT-PCR. Our results suggested bleomycin administration upregulated the expression of COX-1, COX-2, PGE synthase1, 3, and EP2 in $VHL^{+/+}$ mice (figure 4.5C-4.5H), which is consistent with previous reports that there is compensatory induction of PGE_2 production and COX-2 expression immediately after bleomycin administration (160, 161). However, PGE synthase2 levels had no significant change (figure 4.5F). Interestingly, this compensatory elevation did not appear in the Fsp-$VHL^{+/-}$ and Fsp-$VHL^{-/-}$ mice treated with bleomycin (figure 4.5C-4.5F). In summary, these data indicate that suppression of VHL plays an essential role in maintaining PGE_2 homeostatis and prevent the development of pulmonary fibrosis.

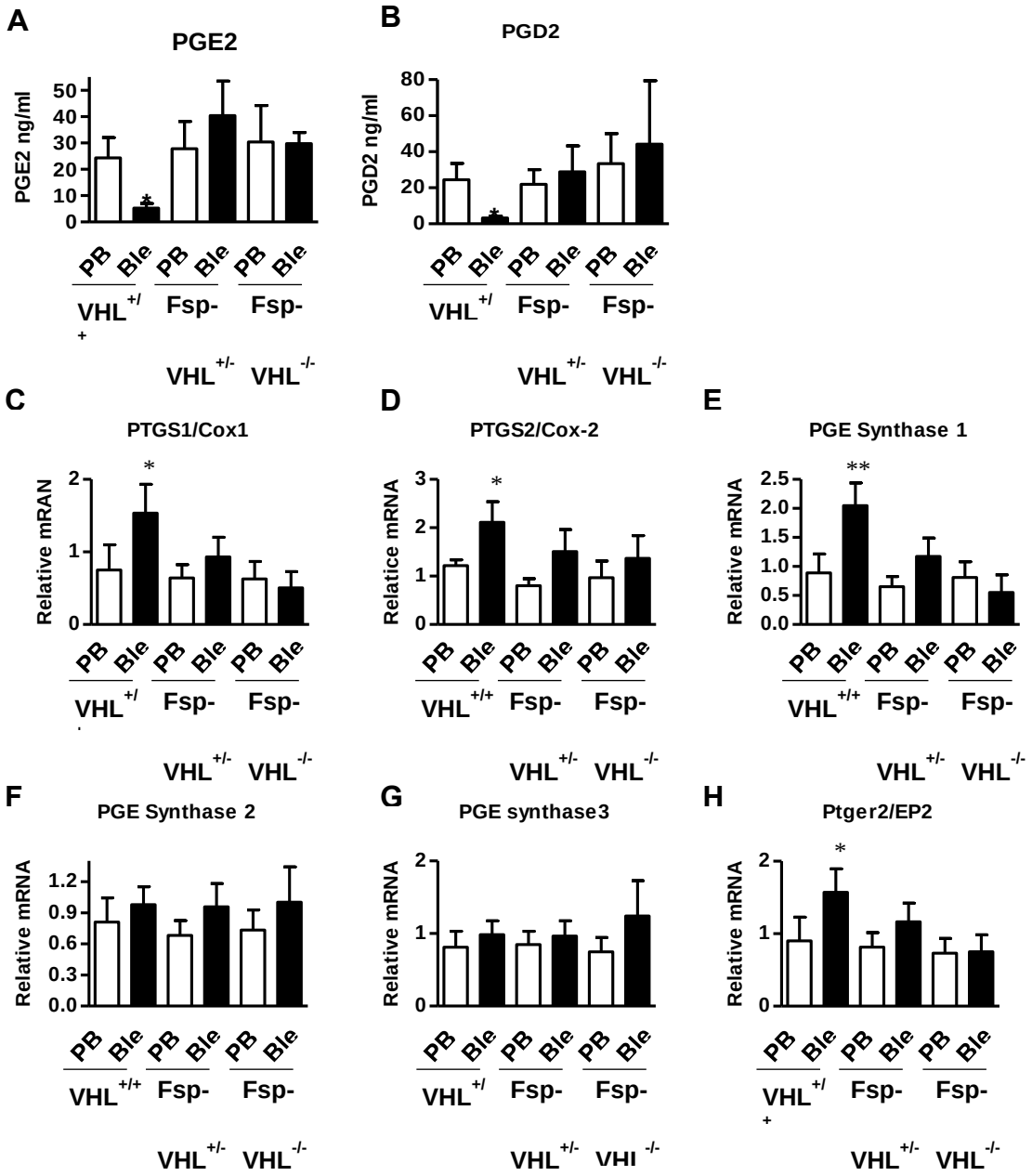

Figure 4.5. Loss of VHL protects bleomycin-mediated suppression of PGE2 and PGD2 in the fibrotic stage. We collected the BAL fluid from the $VHL^{+/+}$, Fsp-$VHL^{+/-}$, and Fsp-$VHL^{-/-}$ mice 21 days after administration of PBS and bleomycin and measured the contents of prostaglandin E (PGE_2) (A) and prostaglandin D (PGD_2) (B). C-H) We measured the mRNA levels of PTGS1/Cox1 (C), PTGS2(Cox2) (D), PGE synthase 1 (E), PGE synthase 2 (F), PGE synthase 3 (G), and Ptger2/EP2 (H) in lungs of these mice by real time qRT-PCR. RPL19 gene was used as internal control for qRT-PCR. n≥5; *, $p<0.05$; **, $p<0.01$; n.s, no significance. * and ** compare the difference between PBS and other groups.

4.3.6 Suppression of VHL in Pulmonary Fibroblasts Has Little Effect on Bleomycin-Mediated Lung Injury and Inflammation *in Vivo*

Inflammation may precede IPF and may be the first step of fibrogenesis. Profibrotic cytokines were secreted by inflammatory cells to stimulate fibroblasts which contribute to pulmonary fibrosis (162, 163). In the bleomycin-mediated pulmonary fibrosis, an initial acute lung injury and inflammatory response may precede lung fibrosis (138, 164) and lung fibrosis is maximal at ~ 21 days after bleomycin administration (165, 166). To explore whether suppression of VHL prevents bleomycin-induced lung injury and inflammation, we drew bronchoalveolar lavage (BAL) fluid from $VHL^{+/+}$, Fsp-$VHL^{+/-}$, and Fsp-$VHL^{-/-}$ mice which were treated with PBS or bleomycin for 5 days and analyzed the protein amount, cell counts and cell differentiation. Briefly, our results showed that $VHL^{+/+}$ and Fsp-$VHL^{+/-}$ mice had similar BALF protein amount, cell counts and cell differentiation, comparing with Fsp-$VHL^{-/-}$ mice which exhibited higher protein amount and cell differentiation (figure 4.6A-4.6C). TGF-β1 is reported to be a potent pro-fibrotic cytokine, however, suppression of VHL had no effect on the bleomycin-induced production of TGF-β1 in BALF (figure 4.6D). We also analyzed the gene expression of cytokines which were reported to involve in pulmonary fibrosis. These results showed that deletion of pVHL did not result in any significant changes on IL-1a, IL-1b, and IL-10 after bleomycin administration, but bleomycin-induced IL-6 expression was suppressed by the deletion of pVHL. Above all, our data indicates suppression of VHL has no effect on bleomycin induced lung injury and inflammation.

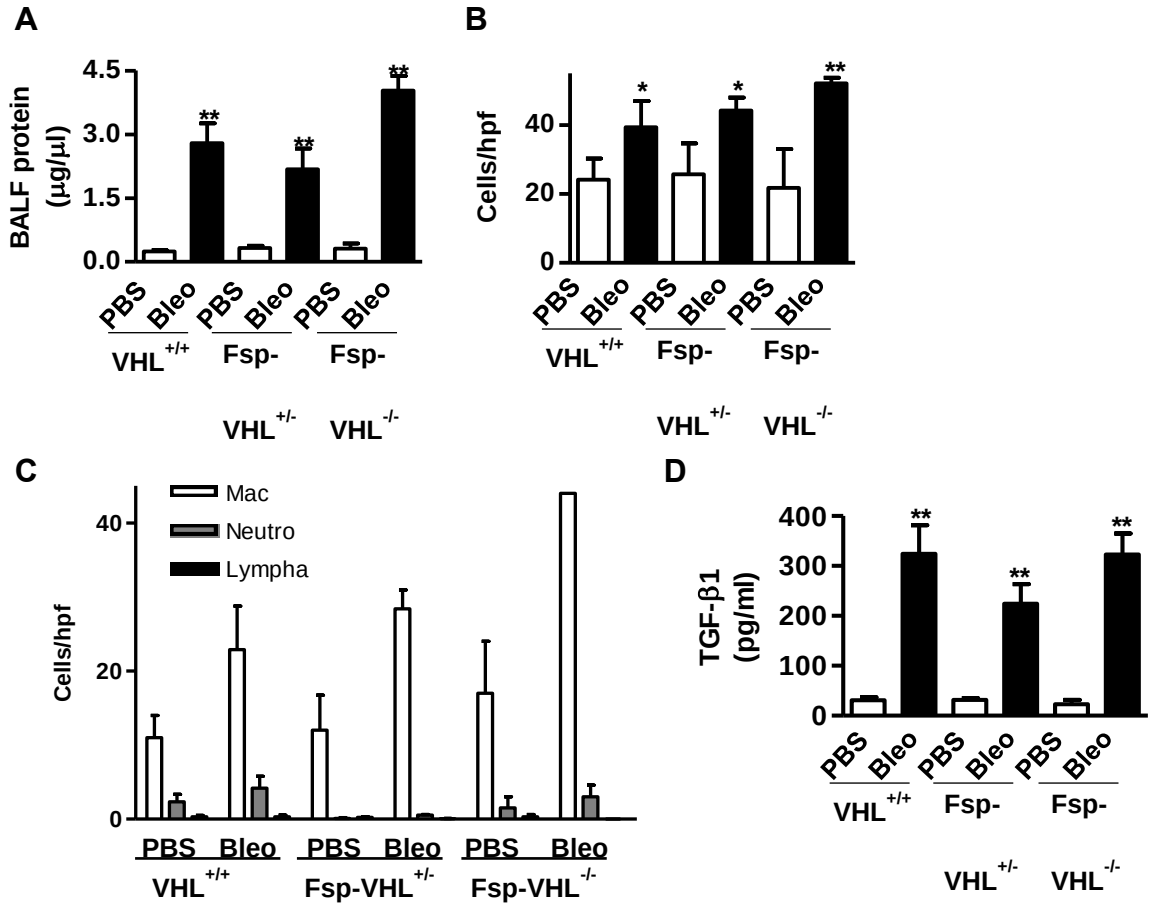

Figure 4.6. Suppression of pVHL in fibroblasts has no effect on bleomycin-induced lung injury and inflammation in the early stage. Wild type ($VHL^{+/+}$) mice and Fsp-$VHL^{+/-}$ and Fsp-$VHL^{-/-}$ mice were administered with PBS or bleomycin intratracheally, 5 days later, mouse bronchoalveolar lavage fluids (BALF) were collected and used to determine the protein concentration (A). Aliquots of 180 μ BALF were applied to cytospin and Wright staining to determine total cell counts (B) and differential cell counts (C) under microscope (200X magnification). The cell counts were expressed as numbers of cells/high power field (hpf). (D) The BALF was also used to determining the TGF-β1 concentration. n≥5; * and #, $p<0.05$; ** and ##, $p<0.01$; n.s, no significance. * and ** compare the difference between PBS and other groups. #, ##, and n.s. compare the difference between the high dose AD vector group and the bleomycin group.

Table V Primers for PCR

Gene	Forward primer (5'to 3')	Reverse primer (5'to 3')	Application
VHL	CTCAggTCATCTTCTgCAACC	TCTgTCTTggCCTCCTgAgT	genotyping
Cre	TCCTGCCCTTAGGTCTCAAC	CCTGTTTTGCACGTTCACCG	genotyping
VHL (mouse)	GCTCCTGCTGTAGTCCTG	CTTCTCTGCTGTAACTGTCTG	qRT-PCR
Col1a1 (mouse)	GCACGAGTCACACCGGAACT	AAGGGAGCCACATCGATGAT	qRT-PCR
Col1a2 (mouse)	CTACTGGTGAAACCTGCATCCA	GGGCGCGGCTGTATGAG	qRT-PCR
PCNA (mouse)	GCCAGACCTCGTTCCTCTTAGA	TCAGGCGTGCCTCAAACAT	qRT-PCR
Acta2 (mouse)	CGGGAGAAAATGACCCAGATT	GGACAGCACAGCCTGAATAGC	qRT-PCR
Integrin α5 (mouse)	AGGTGGGCAGGGTCTACATCT	CGAATCGGCTGAACTCATCTT	qRT-PCR
MMP2 (mouse)	GGACAGTGACACCACGTGACA	GGCCTCATACACAGCGTCAAT	qRT-PCR
MMP9 (mouse)	GGACGACGTGGGCTACGT	CACGGTTGAAGCAAAGAAGGA	qRT-PCR
Wnt5b (mouse)	CCAAGACGGGCATCAGAGA	CACGGTGCTGCAGTTCCA	qRT-PCR
Wnt16 (mouse)	TGTATGGTCGCCACTACCACTT	CGCTACTCAGCTCATAGCCAAA	qRT-PCR
Lrp6 (mouse)	TGGCTTGGCGGTGTGAT	TGCCCGCTGGCACACT	qRT-PCR
PTGS1/Cox1 (mouse)	TTCCGAGCCCAGTTCCAATA	GGATGCCAGTGATAGAGATGGTT	qRT-PCR
PTGS2/Cox2 (mouse)	CAGGTCATTGGTGGAGAGGTGTA	GGATGTGAGGAGGGTAGATCATCT	qRT-PCR
PGE synthase 1 (mouse)	TGGAGCGCTGCCTCAGA	AAGCCGAGGAAGAGGAAAGG	qRT-PCR
PGE synthase 2 (mouse)	AGGCCTTCGACGACCTGAT	TCAATGGCCCGCTCCAT	qRT-PCR
PGE synthase 3 (mouse)	CGCCCACCCGTTTGTCT	TCGATCGTACCACTTTGCAGAA	qRT-PCR
Ptger2/EP2 (mouse)	GCAACATCAGCGTTATCCTCAA	AATCCGCAGCGGCTTCTT	qRT-PCR
IL-1a (mouse)	GCCCGTGTTGCTGAAGGA	AGAAGAAAATGAGGTCGGTCTCA	qRT-PCR
IL-1b (mouse)	CTACAGGCTCCGAGATGAACAAC	TCCATTGAGGTGGAGAGCTTTC	qRT-PCR
IL-6 (mouse)	CGCTATGAAGTTCCTCTCTGCAA	GGAAGGCCGTGGTTGTCA	qRT-PCR
TNF-α (mouse)	CCCAAGGCGCCACATCT	CCACGTCGCGGATCATG	qRT-PCR
TGF-β1 (mouse)	TCGACATGGAGCTGGTGAAA	CTGGCGAGCCTTAGTTTGGA	qRT-PCR
TGF-β2 (mouse)	ACCTTTTTGCTCCTGCATCTG	TGCGCATAAACTGATCCATGTC	qRT-PCR
TGF-β3 (mouse)	TGACCCACGTCCCCTATCAG	CCCCGTGCATCTCTTCCA	qRT-PCR

5. CONCLUSION AND DISCUSSION

The current theory proposes that suppression of pVHL activates HIF, which leads to pulmonary fibrosis by enhancing epithelial mesenchymal transition or pulmonary hypertension (133, 143). Interestingly, fibrotic fibroblasts upregulate pVHL, overexpression of which enhances fibroproliferation and production of collagen and fibronectin, independently of HIF function (135). Consistently, our results suggest that bleomycin-induced lung fibrosis is prevented in both Fsp-VHL$^{+/-}$ and Fsp-VHL$^{-/-}$ mice (figure 4.2). Thus, this study makes the first causal link between VHL in fibroblasts and fibrosis using mouse models. Furthermore, our results suggest that resistance to bleomycin-induced pulmonary fibrosis (figure 4.2) in both Fsp-VHL$^{+/-}$ (HIF is not activated, figure 4.1) and Fsp-VHL$^{-/-}$ (HIF is activated, figure 4.1) mice is mediated by a HIF independent function of pVHL. These results support our previous finding that overexpression of VHL induces fibroblast proliferation and expression of collagen and Fn (fibronectin) in an HIF independent pathway, but not fibronectin/integrin/FAK dependent pathway (figure 4.7) (135). Therefore, our study shifts the paradigm of the role of pVHL in fibrosis from loss-of-function to a gain-of-function and HIF-independent function of pVHL in promoting fibrogenesis.

It is worth pointing out that there is a mild elevation of collagen in Fsp-VHL$^{-/-}$ mice both with and without bleomycin administration, indicating there might be a spontaneous pulmonary fibrosis in Fsp-VHL$^{-/-}$ mice. In addition, researchers reported that mice with mutation of the pVHL at codon 200 (R200W) exhibited pulmonary vascular remodeling, hemorrhage, edema, and macrophage infiltration and fibrosis in the end stage assumably via a HIF2-dependent pathway (143). We assumed that HIF will be stabilized by losing both alleles of VHL in Fsp-VHL$^{-/-}$mice, which may activate the recruitment and migration of fibrocytes to wound sites, causing pulmonary fibrosis (167-170). Overall, the role of pVHL in lung fibrosis may be complicated and involves in both HIF independent and HIF dependent pathways.

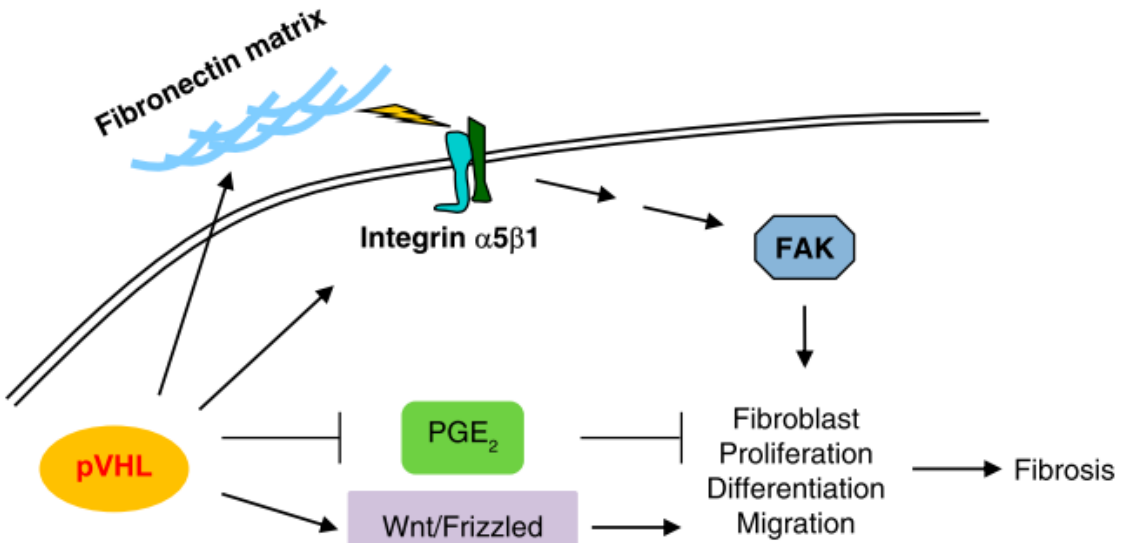

Figure 4.7 A schematic diagram depicting the role of pVHL on fibroblast phenotype and pulmonary fibrosis. pVHL may act at multiple levels, such as Fn/integrin α5β1/focal adhesion kinase (FAK), PGE 2 , and Wnt/Frizzled pathways to coordinately regulate fibroblast proliferation, differentiation, and migration during fibrogenesis.

Fibrotic diseases including IPF are characterized with hyperproliferation of fibroblasts, differentiation of fibroblasts into collagen-producing myofibroblasts, and deregulated ECM remodeling. Inhibition of pVHL in fibroblasts leads to decreased expression of PCNA and α-SMA in mice administrated with bleomycin (figure 4.3A and 4.3B), indicating that fibroblastic pVHL is required for fibroblast proliferation and differentiation into myofibrolasts. Our results show that overexpression of pVHL activates fibroblast proliferation via an integrin α5 dependent function (135). Consistently, we have reported that inhibition of fibrotic pVHL alleviates the expression of bleomycin-induced integrin α5 (figure 4.3C). ECM protein synthesis and degradation are controlled by several mechanisms and degradation of ECM proteins is mainly regulated by MMPs, among of which MMP2 and MMP9 are dysregulated and overexpressed in fibrotic diseases including IPF (171). Our results also indicated that both MMP2 and MMP9 mRNA are overexpressed in bleomycin-administrated mice, and that inhibition of pVHL only suppresses bleomycin-induced of MMP9 (figure 4.3D and 4.3E), indicating an MMP9 specific signaling pathway in pVHL-mediated pulmonary fibrosis, similar to adenoviruses infection-induced fibrosis (172).

Previous reports showed that IPF patients have increased levels of Wnt2, Wnt2b, Wnt5b and Fz-related protein which are well reported to induce pulmonary fibrosis (150-152). Moreover, bleomycin-mediated pulmonary fibrosis in mice can be prevented by inhibiting the Wnt/β-catenin signaling pathway (173). We found that overexpression of pVHL in fibroblasts activates Wnt signaling pathway, whereas suppression of pVHL blocks bleomycin-induced Wnt5b and Wnt16 and decreases the level of Lrp6 in bleomycin-treated mice (figure 4.4). Therefore, according to these data, we conclude that there is a link between pVHL-Wnt-fibrosis. However, the mechanism how pVHL regulates Wnt signaling pathway remains unknown and needs further study.

During the pathogenesis of pulmonary fibrosis, researchers have reported that PGE_2 production decreased and induced pulmonary fibrogenesis via activation of lung myofibroblast differentiation and migration (153-156). Similarly, our results showed that production of PGE_2 levels in the fibrotic lungs of $VHL^{+/-}$ mice were reduced after bleomycin administration, whereas PGE_2 levels in Fsp-$VHL^{+/-}$ and Fsp-$VHL^{-/-}$ mice remains unchanged after bleomycin treatment (**Fig 4.5F-5B)**, implicating that pVHL is required in controlling the homeostasis of PGE_2 signaling pathway. Previous reports indicate that a compensatory up-regulated expression of PGE_2 signaling genes, including COX-1, COX-2, PGE synthase1, 3, and EP2, occurs in $VHL^{+/-}$ mice treated with

bleomycin (160, 161). Furthermore, our results showed that there is no such a compensatory induction of COX-1, COX-2, PGE synthase1, 3, and EP2 in Fsp-VHL$^{+/-}$ and Fsp-VHL$^{-/-}$ mice treated with bleomycin (figure 4.5C-4.5H), further confirming the function of pVHL in the homeostasis of PGE_2 signaling pathway. Further investigations are necessary to explore the molecular mechanisms how pVHL regulates PGE_2 signaling pathway.

Bleomycin administration is not only widely used to induce acute lung injury (ALI) and lung inflammation, which showed increase in pro-inflammatory cytokines, leukocyte infiltration, pulmonary edema and significant oxidative stress, but also leads to pulmonary fibrosis, which is accompanied with fibroblasts proliferation, differentiation of fibroblasts into collagen-producing myofibroblasts, and deregulated ECM remodeling. However, Fsp-VHL$^{+/-}$ mice and their littermates had similar BALF protein amount, cell counts and cell differentiation, Fsp-VHL$^{-/-}$ mice displayed higher protein amount, cell counts, cell differentiation (figure 4.6A-4.6C), indicating that pVHL has little effect on lung BLM induced acute lung injury. Furthermore, similar levels of bleomycin-induced TGF-β1 were shown in wild type mice, Fsp-VHL$^{+/-}$ mice and Fsp-VHL$^{-/-}$ mice have, implicating that pVHL has little effect on BLM induced TGF-β1signaling pathway (figure 4.6D). Above all, pVHL likely acts on the fibrotic stage in the bleomycin model. Furthermore, we found that suppression of pVHL in fibroblasts inhibits bleomycin-induced IL-1b, IL-6, TNF-α, TGFb1, and TGFb3 in the fibrotic stage (figure 4.7), suggesting that loss of pVHL caused prevention of fibrosis also inhibits the sustained inflammation.

We used the bleomycin-mediated pulmonary fibrosis model in this study, which does share the similar pathogenesis with idiopathic pulmonary fibrosis. In the future, other fibrosis models also can be used to confirm our findings. Although Fsp-1 was originally thought to be expressed only in fibroblasts, emerging evidence show that other cell types also express Fsp-1. Thus, it is possible that, in our bleomycin-induced fibrosis model, other cell types may play a role in the phenotype change of pVHL knockout mice. It is likely that fibroblast specific protein-1 (Fsp-1) positive fibroblasts only represent a portion of the total lung fibroblast population, and thus the role of Fsp-1 driven knockout of pVHL in the pathogenesis of pulmonary fibrosis suggests the essential role of this subpopulation of fibroblasts in fibrogenesis. Recent reports also indicate that Fsp-1 is also expressed in fibrocytes and epithelial cells experiencing EMT (174-177). Therefore, knockout of pVHL with Fsp-Cre may ablate pVHL expression in interstitial fibroblasts and fibroblasts/myofibroblasts derived from epithelial cells and fibrocytes. Thus, alleviation of lung

fibrosis in Fsp-VHL$^{+/-}$ and Fsp-VHL$^{-/-}$ mice may suggest the comprehensive contribution of all these types of cells.

Together, our results indicate that pVHL is required for pulmonary fibrosis by controlling fibroblast proliferation, differentiation and ECM dysregulation, possibly via an HIF independent pathway, and that pVHL also mediates the fibrogenesis by altering BLM-induced MMP9, Wnt signaling and prostaglandin E2 (PGE2) signaling **(Fig 4.8)**. Further studies are warranted to investigate how pVHL regulates MMP9, Wnt and PGE2 signaling.

REFERENCES

1. Moolenaar WH. Lysophosphatidic acid, a multifunctional phospholipid messenger. *J Biol Chem.* 1995; 270(22):12949-52.

2. Mills GB, Moolenaar WH. The emerging role of lysophosphatidic acid in cancer. Nat Rev Cancer. 2003; 3(8):582-91.

3. Panupinthu N, Lee HY, Mills GB. Lysophosphatidic acid production and action: critical new players in breast cancer initiation and progression. Br J Cancer. 2010; 102(6):941-6.

4. KIRSCHNER H, VOGT W. Pharmacologically active lipidsoluble acids in brain extracts: isolation of lysophosphatidic acid and ganglioside. Biochem Pharmacol. 1961; 8:224-34

5. Yung YC, Stoddard NC, Chun J. LPA receptor signaling: pharmacology, physiology, and pathophysiology. J Lipid Res. 2014; 55(7):1192-214.

6. Aoki J. Mechanisms of lysophosphatidic acid production. Semin Cell Dev Biol. 2004; 15(5):477-89.

7. Aoki J, Taira A, Takanezawa Y, Kishi Y, Hama K, Kishimoto T, Mizuno K, Saku K, Taguchi R, Arai H. Serum lysophosphatidic acid is produced through diverse phospholipase pathways. J Biol Chem. 2002; 277(50):48737-44.

8. Aoki J, Inoue A, Okudaira S. Two pathways for lysophosphatidic acid production. Biochim Biophys Acta. 2008; 1781(9):513-8.

9. Sugiura T., Nakane S., Kishimoto S., Waku K., Yoshioka Y., Tokumura A., Hanahan D. J. Occurrence of lysophosphatidic acid and its alkyl ether-linked analog in rat brain and comparison of their biological activities toward cultured neural cells. Biochim. Biophys. Acta. 1999; 1440: 194–204.

10. Hosogaya S., Yatomi Y., Nakamura K., Ohkawa R., Okubo S., Yokota H., Ohta M., Yamazaki H., Koike T., Ozaki Y. Measurement of plasma lysophosphatidic acid concentration in healthy subjects: strong correlation with lysophospholipase D activity. Ann Clin Biochem. 2008; 45(Pt 4):364-8.

11. Watanabe N, Ikeda H, Nakamura K, Ohkawa R, Kume Y, Aoki J, Hama K, Okudaira S, Tanaka M, Tomiya T, Yanase M, Tejima K, Nishikawa T, Arai M, Arai H, Omata M, Fujiwara K, Yatomi Y. Both plasma lysophosphatidic acid and serum autotaxin levels are increased in chronic hepatitis C. J Clin Gastroenterol. 2007; 41(6):616-23.

12. Kawagoe H, Soma O, Goji J, Nishimura N, Narita M, Inazawa J, Nakamura H, Sano K. Molecular cloning and chromosomal assignment of the human brain-type phosphodiesterase I/nucleotide pyrophosphatase gene (PDNP2). Genomics. 1995; 30(2):380-4.

13. Jansen S, Stefan C, Creemers JW, Waelkens E, Van Eynde A, Stalmans W, Bollen M. Proteolytic maturation and activation of autotaxin (NPP2), a secreted metastasis-enhancing lysophospholipase D. J Cell Sci. 2005; 118(Pt 14):3081-9.

14. Perrakis A, Moolenaar WH. Autotaxin: structure-function and signaling. J Lipid Res. 2014; 55(6):1010-8.

15. Yuelling LM, Fuss B. Autotaxin (ATX): a multi-functional and multi-modular protein possessing enzymatic lysoPLD activity and matricellular properties. Biochim Biophys Acta. 2008; 1781(9):525-30.

16. van Meeteren LA1, Ruurs P, Christodoulou E, Goding JW, Takakusa H, Kikuchi K, Perrakis A, Nagano T, Moolenaar WH. Inhibition of autotaxin by lysophosphatidic acid and sphingosine 1-phosphate. J Biol Chem. 2005; 280(22):21155-61.

17. Tanaka M, Okudaira S, Kishi Y, Ohkawa R, Iseki S, Ota M, Noji S, Yatomi Y, Aoki J, Arai H. Autotaxin stabilizes blood vessels and is required for embryonic vasculature by producing lysophosphatidic acid. J Biol Chem. 2006; 281(35):25822-30.

18. Alvarez SE, Milstien S, Spiegel S. Autocrine and paracrine roles of sphingosine-1-phosphate. Trends Endocrinol Metab. 2007; 18(8):300-7.

19. Bai Z, Cai L, Umemoto E, Takeda A, Tohya K, Komai Y, Veeraveedu PT, Hata E, Sugiura Y, Kubo A, Suematsu M, Hayasaka H, Okudaira S, Aoki J, Tanaka T, Albers HM, Ovaa H, Miyasaka M. Constitutive lymphocyte transmigration across the basal lamina of high endothelial venules is regulated by the autotaxin/lysophosphatidic acid axis. J Immunol. 2013; 190(5):2036-48.

20. Kanda H, Newton R, Klein R, Morita Y, Gunn MD, Rosen SD. Autotaxin, an ectoenzyme that produces lysophosphatidic acid, promotes the entry of lymphocytes into secondary lymphoid organs. Nat Immunol. 2008; 9(4):415-23.

21. Karliner JS, Honbo N, Summers K, Gray MO, Goetzl EJ. The lysophospholipids sphingosine-1-phosphate and lysophosphatidic acid enhance survival during hypoxia in neonatal rat cardiac myocytes. J Mol Cell Cardiol. 2001; 33(9):1713-7.

22. Chen J, Baydoun AR, Xu R, Deng L, Liu X, Zhu W, Shi L, Cong X, Hu S, Chen X. Lysophosphatidic acid protects mesenchymal stem cells against hypoxia and serum deprivation-induced apoptosis. Stem Cells. 2008; 26(1):135-45.

23. Okusa MD, Ye H, Huang L, Sigismund L, Macdonald T, Lynch KR. Selective blockade of lysophosphatidic acid LPA3 receptors reduces murine renal ischemia-reperfusion injury. Am J Physiol Renal Physiol. 2003; 285(3):F565-74.

24. Hilal-Dandan R, Means CK, Gustafsson AB, Morissette MR, Adams JW, Brunton LL, Heller Brown J. Lysophosphatidic acid induces hypertrophy of neonatal cardiac myocytes via activation of Gi and Rho. J Mol Cell Cardiol. 2004; 36(4):481-93.

25. Chen J, Chen Y, Zhu W, Han Y, Han B, Xu R, Deng L, Cai Y, Cong X, Yang Y, Hu S, Chen X. Specific LPA receptor subtype mediation of LPA-induced hypertrophy of cardiac myocytes and involvement of Akt and NFkappaB signal pathways. J Cell Biochem. 2008; 103(6):1718-31.

26. Pulinilkunnil T, An D, Ghosh S, Qi D, Kewalramani G, Yuen G, Virk N, Abrahani A, Rodrigues B. Lysophosphatidic acid-mediated augmentation of cardiomyocyte lipoprotein lipase involves actin cytoskeleton reorganization. Am J Physiol Heart Circ Physiol. 2005; 288(6):H2802-10.

27. Blumberg HP, Kaufman J, Martin A, Charney DS, Krystal JH, Peterson BS. Significance of adolescent neurodevelopment for the neural circuitry of bipolar disorder. Ann N Y Acad Sci. 2004;1021:376-83.

28. Pulinilkunnil T, An D, Ghosh S, Qi D, Kewalramani G, Yuen G, Virk N, Abrahani A, Rodrigues B. Lysophosphatidic acid-mediated augmentation of cardiomyocyte lipoprotein lipase involves actin cytoskeleton reorganization. Am J Physiol Heart Circ Physiol. 2005; 288(6):H2802-10.

29. Ishii I, Fukushima N, Ye X, Chun J. Lysophospholipid receptors: signaling and biology. Annu Rev Biochem. 2004; 73:321-54.

30. Imamura F, Horai T, Mukai M, Shinkai K, Sawada M, Akedo H. Induction of in vitro tumor cell invasion of cellular monolayers by lysophosphatidic acid or phospholipase D. Biochem Biophys Res Commun. 1993; 193(2):497-503.

31. Kim KJ, Li B, Winer J, Armanini M, Gillett N, Phillips HS, Ferrara N. Inhibition of vascular endothelial growth factor-induced angiogenesis suppresses tumour growth in vivo. Nature. 1993; 362(6423):841-4.

32. Dash PK, Orsi SA, Moody M, Moore AN. A role for hippocampal Rho-ROCK pathway in long-term spatial memory. Biochem Biophys Res Commun. 2004; 322(3):893-8.

33. Das AK, Hajra AK. Quantification, characterization and fatty acid composition of lysophosphatidic acid in different rat tissues. Lipids. 1989; 24(4):329-33.

34. Fukushima N, Morita Y. Actomyosin-dependent microtubule rearrangement in lysophosphatidic acid-induced neurite remodeling of young cortical neurons. Brain Res. 2006;1094(1):65-75.

35. Ye X. Lysophospholipid signaling in the function and pathology of the reproductive system. Hum Reprod Update. 2008; 14(5):519-36.

36. Ziecik AJ, Waclawik A, Bogacki M. Conceptus signals for establishment and maintenance of pregnancy in pigs - lipid signaling system. Exp Clin Endocrinol Diabetes. 2008; 116(7):443-9.

37. Liszewska E, Reinaud P, Billon-Denis E, Dubois O, Robin P, Charpigny G. Lysophosphatidic acid signaling during embryo development in sheep: involvement in prostaglandin synthesis. Endocrinology. 2009;150(1):422-34.

38. Hashimoto T, Yamashita M, Ohata H, Momose K. Lysophosphatidic acid enhances in vivo infiltration and activation of guinea pig eosinophils and neutrophils via a Rho/Rho-associated protein kinase-mediated pathway. J Pharmacol Sci. 2003; 91(1):8-14.

39. Zhao Y, He D, Zhao J, Wang L, Leff AR, Spannhake EW, Georas S, Natarajan V. Lysophosphatidic acid induces interleukin-13 (IL-13) receptor alpha2 expression and inhibits IL-13 signaling in primary human bronchial epithelial cells. J Biol Chem. 2007; 282(14):10172-9.

40. Saatian B, Zhao Y, He D, Georas SN, Watkins T, Spannhake EW, Natarajan V. Transcriptional regulation of lysophosphatidic acid-induced interleukin-8 expression and secretion by p38 MAPK and JNK in human bronchial epithelial cells. Biochem J. 2006; 393(Pt 3):657-68.

41. Rubenfeld J, Guo J, Sookrung N, Chen R, Chaicumpa W, Casolaro V, Zhao Y, Natarajan V,

Georas S. Lysophosphatidic acid enhances interleukin-13 gene expression and promoter activity in T cells. Am J Physiol Lung Cell Mol Physiol. 2006; 290(1):L66-74.

42. Toews ML, Ustinova EE, Schultz HD. Lysophosphatidic acid enhances contractility of isolated airway smooth muscle. J Appl Physiol. 1997; 83(4):1216-22.

43. Zhao Y, Natarajan V. Lysophosphatidic acid signaling in airway epithelium: role in airway inflammation and remodeling. Cell Signal. 2009; 21(3):367-77.

44. Ediger TL, Toews ML. Synergistic stimulation of airway smooth muscle cell mitogenesis. J Pharmacol Exp Ther. 2000; 294(3):1076-82.

45. Xie WL, Chipman JG, Robertson DL, Erikson RL, Simmons DL. Expression of a mitogen-responsive gene encoding prostaglandin synthase is regulated by mRNA splicing. Proc Natl Acad Sci USA. 1991; 88(7):2692-6.

46. Cuendet M, Mesecar AD, DeWitt DL, Pezzuto JM. An ELISA method to measure inhibition of the COX enzymes. Nat Protoc. 2006; 1(4):1915-21.

47. Kis B, Snipes JA, Isse T, Nagy K, Busija DW. Putative cyclooxygenase-3 expression in rat brain cells. J Cereb Blood Flow Metab. 2003; 23(11):1287-92.

48. Kurumbail RG, Stevens AM, Gierse JK, McDonald JJ, Stegeman RA, Pak JY, Gildehaus D, Miyashiro JM, Penning TD, Seibert K, Isakson PC, Stallings WC. Structural basis for selective inhibition of cyclooxygenase-2 by anti-inflammatory agents. Nature. 1996; 384(6610):644-8.

49. Afshin Zarghi and Sara Arfaei. Selective COX-2 Inhibitors: A Review of Their Structure-Activity Relationships. Iran J Pharm Res. 2011; 10(4): 655–683.

50. Dixon DA, Kaplan CD, McIntyre TM, Zimmerman GA, Prescott SM. Post-transcriptional control of cyclooxygenase-2 gene expression: the role of the 3′-untranslated region. J Biol Chem. 2000; 275(16):11750-7.

51. Shao J, Sheng H, Inoue H, Morrow JD, Dubois RN. Regulation of constitutive cyclooxygenase-2 expression in colon carcinoma cells. J Biol Chem. 2000; 275(43):33951-6.

52. Subbaramaiah K, Dannenberg AJ. Cyclooxygenase 2: a molecular target for cancer prevention and treatment. Trends Pharmacol Sci. 2003; 24(2):96-102..

53. Dubois RN, Abramson SB, Crofford L, Gupta RA, Simon LS, Van De Putte LB, Lipsky PE. Cyclooxygenase in biology and disease. FASEB J. 1998; 12:1063-1073.

54. Pierce KL, Fujino H, Srinivasan D, Regan JW. Activation of FP prostanoid receptor isoforms leads to Rho-mediated changes in cell morphology and in the cell cytoskeleton. J Biol Chem. 1999; 274:35944-35949.

55. Moriyama T, Higashi T, Togashi K, Iida T, Segi E, Sugimoto Y, Tominaga T, Narumiya S, Tominaga M. Sensitization of TRPV1 by EP1 and IP reveals peripheral nociceptive mechanism of prostaglandins. Mol Pain. 2005; 1:3.

56. Funk CD. Prostaglandins and leukotrienes: advances in eicosanoid biology. Science. 2001;

294(5548):1871-5.

57. Samuelsson B, Morgenstern R, Jakobsson PJ. Membrane prostaglandin E synthase-1: a novel therapeutic target. Pharmacol Rev. 2007; 59:207-24.

58. Tanioka T, Nakatani Y, Semmyo N, Murakami M, Kudo I. Molecular identification of cytosolic prostaglandin E2 synthase that is functionally coupled with cyclooxygenase-1 in immediate prostaglandin E2 biosynthesis. J Biol Chem. 2000; 275:32775-32782.

59. Nakatani Y, Hokonohara Y, Kakuta S, Sudo K, Iwakura Y, Kudo I. Knockout mice lacking cPGES/p23, a constitutively expressed PGE2 synthetic enzyme, are perinatally lethal. Biochem Biophys Res Commun. 2007; 362:387-392.

60. Trebino CE, Stock JL, Gibbons CP, Naiman BM, Wachtmann TS, Umland JP, Pandher K, Lapointe JM, Saha S, Roach ML, Carter D, Thomas NA, Durtschi BA, McNeish JD, Hambor JE, Jakobsson PJ, Carty TJ, Perez JR, Audoly LP. Impaired inflammatory and pain responses in mice lacking an inducible prostaglandin E synthase. Proc Natl Acad Sci USA. 2003;100: 9044-9049.

61. Kamei D, Yamakawa K, Takegoshi Y, Mikami-Nakanishi M, Nakatani Y, Oh-Ishi S, Yasui H, Azuma Y, Hirasawa N, Ohuchi K, Kawaguchi H, Ishikawa Y, Ishii T, Uematsu S, Akira S, Murakami M, Kudo I. Reduced pain hypersensitivity and inflammation in mice lacking microsomal prostaglandin E synthase-1. J Biol Chem. 2004; 279:33684-33695.

62. Wang M, Zukas AM, Hui Y, Ricciotti E, Pure E, FitzGerald GA. Deletion of microsomal prostaglandin E synthase-1 augments prostacyclin and retards atherogenesis. Proc Natl Acad Sci USA. 2006; 103:14507-14512.

63. Egan KM, Lawson JA, Fries S, Koller B, Rader DJ, Smyth EM, Fitzgerald GA. COX-2-derived prostacyclin confers atheroprotection on female mice. Science. 2004;306:1954-1957.

64. Yao C, Sakata D, Esaki Y, Li Y, Matsuoka T, Kuroiwa K, Sugimoto Y, Narumiya S. Prostaglandin E2-EP4 signaling promotes immune inflammation through Th1 cell differentiation and Th17 cell expansion. Nat Med. 2009;15(6):633-40.

65. Harris SG, Padilla J, Koumas L, Ray D, Phipps RP. Prostaglandins as modulators of immunity. Trends Immunol. 2002;23:144-150.

66. Jowsey IR, Thomson AM, Flanagan JU, Murdock PR, Moore GB, Meyer DJ, Murphy GJ, Smith SA, Hayes JD. Mammalian class Sigma glutathione S-transferases: catalytic properties and tissue-specific expression of human and rat GSH-dependent prostaglandin D2 synthases. Biochem J. 2001; 359(Pt 3):507-16.

67. Urade Y, Hayaishi O. Prostaglandin D2 and sleep regulation. Biochim Biophys Acta. 1999; 1436:606-615.

68. Lewis RA, Soter NA, Diamond PT, Austen KF, Oates JA, Roberts LJ., II Prostaglandin D2 generation after activation of rat and human mast cells with anti-IgE. J Immunol. 1982;129:1627-1631.

69. Murray JJ, Tonnel AB, Brash AR, Roberts LJ, 2nd, Gosset P, Workman R, Capron A, Oates JA. Release of prostaglandin D2 into human airways during acute antigen challenge. N Engl J Med.

1986; 315:800-804.

70. Urade Y, Ujihara M, Horiguchi Y, Ikai K, Hayaishi O. The major source of endogenous prostaglandin D2 production is likely antigenpresenting cells. Localization of glutathione-requiring prostaglandin D synthetase in histiocytes, dendritic, and Kupffer cells in various rat tissues. J Immunol. 1989;143:2982-2989.

71. Hardy CC, Robinson C, Tattersfield AE, Holgate ST. The bronchoconstrictor effect of inhaled prostaglandin D2 in normal and asthmatic men. N Engl J Med. 1984; 311:209-213.

72. Fujitani Y, Kanaoka Y, Aritake K, Uodome N, Okazaki-Hatake K, Urade Y. Pronounced eosinophilic lung inflammation and Th2 cytokine release in human lipocalin-type prostaglandin D synthase transgenic mice. J Immunol. 2002;168:443-449.

73. Hammad H, de Heer HJ, Soullie T, Hoogsteden HC, Trottein F, Lambrecht BN. Prostaglandin D2 inhibits airway dendritic cell migration and function in steady state conditions by selective activation of the D prostanoid receptor 1. J Immunol. 2003;171:3936-3940.

74. Tsukada T, Rosenfeld M, Ross R, Gown AM. Immunocytochemical analysis of cellular components in lesions of atherosclerosis of the Watanabe and fat-fed rabbit using monoclonal antibodies. Arteriosclerosis. 1986; 6:601-613.

75. Hirawa N, Uehara Y, Yamakado M, Toya Y, Gomi T, Ikeda T, Eguchi Y, Takagi M, Oda H, Seiki K, Urade Y, Umemura S. Lipocalin-type prostaglandin dsynthase in essential hypertension. Hypertension. 2002;39:449-454.

76. Nagoshi H, Uehara Y, Kanai F, Maeda S, Ogura T, Goto A, Toyo-oka T, Esumi H, Shimizu T, Omata M. Prostaglandin D2 inhibits inducible nitric oxide synthase expression in rat vascular smooth muscle cells. Circ Res. 1998;82: 204-209.

77. Tanaka R, Miwa Y, Mou K, Tomikawa M, Eguchi N, Urade Y, Takahashi-Yanaga F, Morimoto S, Wake N, Sasaguri T. Knockout of the l-pgds gene aggravates obesity and atherosclerosis in mice. Biochem Biophys Res Commun. 2009;378:851-856.

78. Nelson H.S. The importance of allergens in the development of asthma and the persistence of symptoms. Dis Mon. 2001; 47(1):5-15.

79. Jenna R. Murdoch and Clare M. Lloyd. Chronic inflammation and asthma. Mutat Res. 2010; 690(1-2): 24–39.

80. Hashimoto, T., Yamashita, M., Ohata, H. & Momose, K. Lysophosphatidic acid enhances in vivo infiltration and activation of guinea pig eosinophils and neutrophils via a Rho/Rho-associated protein kinase-mediated pathway. J Pharmacol Sci 91, 8-14 (2003).

81. Zhao Y, He D, Zhao J, Wang L, Leff AR, Spannhake EW, Georas S, Natarajan V.. Lysophosphatidic acid induces interleukin-13 (IL-13) receptor alpha2 expression and inhibits IL-13 signaling in primary human bronchial epithelial cells. J Biol Chem. 2007; 282(14):10172-9.

82. Toews ML, Ustinova EE, Schultz HD. Lysophosphatidic acid enhances contractility of isolated airway smooth muscle. J Appl Physiol (1985). 1997; 83(4):1216-22.

83. Ediger TL, Toews ML. Synergistic Stimulation of Airway Smooth Muscle Cell Mitogenesis. J Pharmacol Exp Ther. 2000; 294(3):1076-82.

84. Goplen N, Karim MZ, Liang Q, Gorska MM, Rozario S, Guo L, Alam R.. Combined sensitization of mice to extracts of dust mite, ragweed, and Aspergillus species breaks through tolerance and establishes chronic features of asthma. J Allergy Clin Immunol. 2009;123(4):925-32.

85. Choi JW, Herr DR, Noguchi K, Yung YC, Lee CW, Mutoh T, Lin ME, Teo ST, Park KE, Mosley AN, Chun J. LPA receptors: subtypes and biological actions. Annu Rev Pharmacol Toxicol. 2010;50:157-86.

86. Contos JJ, Ishii I, Fukushima N, Kingsbury MA, Ye X, Kawamura S, Brown JH, Chun J. Characterization of lpa2 (Edg4) and lpa1/lpa2 (Edg2/Edg4) Lysophosphatidic Acid Receptor Knockout Mice: Signaling Deficits without Obvious Phenotypic Abnormality Attributable to lpa2. Mol Cell Biol. 2002;22(19):6921-9.

87. Pamuklar Z, Federico L, Liu S, Umezu-Goto M, Dong A, Panchatcharam M, Fulkerson Z, Berdyshev E, Natarajan V, Fang X, van Meeteren LA, Moolenaar WH, Mills GB, Morris AJ, Smyth SS. . Autotaxin/Lysopholipase D and Lysophosphatidic Acid Regulate Murine Hemostasis and Thrombosis. J Biol Chem. 2009; 284(11):7385-94.

88. Oikonomou N, Mouratis MA, Tzouvelekis A, Kaffe E, Valavanis C, Vilaras G, Karameris A, Prestwich GD, Bouros D, Aidinis V.. Pulmonary Autotaxin Expression Contributes to the Pathogenesis of Pulmonary Fibrosis. Am J Respir Cell Mol Biol. 2012;47(5):566-74.

89. Barnes PJ. The cytokine network in asthma and chronic obstructive pulmonary disease. J Clin Invest. 2008;118(11):3546-56.

90. Nagai H. Recent research and developmental strategy of anti-asthma drugs. Pharmacol Ther. 2012;133(1):70-8.

91. Hausmann J, Kamtekar S, Christodoulou E, Day JE, Wu T, Fulkerson Z, Albers HM, van Meeteren LA, Houben AJ, van Zeijl L, Jansen S, Andries M, Hall T, Pegg LE, Benson TE, Kasiem M, Harlos K, Kooi CW, Smyth SS, Ovaa H, Bollen M, Morris AJ, Moolenaar WH, Perrakis A. Structural basis of substrate discrimination and integrin binding by autotaxin. Nat Struct Mol Biol. 2011;18(2):198-204.

92. Tanaka M, Okudaira S, Kishi Y, Ohkawa R, Iseki S, Ota M, Noji S, Yatomi Y, Aoki J, Arai H., Autotaxin stabilizes blood vessels and is required for embryonic vasculature by\ producing lysophosphatidic acid. J Biol Chem. 2006; 281(35): 25822-30.

93. Mills, G.B. and W.H. Moolenaar, The emerging role of lysophosphatidic acid in cancer. Nat Rev Cancer, 2003; 3(8): 582-91.

94. Kanda H, Newton R, Klein R, Morita Y, Gunn MD, Rosen SD.., Autotaxin, an ectoenzyme that produces lysophosphatidic acid, promotes the entry of lymphocytes into secondary lymphoid organs. Nat Immunol, 2008; 9(4): 415-23.

95. Tager AM, LaCamera P, Shea BS, Campanella GS, Selman M, Zhao Z, Polosukhin V, Wain J, Karimi-Shah BA, Kim ND, Hart WK, Pardo A, Blackwell TS, Xu Y, Chun J, Luster AD., The

lysophosphatidic acid receptor LPA1 links pulmonary fibrosis to lung injury by mediating fibroblast recruitment and vascular leak. Nat Med, 2008;14(1): 45-54.

96. Kremer AE, Martens JJ, Kulik W, Ruëff F, Kuiper EM, van Buuren HR, van Erpecum KJ, Kondrackiene J, Prieto J, Rust C, Geenes VL, Williamson C, Moolenaar WH, Beuers U, Oude Elferink RP., Lysophosphatidic acid is a potential mediator of cholestatic pruritus. Gastroenterology, 2010;139(3): 1008-18, 1018 e1.

97. Saga H, Ohhata A, Hayashi A, Katoh M, Maeda T, Mizuno H, Takada Y, Komichi Y, Ota H, Matsumura N, Shibaya M, Sugiyama T, Nakade S, Kishikawa K., A novel highly potent autotaxin/ENPP2 inhibitor produces prolonged decreases in plasma lysophosphatidic acid formation in vivo and regulates urethral tension. PLoS One, 2014; 9(4): e93230.

98. van Meeteren LA, Ruurs P, Christodoulou E, Goding JW, Takakusa H, Kikuchi K, Perrakis A, Nagano T, Moolenaar WH., Inhibition of autotaxin by lysophosphatidic acid and sphingosine 1-phosphate. J Biol Chem, 2005;280(22): 21155-61.

99. Tokumura A, Miyake M, Yoshimoto O, Shimizu M, Fukuzawa K., Metal-ion stimulation and inhibition of lysophospholipase D which generates\ bioactive lysophosphatidic acid in rat plasma. Lipids, 1998; 33(10): 1009-15.

100. Albers HM, Dong A, van Meeteren LA, Egan DA, Sunkara M, van Tilburg EW, Schuurman K, van Tellingen O, Morris AJ, Smyth SS, Moolenaar WH, Ovaa H., Boronic acid-based inhibitor of autotaxin reveals rapid turnover of LPA in the\ circulation. Proc Natl Acad Sci U S A, 2010; 107(16): 7257-62.

101. Albers HM, van Meeteren LA, Egan DA, van Tilburg EW, Moolenaar WH, Ovaa H., Discovery and optimization of boronic acid based inhibitors of autotaxin. J Med Chem, 2010; 53(13): 4958-67.

102. Imamura, S. and Y. Horiuti, Enzymatic determination of phospholipase D activity with choline oxidase. J Biochem, 1978; 83(3): 677-80.

103. Scherer, M., G. Schmitz, and G. Liebisch, High-throughput analysis of sphingosine 1-phosphate, sphinganine 1-phosphate, and lysophosphatidic acid in plasma samples by liquid chromatography-tandem mass spectrometry. Clin Chem; 2009; 55(6): 1218-22.

104. Murph M, Tanaka T, Pang J, Felix E, Liu S, Trost R, Godwin AK, Newman R, Mills G., Liquid chromatography mass spectrometry for quantifying plasma lysophospholipids: potential biomarkers for cancer diagnosis. Methods Enzymol, 2007; 433: 1-25.

105. Zhao YZ, van Breemen RB, Nikolic D, Huang CR, Woodbury CP, Schilling A, Venton DL., Screening solution-phase combinatorial libraries using pulsed\ ultrafiltration/electrospray mass spectrometry. J Med Chem, 1997;40(25): 4006-12.

106. van Breemen RB, Huang CR, Nikolic D, Woodbury CP, Zhao YZ, Venton DL., Pulsed ultrafiltration mass spectrometry: a new method for screening combinatorial libraries. Anal Chem, 1997;69(11): 2159-64.

107. Choi Y, Jermihov K, Nam SJ, Sturdy M, Maloney K, Qiu X, Chadwick LR, Main M, Chen SN, Mesecar AD, Farnsworth NR, Pauli GF, Fenical W, Pezzuto JM, van Breemen RB., Screening

natural products for inhibitors of quinone reductase-2 using ultrafiltration LC-MS. Anal Chem, 2011;83(3): 1048-52.

108. Nikolic D, Habibi-Goudarzi S, Corley DG, Gafner S, Pezzuto JM, van Breemen RB., Evaluation of cyclooxygenase-2 inhibitors using pulsed ultrafiltration mass spectrometry. Anal Chem, 2000;72(16): 3853-9.

109. Cao H, Yu R, Choi Y, Ma ZZ, Zhang H, Xiang W, Lee DY, Berman BM, Moudgil KD, Fong HH, van Breemen RB., Discovery of cyclooxygenase inhibitors from medicinal plants used to treat inflammation. Pharmacol Res, 2010;61(6): 519-24.

110. Sun Y, Gu C, Liu X, Liang W, Yao P, Bolton JL, van Breemen RB., Ultrafiltration tandem mass spectrometry of estrogens for characterization of structure and affinity for human estrogen receptors. J Am Soc Mass Spectrom, 2005;16(2): 271-9.

111. Liu D, Guo J, Luo Y, Broderick DJ, Schimerlik MI, Pezzuto JM, van Breemen RB., Screening for ligands of human retinoid X receptor-alpha using ultrafiltration mass spectrometry. Anal Chem, 2007;79(24): 9398-402.

112. Tokumura A, Majima E, Kariya Y, Tominaga K, Kogure K, Yasuda K, Fukuzawa K., Identification of human plasma lysophospholipase D, a lysophosphatidic acid-producing enzyme, as autotaxin, a multifunctional phosphodiesterase. J Biol Chem, 2002; 277(42): 39436-42.

113. Clair T, Aoki J, Koh E, Bandle RW, Nam SW, Ptaszynska MM, Mills GB, Schiffmann E, Liotta LA, Stracke ML., Autotaxin hydrolyzes sphingosylphosphorylcholine to produce the regulator of\ migration, sphingosine-1-phosphate. Cancer Res, 2003;63(17): 5446-53.

114. Umezu-Goto M, Kishi Y, Taira A, Hama K, Dohmae N, Takio K, Yamori T, Mills GB, Inoue K, Aoki J, Arai H., Autotaxin has lysophospholipase D activity leading to tumor cell growth and\ motility by lysophosphatidic acid production. J Cell Biol, 2002;158(2): 227-33.

115. Croset M, Brossard N, Polette A, Lagarde M., Characterization of plasma unsaturated lysophosphatidylcholines in human and rat. Biochem J, 2000;345 Pt 1: 61-7.

116. Asl, M.N. and H. Hosseinzadeh, Review of pharmacological effects of Glycyrrhiza sp. and its bioactive compounds. Phytother Res, 2008;22(6): 709-24.

117. Simmler, C., G.F. Pauli, and S.N. Chen, Phytochemistry and biological properties of glabridin. Fitoterapia, 2013;90: 160-84.

118. Barbayianni E, Magrioti V, Moutevelis-Minakakis P, Kokotos G., Autotaxin inhibitors: a patent review. Expert Opin Ther Pat, 2013;23(9): 1123-32.

119. Raghu G, Selman M. Nintedanib and pirfenidone. New antifibrotic treatments indicated for idiopathic pulmonary fibrosis offer hopes and raises questions. Am J Respir Crit Care Med 2015;191(3):252-254.

120. Bishop T, Lau KW, Epstein AC, Kim SK, Jiang M, O'Rourke D, Pugh CW, Gleadle JM, Taylor MS, Hodgkin J, et al. Genetic analysis of pathways regulated by the von hippel-lindau tumor suppressor in caenorhabditis elegans. Plos Biology 2004;2(10):e289.

121. Kapitsinou PP, Haase VH. The vhl tumor suppressor and hif: Insights from genetic studies in mice. Cell Death Differ 2008;15(4):650-659.

122. Ivan M, Kondo K, Yang H, Kim W, Valiando J, Ohh M, Salic A, Asara JM, Lane WS, Kaelin WG, Jr. Hifalpha targeted for vhl-mediated destruction by proline hydroxylation: Implications for o2 sensing.[see comment]. Science 2001;292(5516):464-468.

123. Jaakkola P, Mole DR, Tian YM, Wilson MI, Gielbert J, Gaskell SJ, Kriegsheim A, Hebestreit HF, Mukherji M, Schofield CJ, et al. Targeting of hif-alpha to the von hippel-lindau ubiquitylation complex by o2-regulated prolyl hydroxylation. Science 2001;292(5516):468-472.

124. Masson N, Willam C, Maxwell PH, Pugh CW, Ratcliffe PJ. Independent function of two destruction domains in hypoxia-inducible factor-alpha chains activated by prolyl hydroxylation. EMBO Journal 2001;20(18):5197-5206.

125. Frew IJ, Krek W. Multitasking by pvhl in tumour suppression. Curr Opin Cell Biol 2007;19(6):685-690.

126. Ohh M, Yauch RL, Lonergan KM, Whaley JM, Stemmer-Rachamimov AO, Louis DN, Gavin BJ, Kley N, Kaelin WG, Jr., Iliopoulos O. The von hippel-lindau tumor suppressor protein is required for proper assembly of an extracellular fibronectin matrix. Mol Cell 1998;1(7):959-968.

127. Kurban G, Hudon V, Duplan E, Ohh M, Pause A. Characterization of a von hippel lindau pathway involved in extracellular matrix remodeling, cell invasion, and angiogenesis. Cancer Res 2006;66(3):1313-1319.

128. Tang N, Mack F, Haase VH, Simon MC, Johnson RS. Pvhl function is essential for endothelial extracellular matrix deposition. Mol Cell Biol 2006;26(7):2519-2530.

129. Biju MP, Neumann AK, Bensinger SJ, Johnson RS, Turka LA, Haase VH. Vhlh gene deletion induces hif-1-mediated cell death in thymocytes. Mol Cell Biol 2004;24(20):9038-9047.

130. Pfander D, Kobayashi T, Knight MC, Zelzer E, Chan DA, Olsen BR, Giaccia AJ, Johnson RS, Haase VH, Schipani E. Deletion of vhlh in chondrocytes reduces cell proliferation and increases matrix deposition during growth plate development. Development 2004;131(10):2497-2508.

131. Mack FA, Patel JH, Biju MP, Haase VH, Simon MC. Decreased growth of vhl-/- fibrosarcomas is associated with elevated levels of cyclin kinase inhibitors p21 and p27. Mol Cell Biol 2005;25(11):4565-4578.

132. Goda N, Ryan HE, Khadivi B, McNulty W, Rickert RC, Johnson RS. Hypoxia-inducible factor 1alpha is essential for cell cycle arrest during hypoxia. Mol Cell Biol 2003;23(1):359-369.

133. Higgins DF, Kimura K, Bernhardt WM, Shrimanker N, Akai Y, Hohenstein B, Saito Y, Johnson RS, Kretzler M, Cohen CD, et al. Hypoxia promotes fibrogenesis in vivo via hif-1 stimulation of epithelial-to-mesenchymal transition. J Clin Invest 2007;117(12):3810-3820.

134. Jatta K, Eliason G, Portela-Gomes GM, Grimelius L, Caro O, Nilholm L, Sirjso A, Piehl-Aulin K, Abdel-Halim SM. Overexpression of von hippel-lindau protein in skeletal muscles of patients with chronic obstructive pulmonary disease. J Clin Pathol 2009;62(1):70-76.

135. Zhou Q, Pardo A, Konigshoff M, Eickelberg O, Budinger GRS, Thavarajah K, Gottardi CJ, Jones J, Varga J, Selman M, et al. Role of von hippel-lindau protein in fibroblast proliferation and fibrosis. FASEB J 2011;25(9):3032-3044.

136. Haase VH, Glickman JN, Socolovsky M, Jaenisch R. Vascular tumors in livers with targeted inactivation of the von hippel-lindau tumor suppressor. Proc Natl Acad Sci U S A 2001;98(4):1583-1588.

137. Trimboli AJ, Fukino K, de Bruin A, Wei G, Shen L, Tanner SM, Creasap N, Rosol TJ, Robinson ML, Eng C, et al. Direct evidence for epithelial-mesenchymal transitions in breast cancer. Cancer Res 2008;68(3):937-945.

138. Budinger GR, Mutlu GM, Eisenbart J, Fuller AC, Bellmeyer AA, Baker CM, Wilson M, Ridge K, Barrett TA, Lee VY, et al. Proapoptotic bid is required for pulmonary fibrosis. Proc Natl Acad Sci U S A 2006;103(12):4604-4609.

139. Cao H, Xiao L, Park G, Wang X, Azim AC, Christman JW, van Breemen RB. An improved lc-ms/ms method for the quantification of prostaglandins e(2) and d(2) production in biological fluids. Anal Biochem 2008;372(1):41-51.

140. Irizarry RA, Hobbs B, Collin F, Beazer-Barclay YD, Antonellis KJ, Scherf U, Speed TP. Exploration, normalization, and summaries of high density oligonucleotide array probe level data. Biostatistics 2003;4(2):249-264.

141. Strutz F, Okada H, Lo CW, Danoff T, Carone RL, Tomaszewski JE, Neilson EG. Identification and characterization of a fibroblast marker: Fsp1. J Cell Biol 1995;130(2):393-405.

142. Lawson WE, Polosukhin VV, Zoia O, Stathopoulos GT, Han W, Plieth D, Loyd JE, Neilson EG, Blackwell TS. Characterization of fibroblast-specific protein 1 in pulmonary fibrosis. Am J Respir Crit Care Med 2005;171(8):899-907.

143. Hickey MM, Richardson T, Wang T, Mosqueira M, Arguiri E, Yu H, Yu QC, Solomides CC, Morrisey EE, Khurana TS, et al. The von hippel-lindau chuvash mutation promotes pulmonary hypertension and fibrosis in mice. J Clin Invest 2010;120(3):827-839.

144. Ramirez G, Hagood JS, Sanders Y, Ramirez R, Becerril C, Segura L, Barrera L, Selman M, Pardo A. Absence of thy-1 results in tgf-beta induced mmp-9 expression and confers a profibrotic phenotype to human lung fibroblasts. Lab Invest 2011;91(8):1206-1218.

145. Garcia-Alvarez J, Ramirez R, Sampieri CL, Nuttall RK, Edwards DR, Selman M, Pardo A. Membrane type-matrix metalloproteinases in idiopathic pulmonary fibrosis. Sarcoidosis Vasc Diffuse Lung Dis 2006;23(1):13-21.

146. Yang IV, Burch LH, Steele MP, Savov JD, Hollingsworth JW, McElvania-Tekippe E, Berman KG, Speer MC, Sporn TA, Brown KK, et al. Gene expression profiling of familial and sporadic interstitial pneumonia.[see comment]. Am J Respir Crit Care Med 2007;175(1):45-54.

147. Selman M, Pardo A, Kaminski N. Idiopathic pulmonary fibrosis: Aberrant recapitulation of developmental programs? PLoS Med 2008;5(3):e62.

148. Flozak AS, Lam AP, Russell S, Jain M, Peled ON, Sheppard KA, Beri R, Mutlu GM, Budinger

GRS, Gottardi CJ. Beta-catenin/t-cell factor signaling is activated during lung injury and promotes the survival and migration of alveolar epithelial cells. J Biol Chem 2010;285(5):3157-3167.

149. Lam AP, Flozak AS, Russell S, Wei J, Jain M, Mutlu GM, Budinger GRS, Feghali-Bostwick CA, Varga J, Gottardi CJ. Nuclear beta-catenin is increased in systemic sclerosis pulmonary fibrosis and promotes lung fibroblast migration and proliferation. Am J Respir Cell Mol Biol 2011;45(5):915-922.

150. Pardo A, Gibson K, Cisneros J, Richards TJ, Yang Y, Becerril C, Yousem S, Herrera I, Ruiz V, Selman M, et al. Up-regulation and profibrotic role of osteopontin in human idiopathic pulmonary fibrosis. PLoS Med 2005;2(9):e251.

151. Zuo F, Kaminski N, Eugui E, Allard J, Yakhini Z, Ben-Dor A, Lollini L, Morris D, Kim Y, DeLustro B, et al. Gene expression analysis reveals matrilysin as a key regulator of pulmonary fibrosis in mice and humans. Proc Natl Acad Sci U S A 2002;99(9):6292-6297.

152. Selman M, Pardo A, Barrera L, Estrada A, Watson SR, Wilson K, Aziz N, Kaminski N, Zlotnik A. Gene expression profiles distinguish idiopathic pulmonary fibrosis from hypersensitivity pneumonitis.[see comment]. Am J Respir Crit Care Med 2006;173(2):188-198.

153. Walker NM, Badri LN, Wadhwa A, Wettlaufer S, Peters-Golden M, Lama VN. Prostaglandin e2 as an inhibitory modulator of fibrogenesis in human lung allografts. Am J Respir Crit Care Med 2012;185(1):77-84.

154. Bauman KA, Wettlaufer SH, Okunishi K, Vannella KM, Stoolman JS, Huang SK, Courey AJ, White ES, Hogaboam CM, Simon RH, et al. The antifibrotic effects of plasminogen activation occur via prostaglandin e2 synthesis in humans and mice. J Clin Invest 2010;120(6):1950-1960.

155. Bozyk PD, Moore BB. Prostaglandin e2 and the pathogenesis of pulmonary fibrosis. Am J Respir Cell Mol Biol 2011;45(3):445-452.

156. Huang SK, Wettlaufer SH, Chung J, Peters-Golden M. Prostaglandin e2 inhibits specific lung fibroblast functions via selective actions of pka and epac-1. Am J Respir Cell Molecular Biol 2008;39(4):482-489.

157. Hara S, Kamei D, Sasaki Y, Tanemoto A, Nakatani Y, Murakami M. Prostaglandin e synthases: Understanding their pathophysiological roles through mouse genetic models. Biochimie;92(6):651-659.

158. Simon LS. Role and regulation of cyclooxygenase-2 during inflammation. Am J Med 1999;106(5B):37S-42S.

159. Narumiya S, Sugimoto Y, Ushikubi F. Prostanoid receptors: Structures, properties, and functions. Physiol Rev 1999;79(4):1193-1226.

160. Hodges RJ, Jenkins RG, Wheeler-Jones CPD, Copeman DM, Bottoms SE, Bellingan GJ, Nanthakumar CB, Laurent GJ, Hart SL, Foster ML, et al. Severity of lung injury in cyclooxygenase-2-deficient mice is dependent on reduced prostaglandin e(2) production. Am J Pathol 2004;165(5):1663-1676.

161. Yoon Y-S, Lee Y-J, Choi J-Y, Cho M-S, Kang JL. Coordinated induction of cyclooxygenase-2/prostaglandin e2 and hepatocyte growth factor by apoptotic cells prevents lung fibrosis. J Leukoc Biol 2013;94(5):1037-1049.

162. Wynn TA. Fibrotic disease and the t(h)1/t(h)2 paradigm. Nat Rev Immunol 2004;4(8):583-594.

163. Rosenbloom J, Castro SV, Jimenez SA. Narrative review: Fibrotic diseases: Cellular and molecular mechanisms and novel therapies. Ann Intern Med 2010;152(3):159-166.

164. Lovgren AK, Kovacs JJ, Xie T, Potts EN, Li Y, Foster WM, Liang J, Meltzer EB, Jiang D, Lefkowitz RJ, et al. Beta-arrestin deficiency protects against pulmonary fibrosis in mice and prevents fibroblast invasion of extracellular matrix. Sci Transl Med 2011;3(74):74ra23.

165. Jones AW, Reeve NL. Ultrastructural study of bleomycin-induced pulmonary changes in mice. J Pathol 1978;124(4):227-233.

166. Schrier DJ, Kunkel RG, Phan SH. The role of strain variation in murine bleomycin-induced pulmonary fibrosis. Am Rev Respir Dis 1983;127(1):63-66.

167. Phillips RJ, Mestas J, Gharaee-Kermani M, Burdick MD, Sica A, Belperio JA, Keane MP, Strieter RM. Epidermal growth factor and hypoxia-induced expression of cxc chemokine receptor 4 on non-small cell lung cancer cells is regulated by the phosphatidylinositol 3-kinase/pten/akt/mammalian target of rapamycin signaling pathway and activation of hypoxia inducible factor-1alpha. J Biol Chem 2005;280(23):22473-22481.

168. Strieter RM, Gomperts BN, Keane MP. The role of cxc chemokines in pulmonary fibrosis. J Clin Invest 2007;117(3):549-556.

169. Ceradini DJ, Kulkarni AR, Callaghan MJ, Tepper OM, Bastidas N, Kleinman ME, Capla JM, Galiano RD, Levine JP, Gurtner GC. Progenitor cell trafficking is regulated by hypoxic gradients through hif-1 induction of sdf-1. Nat Med 2004;10(8):858-864.

170. Staller P, Sulitkova J, Lisztwan J, Moch H, Oakeley EJ, Krek W. Chemokine receptor cxcr4 downregulated by von hippel-lindau tumour suppressor pvhl. Nature 2003;425(6955):307-311.

171. Pardo A, Selman M. Matrix metalloproteases in aberrant fibrotic tissue remodeling. Proc Am Thorac Soc 2006;3(4):383-388.

172. Zhou Q, Chen T, Bozkanat M, Ibe JCF, Christman JW, Raj JU, Zhou G. Intratracheal instillation of high dose adenoviral vectors is sufficient to induce lung injury and fibrosis in mice. PLoS One 2014;9(12):e116142.

173. Henderson WR, Jr., Chi EY, Ye X, Nguyen C, Tien Y-t, Zhou B, Borok Z, Knight DA, Kahn M. Inhibition of wnt/beta-catenin/creb binding protein (cbp) signaling reverses pulmonary fibrosis. Proc Natl Acad Sci U S A 2010;107(32):14309-14314.

174. Okada H, Danoff TM, Kalluri R, Neilson EG. Early role of fsp1 in epithelial-mesenchymal transformation. Am J Physiol 1997;273(4 Pt 2):F563-574.

175. Flier SN, Tanjore H, Kokkotou EG, Sugimoto H, Zeisberg M, Kalluri R. Identification of epithelial to mesenchymal transition as a novel source of fibroblasts in intestinal fibrosis. J Biol

Chem 2010;285(26):20202-20212.

176. Pilling D, Fan T, Huang D, Kaul B, Gomer RH. Identification of markers that distinguish monocyte-derived fibrocytes from monocytes, macrophages, and fibroblasts. PLoS One 2009;4(10):e7475.

177. Spaeth EL, Dembinski JL, Sasser AK, Watson K, Klopp A, Hall B, Andreeff M, Marini F. Mesenchymal stem cell transition to tumor-associated fibroblasts contributes to fibrovascular network expansion and tumor progression. PLoS One 2009;4(4):e4992.

VITA

NAME Yongchao Li

EDUCATION Ph.D., Medicinal Chemistry, University of Illinois, Chicago, Illinois, 2017

M.S., Peking Union Medical College, , Beijing, P. R. China, 2007

M.D., Beijing University of Chinese Medicine, Beijing, P. R. China, 2004

RESEARCH EXPERIENCE Pre-doctoral research assistant, University of Illinois, Chicago, Illinois (05/2009 - Present)

- Developed LC-MS based functional assay to screen and confirm autotaxin inhibitors (thesis)
- Profiling of LPA22: 5 (Autotaxin product) in BAL as a potential biomarker for asthma (thesis)
- Developed LC-MS/MS method to quantitate biomarkers and drug, such as 8-iso-PGF2α in the urine of HCV patients; PGE2 and PGD2 in human BAL; T, DHT and E2 in human serum, adipose and prostate tissue; Sorafenib in rabbit liver; flavonoids and anthocyanidins in human serum and urine; lycopene in cytoplasma and nucleic of primary prostate cells

TEACHING EXPERIENCE	Teaching assistant, University of Illinois, Chicago, Illinois (08/2008 - 05/2009) ▪ PHAR 402, Principles of Drug Action and Therapeutics II (Fall 2007) ▪ PHAR 407, Principles of Drug Action and Therapeutics VII (Spring 2008)
PROFESSIONAL MEMBERSHIPS	American Society of Mass Spectrometry (04/2010 - present) American Association of Clinical Chemistry (06/2013 - present)
HONORS AWARDS	MSACL Young Investigator Travel Award (2016) NIH ODS The Mary Frances Picciano Dietary Supplement Research Practicum (2014) W.E. van Doren Scholar, University of Illinois, Chicago (2014) ASMS Travel award, ASMS Conference Committee (2013)
PUBLICATIONS	van Breemen RB, Wright B, **Li Y**. Standardized grape powder for basic and clinical research (Chapter 1). In: John Pezzuto, "Grapes and Health." (2016) Newsome A, Li Y, van Breemen RB (co-first author) Improved quantification of free and ester-bound gallic acid in foods and beverages by UHPLC-MS/MS. J Agric and Food Chem. 2016; 64(6):1326-34 DG Nosal , Burton T, Wright B, Li Y, van Breemen RB. Quantification of polyphenols in freeze-dried table grape powder. Planta Med 2015; 81 – PR4. Zhou Q, Chen T, Zhang W, Bozkanat M, Li Y, van Breemen RB, Christman JW, Zhou G. Suppression of von Hippel-Lindau protein in

fibroblasts protects against bleomycin-induced pulmonary fibrosis, Am of Respir Cell and Mol Biol. 2016; 54(5):728-39.

Park GY, Li Y, Christman JW. Autotaxin production of lysophosphatidic acid mediates allergic asthmatic inflammation. Am J Respir Crit Care Med. 2013; 188(8):928-40.

Zhao G, Li Y, Xiao L. Pivotal role of reactive oxygen species in differential regulation of lipopolysaccharide-induced prostaglandins production in macrophages. Mol Pharmacol. 2013; 83(1):167-78.

Gaba RC, Li Y, Kumar N. Transarterial sorafenib chemoembolization: preliminary study of technical feasibility in a rabbit model. J Vasc Interv Radiol. 24(5):744-50.

Xiao L, Li Y, Christman JW. Lipopolysaccharide-induced expression of microsomal marrow derived macrophages. PLoS One. 2012; 7 (11):e50244.

Chang M, Li Y, Yang L. Development of methods to monitor ionization modification from dosing vehicles and phospholipids in study samples. Bioanalysis. 2011 Aug 3(15) 1719-1739.

Hoshino J, Park EJ, Kondratyuk TP, Marler L, Pezzuto JM, van Breemen RB, Mo S, Li Y, Cushman M. Selective synthesis andbiological evaluation of sulfate-conjugated resveratrol metabolites. J Med Chem. 2010; 53(13):5033-43.

Cai RL, Li Y, Qi Y. Antifatigue activity of phenylethanoid-rich extract from Cistanche deserticola. Phytother Res. 2010; 24(2): 313-5.

YCH Li, Y Song, Y Qi. Advancement in Pharmacological Research on Radix Angelicae Dahuricae. World Phytomedicines. 2007; 22(4): 161-164. (In Chinese)

Y Qi, RL Cai, M Wang, Y Song, B Liu, YCH Li, DM Zhao. Establishment of the range of normal values of blood biochemicaI measurements in SPF Wistar rats. Chinese J Comparative Med. 2006; 16(4):198-201. (In Chinese)

Y Qi, RL Cai, M Wang, Y Song, B Liu, YCH Li, DM Zhao. Establishment of normal range and values of blood biochemical measurements in beagle dogs. Chinese J Comparative Med. 2006; 16(4): 201-204. (In Chinese)

Y Qi, RL Cai, M Wang, Y Song, B Liu, YCH Li, DM Zhao. Establishment of the range of normal values of blood. Biochemical measurements in SPF SD rats. Chinese J Comparative Med. 2006; 16(4):193-196. (In Chinese)

PRESENTATIONS

Li, Y.; van Breemen, R.B.: Anti-inflammation biomarkers identified by LC-MS based lipidomics study and inhibitors screening by PUF-LCMS and LC-MS functional assay. Proceedings of the 8th Mass Spectrometry Applications to the Clinical Lab (MSACL); Palm Springs, CA, Feb 21-25, 2016.

Li, Y.; Dahl, J.; White, J.; van Breemen, R.B.: Quantitation of 8-iso-$PGF_{2\alpha}$ in human urine using UHPLC-MS-MS. Proceedings of the 61th ASMS Conference on Mass Spectrometry and Applied Topics; Minneapolis, MN, June 9-13, 2013.

Dong, L.; **Li, Y.**; van Breemen, R.B.: Atmospheric pressure photoionization mass of carotinoids using methyl-*tert*-butyl ether as a dopant. Proceedings of the 61th ASMS Conference on Mass Spectrometry and Applied Topics; Minneapolis, MN, June 9-13, 2013.

Nikolic, D.; **Li, Y.**; van Breemen, R.B.: Mass spectrometric characterization of residual pyrrolizidine alkaloids in commercial preparations of borage oil. Proceedings of the 60th ASMS Conference on Mass Spectrometry and Applied Topics; Vancouver, BC, CAN, May 19-24, 2012.

Li, Y.; Ming, C; van Breemen, R.B.: Ion suppression effect of phospholipids on dextromethophan and propranolol. Proceedings of the 59th ASMS Conference on Mass Spectrometry and Applied Topics; Denver, CO, June 5-9, 2011.

Li, Y.; Dong, L.; van Breemen, R.B.: Lycopene sub-cellular localization in primary prostate epithelial and stromal cells. Proceedings of the 58th

ASMS Conference on Mass Spectrometry and Applied Topics; Salt Lake City, UT, May 23-27, 2010.

APPENDICES